Fundamental Study of Bending and Free Vibration Problems of Irregular-Shaped Plates

December 1999

Graduate School of Marine Science and Engineeing

Nagasaki University

Huang Mei

Contents

Chapter 1

General Introduction

1.1 Introduction

This chapter is devoted to describe the background of researches on the problems of irregular-shaped plates and the present work including the equivalent rectangular plate, the discrete method and the outline of this thesis.

1.2 Background of researches on the problems of irregular-shaped plate

The problem of bending and free vibration of irregular-shaped plates is of some importance since these plates are extensively used in aircraft structures, ship structures, traffic, buildings and other structures.

Skew plates are used as floor slabs of skew bridge and elliptical plates are usually used as cover plates for cutouts of structures. In bevel gear design, a cantilevered annular sector plate model replaces the rectangular plate model to analyze the bevel gear tooth and to predict deflections and stresses. Since bevel gear teeth are characterized by a height and thickness taper along the tooth length, the annular sector plate can describe the bevel tooth form more accurately and conveniently than the rectangular plate. In transport vehicle structures, rectangular plates with cutouts are often used to lighten the weight of structure, to connect the components conveniently and to change the resonant frequency of the components or structures. The natural mode shape and frequencies of arbitrarily shaped panels are of considerable interest to the researchers who are examining the flutter margins of aircraft panels. The thin annular plates with clamped boundary conditions can be used to model a wafer machine to investigate its mechanical characteristics.

For their practical application, irregular-shaped plates have been analyzed by many researchers. Usually two kinds of plate theories are used to analyze the plate problems. One is the classical plate theory (Kirchhoff theory). The other is thick plate theory such as Mindlin plate theory. The classical plate theory neglects the transverse shear deformation. It is successfully used to thin plates. But for thick plates, it will make some errors because the shear deformation on thick plates is very important. Mindlin

plate theory takes into account shear deformation. So it provides a more realistic alternative to Kirchhoff theory. Some of the important assumptions used in the development of Mindlin plate theory are: (1) the deflection of the mid-surface of the plate is small compared with the plate thickness, (2) transverse normal stresses are negligible, and (3) the normal to the mid-surface of the plates remains straight after deformation but not necessarily remains normal.

Based on the two kinds of plate theories, lots of researches have been done on irregular-shaped plates such as circular, sector, elliptic, triangular, skew, polygonal plates or plates with cutouts. These researches have been carried out not only on the elastic bending problems, the free vibration problems, but also on the elasto-plastic bending problems.

1.2.1 Elastic bending problems

Conway and Huang [1] analyzed the bending problem of a sectorial plate with clamped edges and uniformly distributed load. They used two different methods of superposition on the elementary solution for a uniformly loaded circular plate with a clamped edge. In the first method, a line loading in the form of a cosine series was applied normally to a diameter of the plate. By superimposing this solution on the elementary solution, the resultant deflections were obtained. By making the resultant deflections equal to zero, the unknown coefficients of the series were determined. In the second method, a number of concentrated loads were applied normally to a diameter of the plate. The magnitudes of the loads were adjusted so that the resultant deflections at their points of application were zero. The flexural behavior of a cantilevered sector plate with variable rigidity, including the effects of shear deformation, was determined by Vaidyanathan et al. [2]. He used the Rayleigh-Ritz method with algebraic polynomial functions to obtain the deflections and stresses of the plate.

Fletcher [3] solved the bending problems of isosceles right triangular plates by two methods. One method used a concentrated diagonal load on a square plate. The other used an antisymmetric load on a square plate. A numerical solution was given for the case of clamped hypotenuse and two simply supported edges. A table was given

to show how to solve fifteen of the possible eighteen problems in which an edge was free, clamped or simply supported. The same problems were also analyzed by Conway [4] who used a special adaptation of the point-matching technique. The numerical solutions were obtained for uniformly loaded triangular plates with clamped or simply supported edges.

Mizusawa[5] analyzed the bending problem of skew plates with arbitrary boundary conditions subjected to uniform load or a concentrated load by using the spline element method. The minimum total potential energy theorem was used to develop the relationship between the unknown parameters and the applied loading. The effects of the degree of B-splines, the number of mesh divisions and refined mesh divisions on the accuracy of the solution were discussed. It has been found that stable convergent results can be obtained with an increase in the number of mesh divisions and in the degree of B-spline function. It has also been found that the refined mesh divisions around the corner region of the plate are useful to improve the defect of uniform mesh divisions and helpful to avoid singularity at obtuse corners.

Lo and Lee [6] determined the deflection of circular plates with variable thickness in one direction by the method of the equivalent systems. An equivalent system of the flat plates subjected to new loading was used to replace the original variable thickness plate. Due to the linearity of the governing equation, the sum of the deflections, bending moments or bending stresses of the flat plates of the equivalent system was equal to that of the corresponding elements of the original variable thickness plate. A simplified equivalent system with constant flexural rigidity was also obtained and could be used to reduce the mathematical complexity of the variable thickness problem.

The bending problems of arbitrarily shaped plates were discussed by Ng and Chen [7] and Hamouche *et al.* [8]. Ng and Chen [7] presented a spline finite strip method with B_3-spline. By using the cubic serendipity shape function, the plate was mapped into a square domain in the natural coordinate plane, and then discretization and analyses were carried out in the square domain. The method can be used for plates with arbitrary intermediate supports and arbitrary point loads. By reducing the order of numerical integrations, the method has solved the problem of shear locking, that is, the influence of the shear terms tends to dominate and the numerical solution may

yield unrealistically over-stiff results as the plate thickness becomes small. Hamouche *et al.* [8] used a spectral solution methodology to solve the biharmonic equation. By transforming the equations to general curvilinear coordinates, the boundary conditions were described exactly as they appeared on the curved lines in the physical plane. The spectral method evaluates the derivatives along the boundaries with spectral accuracy, thus permitting the achievement of a more accurate solution for arbitrarily shaped plates. The results were obtained for a simply-supported triangular plate, a truncated sector plate with mixed boundary conditions, circular and annular plates with different types of boundary conditions.

1.2.2 Free vibration problems

Any plate excited by a time-varying force is subject to vibrations. In order to use plates safely and efficiently, it is necessary to understand their vibration characteristics thoroughly. Consequently, free vibration problems of plates are some of importance and interest many researchers to study.

Vibration problems of rectangular plates have been extensively studied for the past several decades.

Liew, Hung and Lim [9] presented the vibration analysis of shear deformable plates using the Rayleigh-Ritz method with boundary characteristic orthogonal polynomials. Natural frequencies and mode shapes were obtained for simply supported rectangular plates and clamped rectangular plates with different aspect ratios and thickness ratios. It is shown that the presence of shear deformation and rotary inertia effects reduces the flexural rigidity and increases the inertia of the plate. Consequently, the overall vibration frequency parameters tend to decrease as the plate thickness increases. G.Aksu and S.A.Al-kaabi [10] carried out the free vibration analysis of Mindlin plates with linearly varying thickness by using a method based on the variational principles in conjunction with the finite difference technique. Natural frequencies and mode shapes of Mindlin plates with simply supported and clamped edges were obtained for various values of relative thickness ration and the taper thickness constant. Li and Gorman [11] solved the free vibration problem of simply supported rectangular plates with two di-

agonal supports by means of the superposition method. The line support was replaced by point support and the convergence tests have shown that a limited number of point supports provide excellent solution accuracy. Ju, Lee and Lee [12] presented a finite element model for the analysis of the free vibration of plates with multiple stepped variations in thickness resting on non-homogeneous elastic foundations. Natural frequencies and mode shapes of rectangular plates with multiple eccentrically stepped sections resting on non-homogeneous elastic foundations were obtained.

An Rayleigh-Ritz analysis for the free flexure vibration of thin, right triangular plates with different boundary conditions was given by Kim and Dickinson [13]. Simple polynomials were used as the admissible functions. Through the use of a recurrence relationship for the evaluation of the necessary integrals, a simpler analysis could be obtained. Numerical results were given for the isotropic plates. Singh and Saxena [14] solved transverse vibration of a general triangular plate with thickness varying as a linear function of the co-ordinates in the plane of the plate by working out several approximations in the Rayleigh-Ritz. The simple polynomials satisfying the essential boundary conditions have been used. To standardize computations, the given triangle was first mapped into an isosceles right triangle. Numerical results were obtained for arbitrary triangular plates with different boundary conditions and thickness variation. Gorman [15] described a new analytical technique based on the superposition method for the free vibration analysis of simply supported right triangular plates. The governing differential equation was completely satisfied and by means of a judicious choice of building blocks the boundary conditions were satisfied to any desired degree of accuracy. It will be noted that all eigenvalues decrease monotonically with aspect ratio. Mirza and Bijlani [16] solved the problem of the natural frequencies and mode shapes of cantilevered triangular plates with variable thickness and arbitrary plan-form using the finite element technique. The frequencies for the various combinations of four non-dimensional geometric parameters, namely, the aspect ratio, the two thickness ratios along the two coordinate directions and the sweep-back angle were tabulated and a few typical mode shapes have been presented graphically.

Yuan and Dickinson [17] gave natural frequency parameters for the free vibration of annular, circular and sectorial plates which may be supported along only parts of

their boundaries or may have sectorial cut-outs by a Ritz solution. Artificial springs were used to join sectorial elements together and their stiffnesses were permitted to become very high. So the required continuity conditions were satisfied. Lam, Liew and Chow [18] used an approximate method based on the Rayleigh-Ritz principle and a set of admissible orthogonal plate functions to obtain the eigenvalues and eigenvectors of circular and elliptical plates with free, simply supported or fully clamped boundary conditions.

McGee *et al.* [19] used C^0 continuous finite element assemblages of nine-node Lagrangian isoparametric quadrilateral plates based on a higher order shear deformable thick plate theory to analyze the natural vibrations of thick and thin skew plates with clamped and completely free edges. Non-dimensional frequencies and mode shapes were calculated for thick and thin skew plates having various combinations of clamped and free edge conditions, and arbitrary degrees of skewness. Srinivasan and Munaswamy [20] accomplished the free vibration analysis of skew orthotropic plates with point supports by using higher degree skew finite strips. The displacement function for the strips was assumed as a series with polynomials in one direction and beam functions in the other direction.

Ali and Atwal [21] analyzed the vibration of plates with cutouts using a simplified method. The method was based on Rayleigh's principle. The numerical results were obtained for the case of simply supported square plates with square and rectangular cutouts. Young and Dickinson [22] used the Ritz method to obtain an eigenvalue equation for the free vibration of a class of thin, flat plates which involve curved boundaries defined by polynomial expressions. Natural frequency parameters were given for a family of clamped semi-circular plates with free overhangs and family of circular plates with cutouts of different shapes.

Saliba extended superposition techniques developed by Gorman for the free vibration analysis of rectangular plates to the free vibration analysis of quadrilateral non-rectangular plates. Analytical solutions were provided for the simply supported and the fully clamped symmetrical trapezoidal plates with a wide range of plate aspect ratios in 1986 [23] and in 1988 [24], respectively.

The free vibration problems of other irregular-shaped plates, such as rhombic, pen-

tagonal, heptagonal plates, have been also studied.

1.2.3 Elasto-plastic bending problems

Many engineering materials such as steel and aluminum have considerable ductility beyond their elastic limit and the ductility permits a redistribution of stresses beyond the elastic limit. So it makes the structure carry considerable amounts of additional loads. The prediction of deflections and lateral load-carrying capacities, including ultimate capacities, of plates is of interest and importance in the design of structures.

The theory of plastic analysis has developed from two directions, the classical approach known as limit analysis and the fracture-line approach referred to as yield-line theory. Theorems on limit analysis enables one to arrive at upper and lower bounds of the ultimate load for a plate. If a ultimate configuration is assumed, the external loads computed by the principle of "virtual velocities" will be equal to or greater than the true ultimate load. So upper bound of the ultimate load can be obtained. If a stress configuration can be found which exceeds yield nowhere in the structure and which is in equilibrium with the external loads, these external loads will be equal to or less than the true ultimate loads. So the lower bound of the ultimate load can be gotten. The numerical methods such as the finite element methods, the discrete element methods, the finite difference methods are also used for the elasto-plastic bending problems.

Kusuda [25] determined the upper- and lower-bounds ultimate capacities of the plate structures of perfectly plastic material by using the limit analysis.

Anjan and John [26] analyzed the problem of the elasto-plastic plate by finite differences. In order to overcome one of the shortcomings of the finite-difference method, the problem was formulated in two parts. The first part consisted of the equilibrium of forces, which was independent of the material properties. The second part defined the forces according to the local material properties. The combination of these two parts approximated the solution of the actual problem, where a sharp discontinuity was approximated by a gradual curve.

Karakuzu, Özel and Sayman [27] developed a two-dimensional finite element program for elasto-plastic analysis. Isoparametric quadrilateral element with four nodes

was used and Lagrange polynomial was chosen as interpolation function. Residual stresses have been shown in figures and the spread of plastic zones has been illustrated for steel-aluminum composite plates with edge notches.

Alfredo and Leonard [28] suggested a discrete-variable approach to elasto-plastic plates. Numerical solutions were obtained for the flexural analysis of nonlinear elasto-plastic plates.

Ristinmaa [29] derived the consistent stiffness matrix for the generalized trapezoidal rule and paid an attention to the transition from an elastic to an elasto-plastic state. Numerical solutions were presented for a specimen with a notch and a specimen with a cylindrical hole.

Watanabe and Kondo [30] developed a new simplified finite element method for the elasto-plastic analysis of plate bending. In this method, plastic nodal displacement increments of an element were derived from the yield condition. Thus, the elasto-plastic stiffness matrix can be obtained without numerical integration over the domain of the element. Numerical solutions for the elasto-plastic bending problem of circular and rectangular plates were obtained.

1.3 The present work

Generally, the fundamental differential equations of the problems of irregular-shaped plates are the simultaneous partial differential equations with variable coefficients. These coefficients include the flexural rigidity of the plate, the thickness of the plate and etc. It is almost impossible to obtain the analytical solutions. So many numerical method such as Rayleigh-Ritz method, the finite element method, the supposition method, the finite strip element method and etc. are used to analyze the problems. These methods have many advantages in solving elastic bending and vibration problems of a plate. However, it is found that almost all the methods need prior assumption of the deflection. For some cases, they may encounter some difficulties such as the phenomenon of shear locking, the corner problems and etc. In order to solve these problems, special treatment is needed. On the other hand, the problems of irregular-shaped plates are generally more difficult than those of rectangular plates because the

boundary of the irregular-shaped plate is more difficult to be described accurately. All these make the calculation more complex and need more computer memory space and time. As so far, very little work has been done on the free vibration problems of thin or moderately thick rectangular and triangular plates with various thickness in two directions, the free vibration problems and elasto-plastic bending problems of rectangular plates with various-shaped hole located in any part of plates since it is difficult to solve the mathematical complexity in these problems. So it is necessary to find another efficient and simple method to solve the bending and free vibration problems of irregular-shaped plates.

1.3.1 The equivalent rectangular plate

In this thesis, the irregular-shaped plates are always converted into the equivalent rectangular plates with non-uniform thickness by adding some parts. An opening in a plate can be considered as an extremely thin part of the plate, and a non-rectangular plate can be translated into a circumscribed rectangular plate whose additional parts are extremely thin or thick according to the boundary conditions of the original plate. By analyzing the equivalent rectangular plates, the solutions of irregular-shaped plates are obtained.

1.3.2 The discrete method

In this thesis, the fundamental equations replacing the assumption of deflection are used as start pointing. Throughout two steps, the discrete solution is directly obtained. The two steps are as follows.

- Transforming the differential equations into the integral equations.
- Applying trapezoidal rule of numerical integration about the discrete points of intersection of crosswise line divided equally.

The solutions are obtained based on the discrete points. So the method is called discrete method. By increasing the number of crosswise line divided equally, the governing differential equations and the boundary conditions are satisfied to any desired degree

of accuracy in theory. So in fact, the discrete method is a semi-analytical method. The shear forces, the bending moments, the twisting moment, the slopes and the deflection of all the intersection of crosswise line can be obtained.

With the development of the computers, it is possible to obtain much more exact solution than before. The quantities at any intersection point of crosswise line can be finally expressed by the quantities of the boundary points. So the computer time is saved and even not very large-size digital computer can be used to solve the problem of irregular-shaped plates by the discrete method.

By using the discrete method, elastic bending analysis of irregular-shaped plates[31], free vibration analysis of rectangular plates with variable thickness [32, 33], free vibration analysis of irregular-shaped plates [34], free vibration analysis of rectangular plates with variously-shaped holes [35], free vibration analysis of right triangular plate with various thickness [36] and elasto-plastic bending analysis of square plates with various-shaped holes are carried out. The convergency and accuracy of the numerical solutions have been investigated.

1.3.3 The outline of this thesis

The thesis is composed of six chapters which are as follows.

In chapter 1, a general introduction of background of researches on irregular-shaped plate problems and the present work is described.

In chapter 2, at first, the fundamental differential equations of the rectangular plates with variable thickness are converted into integral equations. By applying numerical integration, the discrete solutions based on the Mindlin plate theory are obtained. Then, integral constants and boundary conditions of some rectangular plates are shown in figures. At last, the equivalent rectangular plate is obtained by proper transformation of the irregular-shaped plate.

In chapter 3, in order to investigate the efficiency and accuracy of the discrete solution based on the equivalent rectangular plate, the numerical analyses are carried out for the bending problems of irregular-shaped plates such as plate with opening, circular, semi-circular, elliptic, triangular, skew and rhombic plates. The convergency

and accuracy of the numerical solutions are investigated and compared with those of other literatures.

In chapter 4, the discrete method is extended for the free vibration analysis of irregular-shaped plates. Three sections consist of this chapter. In the first section, the free vibration problems of rectangular plates with different boundary conditions and variable thickness are analyzed. In the second section, under the conception of the equivalent rectangular plate, the discrete method with Green function proposed in the previous section is extended for the free vibration analysis of rectangular plates with various-shaped holes. In the third section, under the conception of an equivalent rectangular plate, the discrete method with Green function is also used for the free vibration analysis of right triangular plates with various thickness, different boundary conditions, aspect ratios and thickness ratios. The convergency and accuracy of these plates are investigated.

In chapter 5, firstly, the fundamental differential equations are obtained for the elasto-plastic bending problems. Then, the discrete solution is obtained by applying numerical integration. An incremental procedure has been used for the elasto-plastic analysis of the rectangular plates with point supports. In order to consider the extension of the yield region in the direction of thickness of the element, the thickness is divided into many layers. Numerical results have been carried out for square plates with square, triangular and circular hole and compared with previously published results. The convergency and accuracy are investigated.

In chapter 6, the conclusions of this work are summarized.

Chapter 2

Basic Theory

2.1 Introduction

In this chapter, at first, the fundamental differential equations of the rectangular plates with variable thickness and point supports are obtained and converted into integral equations. By applying numerical integration, the discrete solutions are obtained. Then, integral constants and boundary conditions of some rectangular plates are shown in figures. At last, the equivalent rectangular plate is obtained by suitable translation of the irregular-shaped plate.

2.2 Fundamental differential equations of plates with variable thickness and point supports

In order to obtain the fundamental differential equations of a rectangular plate with variable thickness and point supports, the rectangular Cartesian coordinates (x, y, z) are used. The xy plane is taken as the middle plane of the plate. The positive direction of the z axis is downward and the origin o is at the corner of the plate, as shown in Figure 2.1. An infinitesimal element is cut out of the plate by two pairs of planes parallel to the xz and yz planes, as shown in Figure 2.2. In this figure, Q_x and Q_y are the shearing forces, $M_{xy}(= M_{yx})$ is the twisting moment, M_x and M_y are the

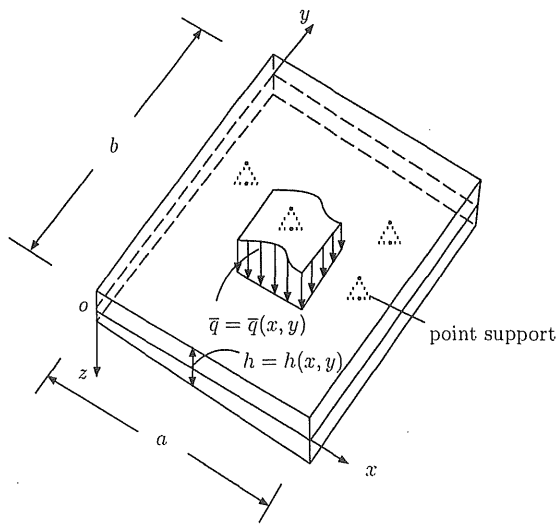

Figure 2.1: Rectangular plate and coordinate system

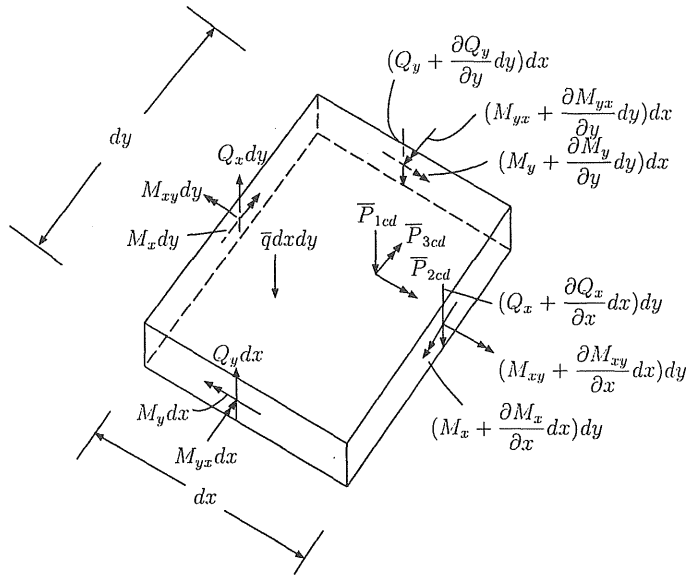

Figure 2.2: Element analysis

bending moments, $\overline{q} = \overline{q}(x, y)$ is the distributed load, $\overline{P}_{1cd}$ is vertical reaction of the point support at (x_c, y_d), $\overline{P}_{2cd}$ and $\overline{P}_{3cd}$ are moment reactions around x and y axis, respectively. Here

$$M_x = \int_h \sigma_x z dz, \qquad M_y = \int_h \sigma_y z dz,$$
$$M_{xy} = \int_h \tau_{xy} z dz, \qquad Q_x = \int_h \tau_{xz} dz,$$
$$Q_y = \int_h \tau_{yz} dz$$

Since the moments and the shearing forces are functions of the coordinates x and y, the small changes of these quantities must be considered when the coordinates x and y change by the small quantities dx and dy. Projecting all the forces acting on the element onto the z axis and taking moments of all the forces acting on the element with respect to the x and y axes, three equations of equilibrium can be obtained. Considering the strain-displacement and stress-strain relationships, another five equations can also be obtained. These eight equations are the fundamental differential equations of plates with variable thickness and point supports. They can be written as:

$$\frac{\partial Q_x}{\partial x}+\frac{\partial Q_y}{\partial y}+\overline{q}+\sum_{c=0}^{m}\sum_{d=0}^{n}\overline{P}_{1cd}\delta(x-x_c)\delta(y-y_d)=0 \tag{2.1a}$$

$$\frac{\partial M_{xy}}{\partial x}+\frac{\partial M_y}{\partial y}-Q_y+\sum_{c=0}^{m}\sum_{d=0}^{n}\overline{P}_{2cd}\delta(x-x_c)\delta(y-y_d)=0 \tag{2.1b}$$

$$\frac{\partial M_x}{\partial x}+\frac{\partial M_{xy}}{\partial y}-Q_x-\sum_{c=0}^{m}\sum_{d=0}^{n}\overline{P}_{3cd}\delta(x-x_c)\delta(y-y_d)=0 \tag{2.1c}$$

$$\frac{\partial \theta_x}{\partial x}+\nu\frac{\partial \theta_y}{\partial y}=\frac{M_x}{D} \tag{2.1d}$$

$$\frac{\partial \theta_y}{\partial y}+\nu\frac{\partial \theta_x}{\partial x}=\frac{M_y}{D} \tag{2.1e}$$

$$\frac{\partial \theta_x}{\partial y}+\frac{\partial \theta_y}{\partial x}=\frac{2}{(1-\nu)}\frac{M_{xy}}{D} \tag{2.1f}$$

$$\frac{\partial w}{\partial x}+\theta_x=\frac{Q_x}{Gt_s} \tag{2.1g}$$

$$\frac{\partial w}{\partial y}+\theta_y=\frac{Q_y}{Gt_s} \tag{2.1h}$$

where θ_x, θ_y are the slopes, w is the deflection, $D = Eh^3/12(1-\nu^2)$ is the flexural rigidity of the plate, E is the modulus of elasticity, G is the shear modulus of elasticity, ν is Poisson's ratio, $h = h(x, y)$ is the thickness of the plate, $t_s = h/1.2$, $\delta(x - x_c)$ and $\delta(y - y_d)$ are the Dirac's delta functions.

2.3 Non-dimensional differential equations

By introducing the following non-dimensional expressions,

$$[\,X_1 \quad X_2\,]=\frac{a^2}{D_0(1-\nu^2)}[\,Q_y \quad Q_x\,],\,[\,X_6 \quad X_7 \quad X_8\,]=[\,\theta_y \quad \theta_x \quad w/a\,]$$

$$[\,X_3 \quad X_4 \quad X_5\,]=\frac{a}{D_0(1-\nu^2)}[\,M_{xy} \quad M_y \quad M_x\,],\,[\,\eta \quad \zeta\,]=[\,x/a \quad y/b\,]$$

the differential equations (2.1a) $\sim$ (2.1h) can be rewritten as follows:

$$\frac{\partial X_1}{\partial \zeta}+\mu\frac{\partial X_2}{\partial \eta}=-q-\sum_{c=0}^{m}\sum_{d=0}^{n}P_{1cd}\delta(\eta-\eta_c)\delta(\zeta-\zeta_d) \tag{2.2a}$$

$$\frac{\partial X_4}{\partial \zeta}+\mu\frac{\partial X_3}{\partial \eta}=\mu X_1-\sum_{c=0}^{m}\sum_{d=0}^{n}P_{2cd}\delta(\eta-\eta_c)\delta(\zeta-\zeta_d) \tag{2.2b}$$

$$\frac{\partial X_3}{\partial \zeta}+\mu\frac{\partial X_5}{\partial \eta}=\mu X_2-\sum_{c=0}^{m}\sum_{d=0}^{n}P_{3cd}\delta(\eta-\eta_c)\delta(\zeta-\zeta_d) \tag{2.2c}$$

$$\frac{\partial X_6}{\partial \zeta}+\nu\mu\frac{\partial X_7}{\partial \eta}=IX_4 \tag{2.2d}$$

$$\nu\frac{\partial X_6}{\partial \zeta}+\mu\frac{\partial X_7}{\partial \eta}=IX_5 \tag{2.2e}$$

$$\frac{\partial X_7}{\partial \zeta}+\mu\frac{\partial X_6}{\partial \eta}=JX_3 \tag{2.2f}$$

$$\frac{\partial X_8}{\partial \eta}+X_7=KX_2 \tag{2.2g}$$

$$\frac{\partial X_8}{\partial \zeta}+\mu X_6=\mu KX_1 \tag{2.2h}$$

where a and b are the length and width of the rectangular plate, respectively, $\mu = b/a$, $q = \overline{q}\mu a^2/D_0(1-\nu^2)$, $D_0 = Eh_0^3/12(1-\nu^2)$ is the standard flexural rigidity of the plate, h_0 is standard thickness of the plate, $I = \mu(1-\nu^2)[h_0/h(x,y)]^3$, $[\,P_{1cd} \quad P_{2cd} \quad P_{3cd}\,] = \mu a^2\,[\,\overline{P}_{1cd}a \quad \overline{P}_{2cd} \quad -\overline{P}_{3cd}\,]/D_0(1-\nu^2)$, $J = 2\mu(1+\nu)[h_0/h(x,y)]^3$, $K = Eh_0^3/(10Ga^2h)$.

2.4 Discrete solution of fundamental differential equations

2.4.1 Introduction

With a rectangular plate divided vertically into m equal-length parts and horizontally into n equal-length parts as shown in Figure 2.3, the plate can be considered as a group of discrete points which are the intersections of the $(m+1)$-vertical and $(n+1)$-horizontal dividing lines. In this thesis, the rectangular area, $0 \le \eta \le \eta_i$, $0 \le \zeta \le \zeta_j$,

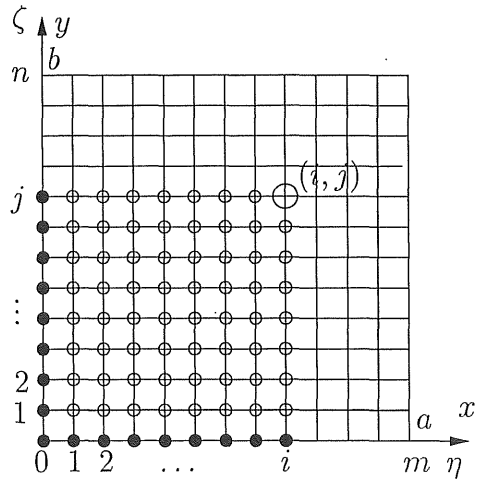

Figure 2.3: Discrete points on plate

corresponding to the arbitrary intersection (i, j) as shown in Figure 2.3 is denoted as the area $[i, j]$, the intersection (i, j) denoted by ○ is called the main point of the area $[i, j]$, the intersections denoted by ∘ are called the inner dependent points of the area, and the intersections denoted by • are called the boundary dependent points of the area.

2.4.2 Translation from differential equations into integral equations

By integrating the equations (2.2a) ∼ (2.2h) over the area $[i, j]$, the integral equations are obtained as:

$$\int_0^{\eta_i}\int_0^{\zeta_j}\frac{\partial X_1(\eta,\zeta)}{\partial\zeta}d\eta d\zeta+\mu\int_0^{\eta_i}\int_0^{\zeta_j}\frac{\partial X_2(\eta,\zeta)}{\partial\eta}d\eta d\zeta$$
$$=-\int_0^{\eta_i}\int_0^{\zeta_j}q(\eta,\zeta)d\eta d\zeta-\int_0^{\eta_i}\int_0^{\zeta_j}\sum_{c=0}^{m}\sum_{d=0}^{n}P_{1cd}\delta(\eta-\eta_c)\delta(\zeta-\zeta_d)d\eta d\zeta \quad (2.3a)$$

$$\int_0^{\eta_i}\int_0^{\zeta_j}\frac{\partial X_4(\eta,\zeta)}{\partial\zeta}d\eta d\zeta+\mu\int_0^{\eta_i}\int_0^{\zeta_j}\frac{\partial X_3(\eta,\zeta)}{\partial\eta}d\eta d\zeta$$
$$=\mu\int_0^{\eta_i}\int_0^{\zeta_j}X_1(\eta,\zeta)d\eta d\zeta-\int_0^{\eta_i}\int_0^{\zeta_j}\sum_{c=0}^{m}\sum_{d=0}^{n}P_{2cd}\delta(\eta-\eta_c)\delta(\zeta-\zeta_d)d\eta d\zeta \quad (2.3b)$$

$$\int_0^{\eta_i}\int_0^{\zeta_j}\frac{\partial X_3(\eta,\zeta)}{\partial\zeta}d\eta d\zeta+\mu\int_0^{\eta_i}\int_0^{\zeta_j}\frac{\partial X_5(\eta,\zeta)}{\partial\eta}d\eta d\zeta$$
$$=\mu\int_0^{\eta_i}\int_0^{\zeta_j}X_2(\eta,\zeta)d\eta d\zeta-\int_0^{\eta_i}\int_0^{\zeta_j}\sum_{c=0}^{m}\sum_{d=0}^{n}P_{3cd}\delta(\eta-\eta_c)\delta(\zeta-\zeta_d)d\eta d\zeta \quad (2.3c)$$

$$\int_0^{\eta_i}\int_0^{\zeta_j}\frac{\partial X_6(\eta,\zeta)}{\partial\zeta}d\eta d\zeta+\nu\mu\int_0^{\eta_i}\int_0^{\zeta_j}\frac{\partial X_7(\eta,\zeta)}{\partial\eta}d\eta d\zeta$$
$$=\int_0^{\eta_i}\int_0^{\zeta_j}I(\eta,\zeta)X_4(\eta,\zeta)d\eta d\zeta \quad (2.3d)$$

$$\nu\int_0^{\eta_i}\int_0^{\zeta_j}\frac{\partial X_6(\eta,\zeta)}{\partial\zeta}d\eta d\zeta+\mu\int_0^{\eta_i}\int_0^{\zeta_j}\frac{\partial X_7(\eta,\zeta)}{\partial\eta}d\eta d\zeta$$
$$=\int_0^{\eta_i}\int_0^{\zeta_j}I(\eta,\zeta)X_5(\eta,\zeta)d\eta d\zeta \quad (2.3e)$$

$$\int_0^{\eta_i}\int_0^{\zeta_j}\frac{\partial X_7(\eta,\zeta)}{\partial\zeta}d\eta d\zeta+\mu\int_0^{\eta_i}\int_0^{\zeta_j}\frac{\partial X_6(\eta,\zeta)}{\partial\eta}d\eta d\zeta$$
$$=\int_0^{\eta_i}\int_0^{\zeta_j}J(\eta,\zeta)X_3(\eta,\zeta)d\eta d\zeta \tag{2.3f}$$

$$\int_0^{\eta_i}\int_0^{\zeta_j}\frac{\partial X_8(\eta,\zeta)}{\partial\eta}d\eta d\zeta+\int_0^{\eta_i}\int_0^{\zeta_j}X_7(\eta,\zeta)d\eta d\zeta$$
$$=\int_0^{\eta_i}\int_0^{\zeta_j}K(\eta,\zeta)X_2(\eta,\zeta)d\eta d\zeta \tag{2.3g}$$

$$\int_0^{\eta_i}\int_0^{\zeta_j}\frac{\partial X_8(\eta,\zeta)}{\partial\zeta}d\eta d\zeta+\mu\int_0^{\eta_i}\int_0^{\zeta_j}X_6(\eta,\zeta)d\eta d\zeta$$
$$=\mu\int_0^{\eta_i}\int_0^{\zeta_j}K(\eta,\zeta)X_1(\eta,\zeta)d\eta d\zeta \tag{2.3h}$$

By using integration by parts, equations (2.3a) $\sim$ (2.3h) are written as:

$$\int_0^{\eta_i}X_1(\eta,\zeta_j)d\eta+\mu\int_0^{\zeta_j}X_2(\eta_i,\zeta)d\zeta$$
$$=\int_0^{\eta_i}X_1(\eta,0)d\eta+\mu\int_0^{\zeta_j}X_2(0,\zeta)d\zeta-\int_0^{\eta_i}\int_0^{\zeta_j}q(\eta,\zeta)d\eta d\zeta$$
$$-\sum_{c=0}^{m}\sum_{d=0}^{n}P_{1cd}u(\eta_i-\eta_c)u(\zeta_j-\zeta_d) \tag{2.4a}$$

$$\int_0^{\eta_i}X_4(\eta,\zeta_j)d\eta+\mu\int_0^{\zeta_j}X_3(\eta_i,\zeta)d\zeta$$
$$=\int_0^{\eta_i}X_4(\eta,0)d\eta+\mu\int_0^{\zeta_j}X_3(0,\zeta)d\zeta+\mu\int_0^{\eta_i}\int_0^{\zeta_j}X_1(\eta,\zeta)d\eta d\zeta$$
$$-\sum_{c=0}^{m}\sum_{d=0}^{n}P_{2cd}u(\eta_i-\eta_c)u(\zeta_j-\zeta_d) \tag{2.4b}$$

$$\int_0^{\eta_i}X_3(\eta,\zeta_j)d\eta+\mu\int_0^{\zeta_j}X_5(\eta_i,\zeta)d\zeta$$
$$=\int_0^{\eta_i}X_3(\eta,0)d\eta+\mu\int_0^{\zeta_j}X_5(0,\zeta)d\zeta+\mu\int_0^{\eta_i}\int_0^{\zeta_j}X_2(\eta,\zeta)d\eta d\zeta$$
$$-\sum_{c=0}^{m}\sum_{d=0}^{n}P_{3cd}u(\eta_i-\eta_c)u(\zeta_j-\zeta_d) \tag{2.4c}$$

$$\int_0^{\eta_i}X_6(\eta,\zeta_j)d\eta+\nu\mu\int_0^{\zeta_j}X_7(\eta_i,\zeta)d\zeta$$
$$=\int_0^{\eta_i}X_6(\eta,0)d\eta+\nu\mu\int_0^{\zeta_j}X_7(0,\zeta)d\zeta+\int_0^{\eta_i}\int_0^{\zeta_j}I(\eta,\zeta)X_4(\eta,\zeta)d\eta d\zeta \tag{2.4d}$$

$$\nu \int_0^{\eta_i} X_6(\eta, \zeta_j) d\eta + \mu \int_0^{\zeta_j} X_7(\eta_i, \zeta) d\zeta$$
$$= \nu \int_0^{\eta_i} X_6(\eta, 0) d\eta + \mu \int_0^{\zeta_j} X_7(0, \zeta) d\zeta + \int_0^{\eta_i} \int_0^{\zeta_j} I(\eta, \zeta) X_5(\eta, \zeta) d\eta d\zeta \tag{2.4e}$$

$$\int_0^{\eta_i} X_7(\eta, \zeta_j) d\eta + \mu \int_0^{\zeta_j} X_6(\eta_i, \zeta) d\zeta$$
$$= \int_0^{\eta_i} X_7(\eta, 0) d\eta + \mu \int_0^{\zeta_j} X_6(0, \zeta) d\zeta + \int_0^{\eta_i} \int_0^{\zeta_j} J(\eta, \zeta) X_3(\eta, \zeta) d\eta d\zeta \tag{2.4f}$$

$$\int_0^{\zeta_j} X_8(\eta_i, \zeta) d\zeta = \int_0^{\zeta_j} X_8(0, \zeta) d\zeta + \int_0^{\eta_i} \int_0^{\zeta_j} [K(\eta, \zeta) X_2(\eta, \zeta) - X_7(\eta, \zeta)] d\eta d\zeta \tag{2.4g}$$

$$\int_0^{\eta_i} X_8(\eta, \zeta_j) d\eta = \int_0^{\eta_i} X_8(\eta, 0) d\eta + \mu \int_0^{\eta_i} \int_0^{\zeta_j} [K(\eta, \zeta) X_1(\eta, \zeta) - X_6(\eta, \zeta)] d\eta d\zeta \tag{2.4h}$$

where

$$u(\eta_i - \eta_c) = \int_0^{\eta_i} \delta(\eta - \eta_c) d\eta, \quad u(\zeta_j - \zeta_d) = \int_0^{\zeta_j} \delta(\zeta - \zeta_d) d\zeta$$

2.4.3 Discrete forms of integral equations

By denoting $X_p(\eta_k, \zeta_l)$ as X_{pkl} and utilizing the trapezoidal rule of the numerical integration, the equations (2.4a) $\sim$ (2.4h) are written as:

$$\sum_{k=0}^{i} \beta_{ik} X_{1kj} + \mu \sum_{l=0}^{j} \beta_{jl} X_{2il}$$
$$= \sum_{k=0}^{i} \beta_{ik} X_{1k0} + \mu \sum_{l=0}^{j} \beta_{jl} X_{20l} - \sum_{k=0}^{i} \sum_{l=0}^{j} \beta_{ik} \beta_{jl} q_{kl} - \sum_{c=0}^{m} \sum_{d=0}^{n} P_{1cd} u_{ic} u_{jd} \tag{2.5a}$$

$$\sum_{k=0}^{i} \beta_{ik} X_{4kj} + \mu \sum_{l=0}^{j} \beta_{jl} X_{3il}$$
$$= \sum_{k=0}^{i} \beta_{ik} X_{4k0} + \mu \sum_{l=0}^{j} \beta_{jl} X_{30l} + \mu \sum_{k=0}^{i} \sum_{l=0}^{j} \beta_{ik} \beta_{jl} X_{1kl} - \sum_{c=0}^{m} \sum_{d=0}^{n} P_{2cd} u_{ic} u_{jd} \tag{2.5b}$$

$$\sum_{k=0}^{i} \beta_{ik} X_{3kj} + \mu \sum_{l=0}^{j} \beta_{jl} X_{5il}$$
$$= \sum_{k=0}^{i} \beta_{ik} X_{3k0} + \mu \sum_{l=0}^{j} \beta_{jl} X_{50l} + \mu \sum_{k=0}^{i} \sum_{l=0}^{j} \beta_{ik} \beta_{jl} X_{2kl} - \sum_{c=0}^{m} \sum_{d=0}^{n} P_{3cd} u_{ic} u_{jd} \tag{2.5c}$$

$$\sum_{k=0}^{i} \beta_{ik} X_{6kj} + \nu\mu \sum_{l=0}^{j} \beta_{jl} X_{7il}$$
$$= \sum_{k=0}^{i} \beta_{ik} X_{6k0} + \nu\mu \sum_{l=0}^{j} \beta_{jl} X_{70l} + \sum_{k=0}^{i} \sum_{l=0}^{j} \beta_{ik}\beta_{jl} I_{kl} X_{4kl} \tag{2.5d}$$

$$\nu \sum_{k=0}^{i} \beta_{ik} X_{6kj} + \mu \sum_{l=0}^{j} \beta_{jl} X_{7il}$$
$$= \nu \sum_{k=0}^{i} \beta_{ik} X_{6k0} + \mu \sum_{l=0}^{j} \beta_{jl} X_{70l} + \sum_{k=0}^{i} \sum_{l=0}^{j} \beta_{ik}\beta_{jl} I_{kl} X_{5kl} \tag{2.5e}$$

$$\sum_{k=0}^{i} \beta_{ik} X_{7kj} + \mu \sum_{l=0}^{j} \beta_{jl} X_{6il}$$
$$= \sum_{k=0}^{i} \beta_{ik} X_{7k0} + \mu \sum_{l=0}^{j} \beta_{jl} X_{60l} + \sum_{k=0}^{i} \sum_{l=0}^{j} \beta_{ik}\beta_{jl} J_{kl} X_{3kl} \tag{2.5f}$$

$$\sum_{l=0}^{j} \beta_{jl} X_{8il} = \sum_{l=0}^{j} \beta_{jl} X_{80l} + \sum_{k=0}^{i} \sum_{l=0}^{j} \beta_{ik}\beta_{jl} [K_{kl} X_{2kl} - X_{7kl}] \tag{2.5g}$$

$$\sum_{k=0}^{i} \beta_{ik} X_{8kj} = \sum_{k=0}^{i} \beta_{ik} X_{8k0} + \mu \sum_{k=0}^{i} \sum_{l=0}^{j} \beta_{ik}\beta_{jl} [K_{kl} X_{1kl} - X_{6kl}] \tag{2.5h}$$

where

$$u_{ic} = u(\eta_i - \eta_c), \quad u_{jd} = u(\zeta_j - \zeta_d),$$

$$u_{ic} = \begin{cases} 0 & \text{if } i < c \\ 0.5 & \text{if } i = c \\ 1 & \text{if } i > c \end{cases}, \quad u_{jd} = \begin{cases} 0 & \text{if } j < d \\ 0.5 & \text{if } j = d \\ 1 & \text{if } j > d \end{cases},$$

$$\alpha_{ik} = \begin{cases} 0.5 & \text{if } k = 0, i \\ 1 & \text{if } k \neq 0, i \end{cases}, \quad \alpha_{jl} = \begin{cases} 0.5 & \text{if } l = 0, j \\ 1 & \text{if } l \neq 0, j \end{cases},$$

$$\beta_{ik} = \alpha_{ik}/m, \qquad \beta_{jl} = \alpha_{jl}/n, \qquad \beta_{ij} = \beta_{ii}\beta_{jj}$$

Putting the quantities at main point (i, j) to the left-hand side and the quantities at the other points to the right-hand side of the equations (2.5a) $\sim$ (2.5h), the simultaneous equations for the unknown quantities at the main point (i, j), which include the dimensionless shear forces, twisting moment, bending moments, rotations

and deflections, can be obtained as follows:

$$\begin{aligned}
&\beta_{ii}X_{1ij} + \mu\beta_{jj}X_{2ij} \\
&= \sum_{k=0}^{i} \beta_{ik}[X_{1k0} - X_{1kj}(1-\delta_{ki})] + \mu\sum_{l=0}^{j} \beta_{jl}[X_{20l} - X_{2il}(1-\delta_{lj})] \\
&\quad - \sum_{k=0}^{i}\sum_{l=0}^{j} \beta_{ik}\beta_{jl}q_{kl} - \sum_{c=0}^{m}\sum_{d=0}^{n} P_{1cd}u_{ic}u_{jd}
\end{aligned} \tag{2.6a}$$

$$\begin{aligned}
&\beta_{ii}X_{4ij} + \mu\beta_{jj}X_{3ij} - \mu\beta_{ii}\beta_{jj}X_{1ij} \\
&= \sum_{k=0}^{i} \beta_{ik}[X_{4k0} - X_{4kj}(1-\delta_{ki})] + \mu\sum_{l=0}^{j} \beta_{jl}[X_{30l} - X_{3il}(1-\delta_{lj})] \\
&\quad + \mu\sum_{k=0}^{i}\sum_{l=0}^{j} \beta_{ik}\beta_{jl}X_{1kl}(1-\delta_{ki}\delta_{lj}) - \sum_{c=0}^{m}\sum_{d=0}^{n} P_{2cd}u_{ic}u_{jd}
\end{aligned} \tag{2.6b}$$

$$\begin{aligned}
&\beta_{ii}X_{3ij} + \mu\beta_{jj}X_{5ij} - \mu\beta_{ii}\beta_{jj}X_{2ij} \\
&= \sum_{k=0}^{i} \beta_{ik}[X_{3k0} - X_{3kj}(1-\delta_{ki})] + \mu\sum_{l=0}^{j} \beta_{jl}[X_{50l} - X_{5il}(1-\delta_{lj})] \\
&\quad + \mu\sum_{k=0}^{i}\sum_{l=0}^{j} \beta_{ik}\beta_{jl}X_{2kl}(1-\delta_{ki}\delta_{lj}) - \sum_{c=0}^{m}\sum_{d=0}^{n} P_{3cd}u_{ic}u_{jd}
\end{aligned} \tag{2.6c}$$

$$\begin{aligned}
&\beta_{ii}X_{6ij} + \nu\mu\beta_{jj}X_{7ij} - \beta_{ii}\beta_{jj}I_{ij}X_{4ij} \\
&= \sum_{k=0}^{i} \beta_{ik}[X_{6k0} - X_{6kj}(1-\delta_{ki})] + \nu\mu\sum_{l=0}^{j} \beta_{jl}[X_{70l} - X_{7il}(1-\delta_{lj})] \\
&\quad + \sum_{k=0}^{i}\sum_{l=0}^{j} \beta_{ik}\beta_{jl}I_{kl}X_{4kl}(1-\delta_{ki}\delta_{lj})
\end{aligned} \tag{2.6d}$$

$$\begin{aligned}
&\nu\beta_{ii}X_{6ij} + \mu\beta_{jj}X_{7ij} - \beta_{ii}\beta_{jj}I_{ij}X_{5ij} \\
&= \nu\sum_{k=0}^{i} \beta_{ik}[X_{6k0} - X_{6kj}(1-\delta_{ki})] + \mu\sum_{l=0}^{j} \beta_{jl}[X_{70l} - X_{7il}(1-\delta_{lj})] \\
&\quad + \sum_{k=0}^{i}\sum_{l=0}^{j} \beta_{ik}\beta_{jl}I_{kl}X_{5kl}(1-\delta_{ki}\delta_{lj})
\end{aligned} \tag{2.6e}$$

$$\begin{aligned}
&\beta_{ii}X_{7ij} + \mu\beta_{jj}X_{6ij} - \beta_{ii}\beta_{jj}J_{ij}X_{3ij} \\
&= \sum_{k=0}^{i} \beta_{ik}[X_{7k0} - X_{7kj}(1-\delta_{ki})] + \mu\sum_{l=0}^{j} \beta_{jl}[X_{60l} - X_{6il}(1-\delta_{lj})]
\end{aligned}$$

$$+\sum_{k=0}^{i}\sum_{l=0}^{j}\beta_{ik}\beta_{jl}J_{kl}X_{3kl}(1-\delta_{ki}\delta_{lj}) \tag{2.6f}$$

$$\begin{aligned}&\beta_{jj}X_{8ij}-\beta_{ii}\beta_{jj}K_{ij}X_{2ij}+\beta_{ii}\beta_{jj}X_{7ij}\\&=\sum_{l=0}^{j}\beta_{jl}[X_{80l}-X_{8jl}(1-\delta_{lj})]\\&+\sum_{k=0}^{i}\sum_{l=0}^{j}\beta_{ik}\beta_{jl}[K_{kl}X_{2kl}-X_{7kl}](1-\delta_{ki}\delta_{lj})\end{aligned} \tag{2.6g}$$

$$\begin{aligned}&\beta_{ii}X_{8ij}-\mu\beta_{ii}\beta_{jj}K_{ij}X_{1ij}+\mu\beta_{ii}\beta_{jj}X_{6ij}\\&=\sum_{k=0}^{i}\beta_{ik}[X_{8k0}-X_{8kj}(1-\delta_{ki})]\\&+\mu\sum_{k=0}^{i}\sum_{l=0}^{j}\beta_{ik}\beta_{jl}[K_{kl}X_{1kl}-X_{6kl}](1-\delta_{ki}\delta_{lj})\end{aligned} \tag{2.6h}$$

where

$$\delta_{ki}=\begin{cases}0 & \text{if } k\neq i\\ 1 & \text{if } k=i\end{cases},\quad \delta_{lj}=\begin{cases}0 & \text{if } l\neq j\\ 1 & \text{if } l=j\end{cases}$$

Rewriting the equations (2.6a) $\sim$ (2.6h) in matrix form yields

$$[\rho_{ep}]\{X_{pij}\}=\{A_e\}\quad (p=1\sim 8,\ e=1\sim 8) \tag{2.7}$$

where $\{A_e\}$ is the right-hand terms of equations (2.6a) $\sim$ (2.6h), $\{X_{pij}\}$ is the quantity at the main point (i,j), the coefficient matrix $[\rho_{ep}]$ (8×8) is as follows:

$$[\rho_{ep}]=\begin{bmatrix}
\beta_{ii} & \mu\beta_{jj} & 0 & 0 & 0 & 0 & 0 & 0\\
-\mu\beta_{ij} & 0 & \mu\beta_{jj} & \beta_{ii} & 0 & 0 & 0 & 0\\
0 & -\mu\beta_{ij} & \beta_{ii} & 0 & \mu\beta_{jj} & 0 & 0 & 0\\
0 & 0 & 0 & -\beta_{ij}I_{ij} & 0 & \beta_{ii} & \nu\mu\beta_{jj} & 0\\
0 & 0 & 0 & 0 & -\beta_{ij}I_{ij} & \nu\beta_{ii} & \mu\beta_{jj} & 0\\
0 & 0 & -\beta_{ij}J_{ij} & 0 & 0 & \mu\beta_{jj} & \beta_{ii} & 0\\
0 & -\beta_{ij}K_{ij} & 0 & 0 & 0 & 0 & \beta_{ij} & \beta_{jj}\\
-\mu\beta_{ij}K_{ij} & 0 & 0 & & 0 & \mu\beta_{ij} & 0 & \beta_{ii}
\end{bmatrix} \tag{2.8}$$

2.4.4 Discrete solution

If the inverse of matrix $[\rho_{ep}]$ is denoted as $[\gamma_{pe}]$, that is, $[\gamma_{pe}]=[\rho_{ep}]^{-1}$, then the equation (2.7) can be written as

$$\{X_{pij}\} = [\rho_{ep}]^{-1}\{A_e\} = [\gamma_{pe}]\{A_e\} \tag{2.9}$$

By substituting the right-hand terms of equations (2.6a) $\sim$ (2.6h) into the vector $\{A_e\}$ and rearranging terms, the following equation can be obtained:

$$\begin{aligned} X_{pij} = \sum_{e=1}^{8}\Big\{ & \sum_{k=0}^{i} \beta_{ik} A_{pe}[X_{ek0} - X_{ekj}(1-\delta_{ki})] \\ & + \sum_{l=0}^{j} \beta_{jl} B_{pe}[X_{e0l} - X_{eil}(1-\delta_{lj})] \\ & + \sum_{k=0}^{i}\sum_{l=0}^{j} \beta_{ik}\beta_{jl} C_{pekl} X_{ekl}(1-\delta_{ki}\delta_{lj})\Big\} \\ & - \sum_{k=0}^{i}\sum_{l=0}^{j} \beta_{ik}\beta_{jl}\gamma_{p1} q_{kl} - \sum_{f=1}^{3}\sum_{c=0}^{m}\sum_{d=0}^{n} \gamma_{pf} P_{fcd} u_{ic} u_{jd} \end{aligned} \tag{2.10}$$

where

$p = 1, 2, \cdots, 8$	$i = 1, 2, \cdots, m$	$j = 1, 2, \cdots, n$
$A_{p1} = \gamma_{p1}$	$B_{p1} = 0$	$C_{p1kl} = \mu(\gamma_{p2} + K_{kl}\gamma_{p8})$
$A_{p2} = 0$	$B_{p2} = \mu\gamma_{p1}$	$C_{p2kl} = \mu\gamma_{p3} + K_{kl}\gamma_{p7}$
$A_{p3} = \gamma_{p3}$	$B_{p3} = \mu\gamma_{p2}$	$C_{p3kl} = J_{kl}\gamma_{p6}$
$A_{p4} = \gamma_{p2}$	$B_{p4} = 0$	$C_{p4kl} = I_{kl}\gamma_{p4}$
$A_{p5} = 0$	$B_{p5} = \mu\gamma_{p3}$	$C_{p5kl} = I_{kl}\gamma_{p5}$
$A_{p6} = \gamma_{p4} + \nu\gamma_{p5}$	$B_{p6} = \mu\gamma_{p6}$	$C_{p6kl} = -\mu\gamma_{p8}$
$A_{p7} = \gamma_{p6}$	$B_{p7} = \mu(\nu\gamma_{p4} + \gamma_{p5})$	$C_{p7kl} = -\gamma_{p7}$
$A_{p8} = \gamma_{p8}$	$B_{p8} = \gamma_{p7}$	$C_{p8kl} = 0$

In the equation (2.10), the quantity X_{pij} at the main point (i, j) of the area $[i, j]$ is related to the quantities X_{ek0} and X_{e0l} at the boundary dependent points of the area and the quantities X_{ekj}, X_{eil} and X_{ekl} at the inner dependent points of the area. With the spreading of the area $[i, j]$ according to the regular order as $[1, 1]$, $[1, 2]$, $\cdots$, $[1, n]$, $[2, 1]$, $[2, 2]$, $\cdots$, $[2, n]$, $\cdots$, $[m, 1]$, $[m, 2]$, $\cdots$, $[m, n]$, a main point of a smaller area becomes one of the inner dependent points of the following larger areas. Whenever

the quantity X_{pij} at the main point (i,j) is obtained by using the equation (2.10) in above mentioned order, the quantities X_{ekj}, X_{eil} and X_{ekl} at the inner dependent points of the following larger areas can be eliminated by substituting the obtained results into the corresponding terms of the right side of equation (2.10). By repeating this process, the quantity X_{pij} at the main point is only related to the quantities X_{rk0}, (r=1,3,4,6,7,8) and X_{s0l},(s=2,3,5,6,7,8) which are six independent quantities at each boundary dependent point along the horizontal axis and the vertical axis in Figure 2.3, respectively. The result is as follows:

$$\begin{aligned}
X_{pij} = &\sum_{k=0}^{i}\Big\{a_{1pijk1}(Q_y)_{k0} + a_{1pijk2}(M_{xy})_{k0} + a_{1pijk3}(M_y)_{k0} \\
&\quad + a_{1pijk4}(\theta_y)_{k0} + a_{1pijk5}(\theta_x)_{k0} + a_{1pijk6}(w)_{k0}\Big\} \\
&+\sum_{l=0}^{j}\Big\{a_{2pijl1}(Q_x)_{0l} + a_{2pijl2}(M_{xy})_{0l} + a_{2pijl3}(M_x)_{0l} \\
&\quad + a_{2pijl4}(\theta_y)_{0l} + a_{2pijl5}(\theta_x)_{0l} + a_{2pijl6}(w)_{0l}\Big\} \\
&+\overline{q}_{pij} + \sum_{f=1}^{3}\sum_{c=0}^{m}\sum_{d=0}^{n}\overline{q}_{fpijcd}P_{fcd}
\end{aligned} \tag{2.11}$$

where the integral constants $(Q_y) = X_1$, $(Q_x) = X_2$, $(M_{xy}) = X_3$, $(M_y) = X_4$, $(M_x) = X_5$, $(\theta_y) = X_6$, $(\theta_x) = X_7$, $(w) = X_8$ and the coefficients

$$\begin{aligned}
a_{1pijuv} = &\sum_{e=1}^{8}\Big\{\sum_{k=0}^{i}\beta_{ik}A_{pe}[a_{1ek0uv} - a_{1ekjuv}(1-\delta_{ki})] \\
&\quad + \sum_{l=0}^{j}\beta_{jl}B_{pe}[a_{1e0luv} - a_{1eiluv}(1-\delta_{lj})] \\
&\quad + \sum_{k=0}^{i}\sum_{l=0}^{j}\beta_{ik}\beta_{jl}C_{pekl}a_{1ekluv}(1-\delta_{ki}\delta_{lj})\Big\} \\
a_{2pijuv} = &\sum_{e=1}^{8}\Big\{\sum_{k=0}^{i}\beta_{ik}A_{pe}[a_{2ek0uv} - a_{2ekjuv}(1-\delta_{ki})] \\
&\quad + \sum_{l=0}^{j}\beta_{jl}B_{pe}[a_{2e0luv} - a_{2eiluv}(1-\delta_{lj})] \\
&\quad + \sum_{k=0}^{i}\sum_{l=0}^{j}\beta_{ik}\beta_{jl}C_{pekl}a_{2ekluv}(1-\delta_{ki}\delta_{lj})\Big\} \\
\overline{q}_{pij} = &\sum_{e=1}^{8}\Big\{\sum_{k=0}^{i}\beta_{ik}A_{pe}[\overline{q}_{ek0} - \overline{q}_{ekj}(1-\delta_{ki})]
\end{aligned}$$

$$
\begin{aligned}
&+\sum_{l=0}^{j}\beta_{jl}B_{pe}[\overline{q}_{e0l}-\overline{q}_{eil}(1-\delta_{lj})]\\
&+\sum_{k=0}^{i}\sum_{l=0}^{j}\beta_{ik}\beta_{jl}C_{pekl}\overline{q}_{ekl}(1-\delta_{ki}\delta_{lj})\Big\}\\
&-\sum_{k=0}^{i}\sum_{l=0}^{j}\beta_{ik}\beta_{jl}\gamma_{p1}q_{kl}\\
\overline{q}_{fpijcd}=&\sum_{e=1}^{8}\Big\{\sum_{k=0}^{i}\beta_{ik}A_{pe}[\overline{q}_{fek0cd}-\overline{q}_{fekjcd}(1-\delta_{ki})]\\
&+\sum_{l=0}^{j}\beta_{jl}B_{pe}[\overline{q}_{fe0lcd}-\overline{q}_{feilcd}(1-\delta_{lj})]\\
&+\sum_{k=0}^{i}\sum_{l=0}^{j}\beta_{ik}\beta_{jl}C_{pekl}\overline{q}_{feklcd}(1-\delta_{ki}\delta_{lj})\Big\}\\
&-\gamma_{pf}u_{ic}u_{jd}\overline{u}_{fcd}
\end{aligned}
$$

where

$$
p=1,2,\cdots,8,\quad i=1,2,\cdots,m,\quad j=1,2,\cdots,n,\quad v=1,2,\cdots,6
$$

$$
u=\begin{cases}0,1,\cdots,i & (h=1)\\ 0,1,\cdots,j & (h=2)\end{cases}
\qquad
\overline{u}_{fcd}=\begin{cases}0:\text{not existing point support}\\ 1:\text{existing point support}\end{cases}
$$

$$
\begin{aligned}
&a_{1ri0iv}=1, && a_{2s0jjv}=1, && a_{25i003}=\frac{\overline{D}_{00}}{\overline{D}_{i0}}\overline{\alpha}_i\\
&a_{140j03}=\frac{\overline{D}_{00}}{\overline{D}_{0j}}\overline{\alpha}_j, && a_{15i0k3}=\nu\frac{\overline{D}_{k0}}{\overline{D}_{i0}}\overline{\beta}_{ik}, && a_{240jl3}=\nu\frac{\overline{D}_{0l}}{\overline{D}_{0j}}\overline{\beta}_{jl}\\
&a_{15i0k5}=\frac{1}{\overline{D}_{i0}}\overline{\gamma}_{ik}, && a_{240jl4}=\frac{1}{\mu\overline{D}_{0j}}\overline{\gamma}_{jl}, && a_{110j01}=\frac{K_{00}}{\overline{K}_{0j}}\overline{\alpha}_j\\
&a_{210jl4}=\frac{1}{K_{0j}}\overline{\beta}_{jl}, && a_{210jl6}=\frac{1}{\mu K_{0j}}\overline{\gamma}_{jl}, && a_{22i001}=\frac{K_{00}}{K_{i0}}\overline{\alpha}_i\\
&a_{12i0k5}=\frac{1}{K_{i0}}\overline{\beta}_{ik}, && a_{12i0k6}=\frac{1}{K_{i0}}\overline{\gamma}_{ik} && \overline{\alpha}_i=(-1)^i\\
&\overline{\alpha}_j=(-1)^j, && \overline{D}_{i0}=D_0/D_{i0}, && \overline{D}_{0j}=\mu D_0/D_{0j}\\
&\overline{\beta}_{ik}=\delta_{ik}+(-1)^{(i+1)}\delta_{0k}, && \overline{\beta}_{jl}=\delta_{jl}+(-1)^{(j+1)}\delta_{0l}, && \overline{\gamma}_{ik}=\frac{4m(-1)^{i+k}}{1+\delta_{ik}+\delta_{0k}}\\
&\overline{\gamma}_{jl}=\frac{4n(-1)^{j+l}}{1+\delta_{jl}+\delta_{0l}}, && \overline{\gamma}_{ik}=\begin{cases}0 & (i<k)\\ \overline{\gamma}_{ik} & (i\geq k)\end{cases}, && \overline{\gamma}_{jl}=\begin{cases}0 & (j<l)\\ \overline{\gamma}_{ik} & (j\geq l)\end{cases}
\end{aligned}
$$

The above coefficients a_{25i003}, a_{140j03}, $\cdots$, a_{22i001}, a_{12i0k5}, a_{12i0k6}, $\overline{\alpha}_i$, $\overline{\beta}_{ik}$, $\overline{\gamma}_{ik}$ and *etc.* are derived in Appendix.

The equation (2.11) is the approximate solution of the equations (2.2a) $\sim$ (2.2h). In this equation, the integral constants can be determined from the boundary conditions.

2.5 Integral constants and boundary conditions

2.5.1 Introduction

The integral constants are all quantities at the discrete points along the edges $y = 0$ ($\zeta = 0$) and $x = 0$ ($\eta = 0$) of the rectangular plate. There are six integral constants at every discrete point except the points at corners, and half of them are self-evident according to the boundary conditions along the edges $y = 0$ and $x = 0$. The remaining three integral constants can be determined by the boundary conditions along the edges $y = b$ and $x = a$.

2.5.2 Integral constants and boundary conditions for some plates

The integral constants and the boundary conditions of rectangular plates with four edges simply supported (SSSS), four edges clamped (CCCC), four edges free (FFFF), three edges free and one edge clamped (FCFF), two adjacent edges simply supported and the other edges clamped (SCCS) or free (SFFS) are shown in Figures 2.4 $\sim$ 2.9, respectively. In this thesis, the symbolism used for the boundary conditions will identify a rectangular plate with the edges $y = 0$, $x = a$, $y = b$ and $x = 0$. For example, a plate having boundary SFFS has a simply supported boundary condition at $y = 0$ ($\zeta = 0$), a free boundary condition at $x = a$ ($\eta = 1$), a free boundary condition at $y = b$ ($\zeta = 1$), a simply supported boundary condition at $x = 0$ ($\eta = 0$). For the plates with symmetrical axes, 1/2 or 1/4 parts cut out of the plates along the horizontal or vertical symmetrical axis or both are designated by (b), (c) or (d) and also shown in these figures. The integral constants and the boundary conditions at the corners of the plates are shown in the boxes. The simply supported, clamped and free edges are shown by solid line, thick solid line and dotted line, respectively.

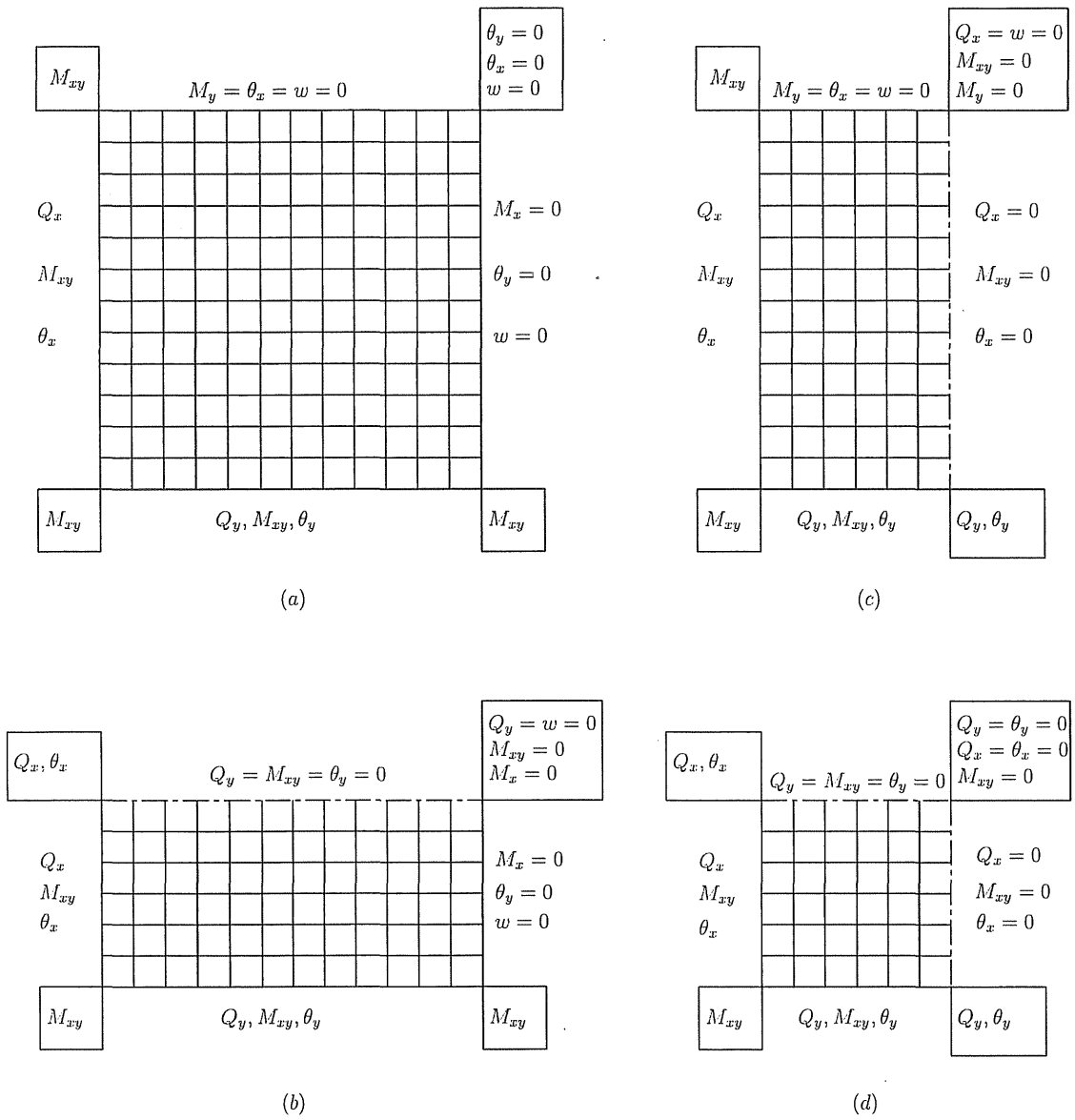

Figure 2.4: Integral constants and boundary conditions of a plate with four simply supported edges (SSSS)

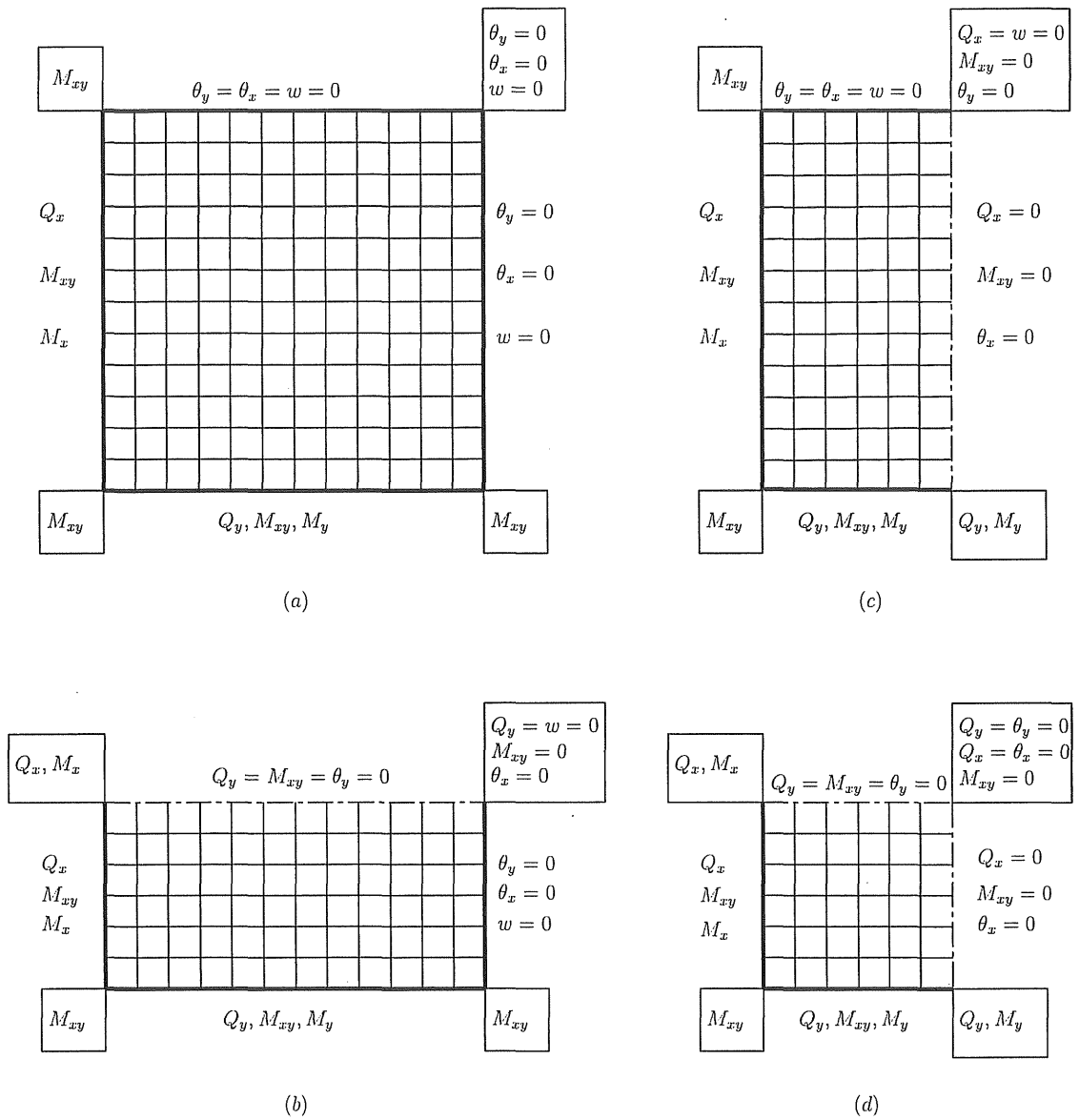

Figure 2.5: Integral constants and boundary conditions of a plate with four clamped edges (CCCC)

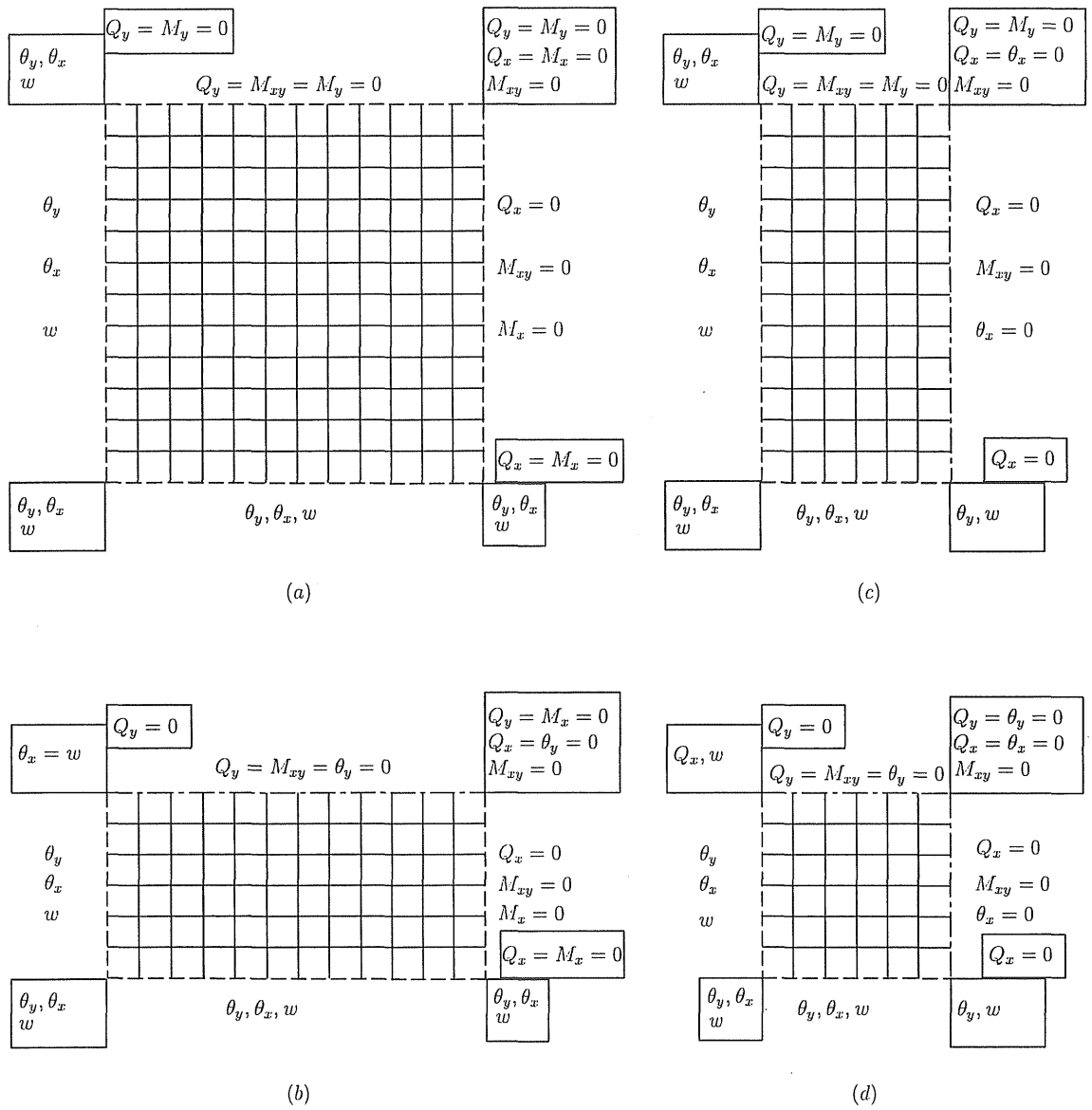

Figure 2.6: Integral constants and boundary conditions of a plate with four free edges (FFFF)

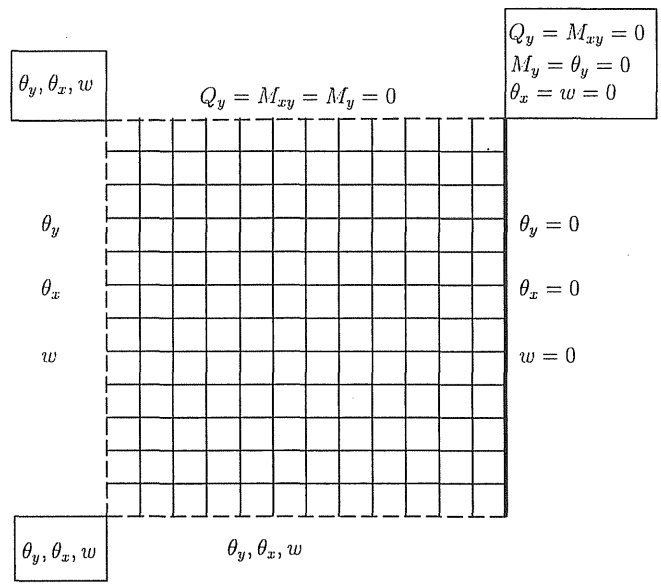

(a)

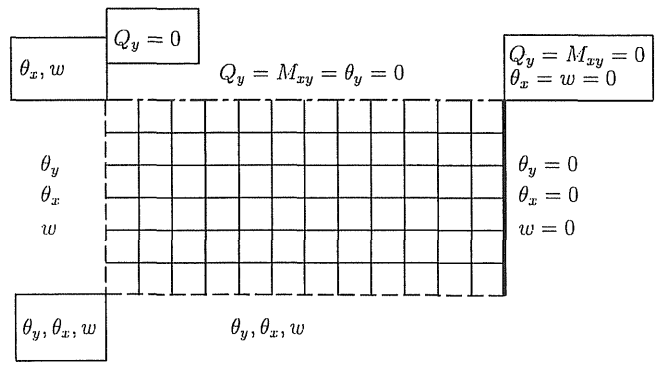

(b)

Figure 2.7: Integral constants and boundary conditions of a cantilever plate (FCFF)

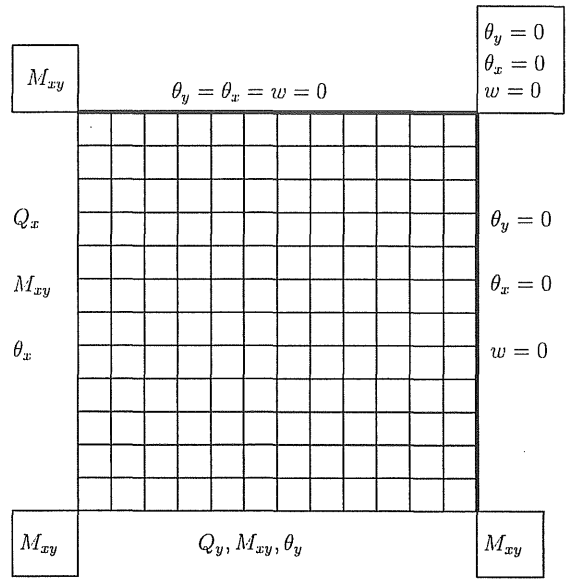

Figure 2.8: Integral constants and boundary conditions of a plate with simply supported edges and clamped edges (SCCS)

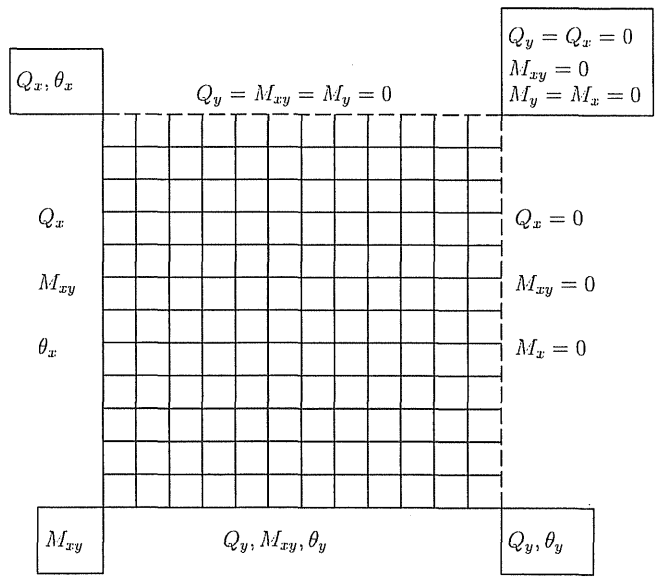

Figure 2.9: Integral constants and boundary conditions of a plate with simply supported edges and free edges (SFFS)

2.5.3 Integral constants and boundary conditions at the corners

There are eight integral constants at each corner. They are Q_y, Q_x, M_{xy}, M_y, M_x, θ_y, θ_x and w. Some of them can be determined to be zero by using the boundary conditions at the corner. For example, in Figure 2.4(a), the rectangular plate is simply supported. The boundary conditions along the the side $x = 0$ and the side $y = 0$ are

$$M_x = 0, \quad \theta_y = 0, \quad w = 0 \qquad \text{for } x = 0$$

$$M_y = 0, \quad \theta_x = 0, \quad w = 0 \qquad \text{for } y = 0$$

so the boundary conditions at the corner $(0, 0)$ are $M_y = M_x = \theta_y = \theta_x = w = 0$. In order to satisfy these conditions, the five integral constants M_y, M_x, θ_y, θ_x and w at the corner $(0, 0)$ must be zero.

Observing that

$$\frac{\partial w}{\partial x} = 0 \qquad \text{when } w = 0 \text{ on the side } y = 0$$

and using equation (2.1g), the following equation can be obtained:

$$\frac{\partial w}{\partial x} = \frac{Q_x}{Gt_s} - \theta_x = 0$$

from which

$$\frac{Q_x}{Gt_s} = \theta_x$$

Considering $\theta_x = 0$ on the side $y = 0$, then

$$Q_x = 0$$

Observing that

$$\frac{\partial w}{\partial y} = 0 \qquad \text{when } w = 0 \text{ on the side } x = 0$$

and using equation (2.1h), $Q_y = 0$ can be also obtained. Therefore, at last, there is only one integral constant M_{xy} at the corner $(0, 0)$.

In the similar manner, the boundary conditions at the corner (a, b) can be obtained. The boundary conditions along the side $x = a$ and the side $y = b$ are

$$M_x = 0, \quad \theta_y = 0, \quad w = 0 \qquad \text{for} \quad x = a$$

$$M_y = 0, \quad \theta_x = 0, \quad w = 0 \qquad \text{for} \quad y = b$$

Hence, the boundary conditions at the corner (a, b) are $M_y = M_x = \theta_y = \theta_x = w = 0$. But not all of these boundary conditions are independent.

By using equation (2.1d) and equation (2.1e), the following equations can be obtained.

$$\frac{\partial \theta_x}{\partial x} = \frac{1}{(1-\nu^2)D}(M_x - \nu M_y)$$
$$\frac{\partial \theta_y}{\partial y} = \frac{1}{(1-\nu^2)D}(M_y - \nu M_x)$$

Observing that

$$\frac{\partial \theta_x}{\partial x} = 0 \qquad \text{when } \theta_x = 0 \text{ on the side } y = b$$

$$\frac{\partial \theta_y}{\partial y} = 0 \qquad \text{when } \theta_y = 0 \text{ on the side } x = a$$

from which

$$M_x = M_y = 0$$

Thus, there are only three independent boundary conditions at the corner (a, b), namely, $\theta_y = 0$, $\theta_x = 0$, $w = 0$.

2.6 Equivalent rectangular plate of an irregular-shaped plate

Irregular-shaped plates such as plate with opening, circular plate, semi-circular plate, triangular plate, skew plate, rhombic plate, trapezoidal plate or the other polygonal plate are usually more complicated than uniform rectangular plates, but they can be considered as a kind of rectangular plate by translating them into the equivalent rectangular plate with non-uniform thickness. An opening in the plate can be considered as an extremely thin part of the equivalent rectangular plate. Furthermore, a non-rectangular plate can be translated into the equivalent rectangular plate whose additional parts are extremely thin or thick according to the boundary condition of the original plate.

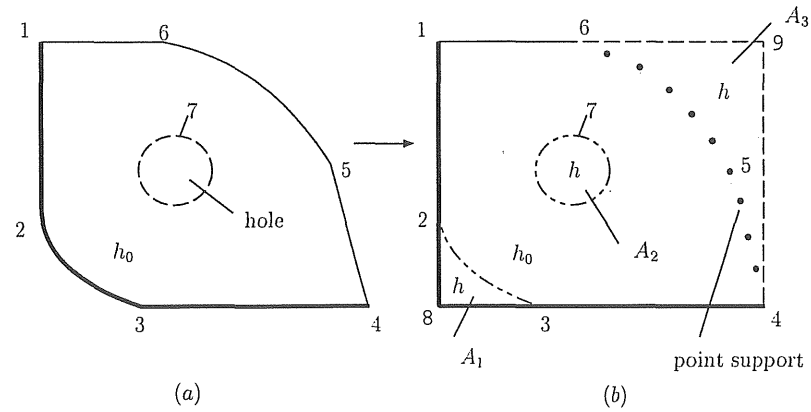

Figure 2.10: An irregular-shaped plate and its equivalent rectangular plate. (a) irregular-shaped plate; (b) equivalent rectangular plate.

A typical translation from an original irregular-shaped plate into its equivalent rectangular plate is shown in Figure 2.10. In Figure 2.10(a), the edge 1-2-3-4 is clamped, the edge 4-5-6-1 is simply supported, the edge 7, which is the periphery of the hole, is free. The thickness of the irregular-shaped plate is denoted by h_0. By adding three parts A_1, A_2, A_3, the irregular-shaped plate is translated into a rectangular plate as shown in Figure 2.10(b). The parts A_1, A_2, A_3 are enclosed by the edges 2-3-8-2, the edge 7 and the edges 4-5-6-9-4, respectively. The thickness of these additional parts is denoted by h. The thickness of the rectangular plate along the curved lines 2-3, 7 and 4-5-6 is taken as $(h_0 + h)/2$. The thickness of the part A_1 is chosen to be extremely thick ($h >> h_0$) and the edges 3-8-2 of the part A_1 are chosen to be clamped because the edge 2-3 of the irregular-shaped plate is clamped. In this case, there will be almost no deflection and slopes along the curved line 2-3 when the rectangular plate is subjected to the bending load. So the curved line 2-3 of the rectangular plate can be approximately considered as clamped. The thickness of the part A_2 is chosen to be extremely thin ($h << h_0$) because the edge 7 of the irregular-shaped plate is free. In this case, the part A_2 is similar to a hole and there are almost no forces along its edge 7 when the rectangular plate is subjected to the bending load. So the edge 7 of the

rectangular plate can be approximately considered as free. The part A_3 is chosen to be an extremely thin overhang ($h << h_0$) and there are many point supports along its edge 4-5-6 because the edge 4-5-6 of the original irregular-shaped plate is simply supported. The values of three reactions P_{1cd}, P_{2cd}, P_{3cd} at each point support of the rectangular plate are adjusted to satisfy the three restrained conditions, $M_n = 0$, $\theta_t = 0$, $w = 0$. The first condition $M_n = 0$ means that the bending moment M_n around the tangential axis of the curved line of point supports is zero. The second condition $\theta_t = 0$ means that the slope θ_t around the normal axis of the curved line of point supports is zero, and the third condition $w = 0$ means the deflection w is zero. So the curved line 4-5-6 can be considered as simply supported when the rectangular plate is subjected to the bending load. By the above translation of an original irregular-shaped plate, an equivalent rectangular plate is finally obtained. The boundary conditions of this equivalent rectangular plate are clamped along the edges 1-2-8 and 8-3-4, free along the edges 4-9 and 9-6, and simply supported along the edge 6-1. This equivalent plate has many point supports along the curved line 4-5-6 and the thickness of the plate is variable. After the equivalent rectangular plate is obtained, all analyses are carried out in the equivalent rectangular plate. A general method is obtained for analyzing the bending and free vibration problems of irregular-shaped plates.

In order to express the conditions $M_n = 0$, $\theta_t = 0$ by means of P_{1cd}, P_{2cd}, P_{3cd}, a relationship between the two coordinate axes, n-t axes and x-y axes, is needed.

In Figure 2.11, point A is any point at the curved line of point supports. The t and n axes are the coordinate axes in the direction of the tangent and the normal at point A, respectively. The angle between n axis and x axis is α. A is the point at (x_0, y_0) in x-y axes. A' is the point at (x, y) in x-y axes and at (u, v) in n-t axes. Then, the following relationship can be obtained as follows:

$$x = x_0 + u \sin\alpha + v \cos\alpha$$

$$y = y_0 + v \sin\alpha - u \cos\alpha$$

From which,

$$\frac{\partial x}{\partial u} = \sin\alpha \qquad \frac{\partial x}{\partial v} = \cos\alpha \qquad \frac{\partial y}{\partial u} = -\cos\alpha \qquad \frac{\partial y}{\partial v} = \sin\alpha$$

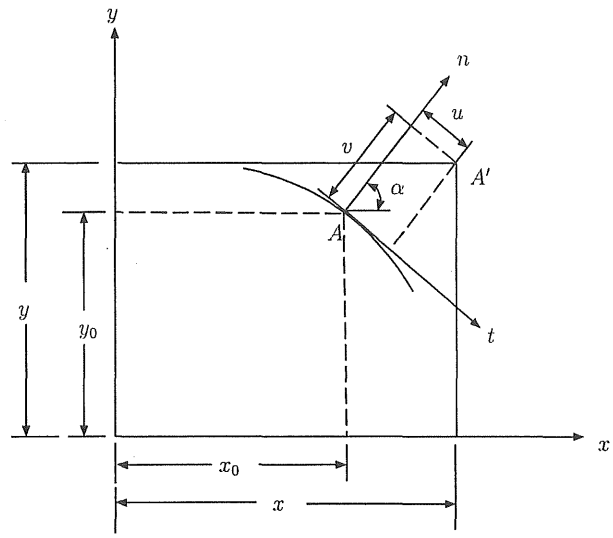

Figure 2.11: Transformation of coordinates

By using the above expressions, the slopes of n and t direction are derived as follows:

$$\begin{aligned}
\theta_n &= -\frac{\partial w}{\partial v} \\
&= -(\frac{\partial w}{\partial x}\frac{\partial x}{\partial v} + \frac{\partial w}{\partial y}\frac{\partial y}{\partial v}) \\
&= -(\frac{\partial w}{\partial x}\cos\alpha + \frac{\partial w}{\partial y}\sin\alpha) \\
&= \theta_x \cos\alpha + \theta_y \sin\alpha \qquad (2.12) \\
\theta_t &= -\frac{\partial w}{\partial u} \\
&= -(\frac{\partial w}{\partial x}\frac{\partial x}{\partial u} + \frac{\partial w}{\partial y}\frac{\partial y}{\partial u}) \\
&= -[\frac{\partial w}{\partial x}\sin\alpha + \frac{\partial w}{\partial y}(-\cos\alpha)] \\
&= \theta_x \sin\alpha - \theta_y \cos\alpha \qquad (2.13)
\end{aligned}$$

The element abc through the point A is shown in Figure 2.12. The normal stress σ_n and the shear stress τ_{nt} on the side ac can be obtained by projecting the forces acting on the element acb onto the n and t direction, respectively, which give following equations

$$\sigma_n ds - (\sigma_x dy)\cos\alpha - (\tau_{xy} dy)\sin\alpha - (\sigma_y dx)\sin\alpha - (\tau_{xy} dx)\cos\alpha = 0$$

$$\tau_{nt} ds - (\sigma_x dy)\sin\alpha + (\tau_{xy} dy)\cos\alpha + (\sigma_y dx)\cos\alpha - (\tau_{xy} dsx)\sin\alpha = 0$$

Observing that

$$dx = ds \sin\alpha \quad dy = ds \cos\alpha$$

after simplifying and rearranging, the values of σ_n and τ_{nt} are obtained

$$\sigma_n = \sigma_x \cos^2\alpha + \sigma_y \sin^2\alpha + 2\tau_{xy} \sin\alpha \cos\alpha \tag{2.14}$$

$$\tau_{nt} = (\sigma_x - \sigma_y) \sin\alpha \cos\alpha + \tau_{xy}(\sin^2\alpha - \cos^2\alpha) \tag{2.15}$$

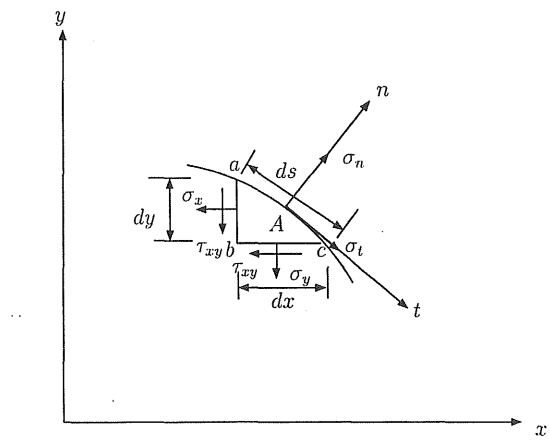

Figure 2.12: Stress element

The bending and twisting moments at point A are as follows:

$$M_n = \int_{-h/2}^{h/2} \sigma_n z dz \qquad M_{nt} = \int_{-h/2}^{h/2} \tau_{nt} z dz \tag{2.16}$$

Using the expressions of σ_n and τ_{nt}, the above equations are written as:

$$M_n = M_x \cos^2\alpha + M_y \sin^2\alpha + 2M_{xy} \sin\alpha \cos\alpha \tag{2.17}$$

$$M_{nt} = M_{xy}(\sin^2\alpha - \cos^2\alpha) + (M_y - M_x) \sin\alpha \cos\alpha \tag{2.18}$$

Therefore, the restrained conditions $M_n = 0$, $\theta_t = 0$, $w = 0$ can be presented as

$$M_n = M_x \cos^2\alpha + M_y \sin^2\alpha + 2M_{xy} \sin\alpha \cos\alpha = 0 \tag{2.19a}$$

$$\theta_t = \theta_x \sin\alpha - \theta_y \cos\alpha = 0 \tag{2.19b}$$

$$w = 0 \tag{2.19c}$$

or in non-dimensional expressions

$$X_M = X_5 \cos^2\alpha + X_4 \sin^2\alpha + 2X_3 \sin\alpha\cos\alpha = 0 \tag{2.20a}$$

$$X_\theta = X_7 \sin\alpha - X_6 \cos\alpha = 0 \tag{2.20b}$$

$$X_8 = 0 \tag{2.20c}$$

Here,

$$X_M = \frac{a^2}{D_0(1-\nu^2)} M_n, \quad X_\theta = \frac{a}{D_0(1-\nu^2)} \theta_t$$

By using the above three restrained conditions and the equation (2.11), three equations including three reactions P_{1cd}, P_{2cd}, P_{3cd} are obtained at each point support. With using the boundary conditions of the equivalent rectangular plate, the integral constants and the reactions can be determined.

2.7 Conclusions

The main work in this chapter is described as follows:

1. The fundamental differential equations are established for the rectangular plates with variable thickness and point supports. By converting the differential equations into integral equations and applying numerical integration, the discrete solutions based on the Mindlin plate theory are obtained.

2. The discrete solutions are only related to the quantities of the discrete points on the boundary. So it can make the calculation more easily and quickly.

3. The discrete solutions give the transverse shear forces, twisting moments, bending moments, rotations and deflections at all the discrete points. Thus, the method does not require prior assumption of the shape of the deflection mode of the plate and it can be considered as a semi-analytical method. With the increase of the numbers of dividing lines, the discrete solutions tend to analytical solutions theoretically.

4. Irregular-shaped plates are different from uniform rectangular plates, but they can be translated into the equivalent rectangular plate with various thickness. An

opening in an original irregular-shaped plate can be considered as an extremely thin part of the equivalent rectangular plate. Furthermore, a non-rectangular plate can be translated into the equivalent rectangular plate by adding some parts which are extremely thin or thick according to the boundary conditions of the original plate. After the equivalent rectangular plate is obtained, the problem of the irregular-shaped plate is translated into the problem of the equivalent rectangular plate. A general method is obtained for the bending and free vibration problems of irregular-shaped plates.

Chapter 3

Elastic Bending Analysis of Irregular-Shaped Plates

3.1 Introduction

In chapter 2, by translating an irregular-shaped plate into an equivalent plate and using the discrete method, the solutions for the bending problems of irregular-shaped plates are obtained. In this chapter, the convergency and accuracy of these solutions are investigated for circular, semi-circular, triangular, skew, rhombic and trapezoidal plates and rectangular plates with opening under uniform load q_0 or a concentrated load P.

3.2 Fundamental differential equations and the discrete solution

The fundamental differential equations of the equivalent rectangular plate with variable thickness and point supports are as follows (see chapter 2)

$$\frac{\partial Q_x}{\partial x}+\frac{\partial Q_y}{\partial y}+\overline{q}+\sum_{c=0}^{m}\sum_{d=0}^{n}\overline{P}_{1cd}\delta(x-x_c)\delta(y-y_d)=0 \tag{3.1a}$$

$$\frac{\partial M_{xy}}{\partial x}+\frac{\partial M_y}{\partial y}-Q_y+\sum_{c=0}^{m}\sum_{d=0}^{n}\overline{P}_{2cd}\delta(x-x_c)\delta(y-y_d)=0 \tag{3.1b}$$

$$\frac{\partial M_x}{\partial x}+\frac{\partial M_{xy}}{\partial y}-Q_x-\sum_{c=0}^{m}\sum_{d=0}^{n}\overline{P}_{3cd}\delta(x-x_c)\delta(y-y_d)=0 \tag{3.1c}$$

$$\frac{\partial \theta_x}{\partial x}+\nu\frac{\partial \theta_y}{\partial y}=\frac{M_x}{D} \tag{3.1d}$$

$$\frac{\partial \theta_y}{\partial y}+\nu\frac{\partial \theta_x}{\partial x}=\frac{M_y}{D} \tag{3.1e}$$

$$\frac{\partial \theta_x}{\partial y}+\frac{\partial \theta_y}{\partial x}=\frac{2}{(1-\nu)}\frac{M_{xy}}{D} \tag{3.1f}$$

$$\frac{\partial w}{\partial x}+\theta_x=\frac{Q_x}{Gt_s} \tag{3.1g}$$

$$\frac{\partial w}{\partial y}+\theta_y=\frac{Q_y}{Gt_s} \tag{3.1h}$$

where Q_x, Q_y are the shearing forces, M_{xy} is the twisting moment, M_x, M_y are the bending moments, $\overline{P}_{1cd}$ is the vertical reaction of the point support at (x_c, y_d), $\overline{P}_{2cd}$ and $\overline{P}_{3cd}$ are moment reactions around x- and y-axis, respectively, $\overline{q}=\overline{q}(x,y)$ is the distributed load, θ_x, θ_y are the slopes, w is the deflection, $D=Eh^3/12(1-\nu^2)$ is the flexural rigidity of the plate, E is the modulus of elasticity, G is the shear modulus

of elasticity, ν is Poisson's ratio, $h = h(x, y)$ is the thickness of the plate, $t_s = h/1.2$, $\delta(x - x_c)$ and $\delta(y - y_d)$ are the Dirac's delta functions.

By introducing the following non-dimensional expressions,

$$[\,X_1 \quad X_2\,] = \frac{a^2}{D_0(1-\nu^2)}[\,Q_y \quad Q_x\,], [\,X_6 \quad X_7 \quad X_8\,] = [\,\theta_y \quad \theta_x \quad w/a\,]$$

$$[\,X_3 \quad X_4 \quad X_5\,] = \frac{a}{D_0(1-\nu^2)}[\,M_{xy} \quad M_y \quad M_x\,], [\,\eta \quad \zeta\,] = [\,x/a \quad y/b\,]$$

the differential equations (3.1a) $\sim$ (3.1h) can be rewritten as follows.

$$\sum_{e=1}^{8}[F_{1te}\frac{\partial X_e}{\partial \zeta} + F_{2te}\frac{\partial X_e}{\partial \eta} + F_{3te}X_e] + \delta_{1t}q + \sum_{f=1}^{3}\sum_{c=0}^{m}\sum_{d=0}^{n} P_{fcd}\delta(\eta - \eta_c)\delta(\zeta - \zeta_d)\delta_{ft} = 0 \tag{3.2}$$

where F_{111}=F_{123}=F_{134}=F_{146}=F_{167}=F_{178}=F_{188}=1, F_{212}=F_{225}=F_{233}=F_{257}=F_{266}=μ, $F_{156} = \nu$, $F_{247} = \nu\mu$, $F_{322} = F_{331} = -\mu$, $F_{344} = F_{355} = -I$, $F_{363} = -J$, $F_{372} = -K$, $F_{377} = 1$, $F_{381} = -\mu K$, $F_{386} = \mu$, other $F_{1te} = 0$, $F_{2te} = 0$, $F_{3te} = 0$, $t = 1 \sim 8$, $\mu = b/a$, a and b are the length of the sides of the rectangular plate, δ_{ft} is Kronecker's delta, $I = \mu(1-\nu^2)[h_0/h(x,y)]^3$, $J = 2\mu(1+\nu)[h_0/h(x,y)]^3$, $K = Eh_0^3/(10Ga^2h)$, $[\,P_{1cd} \quad P_{2cd} \quad P_{3cd}\,] = \mu a^2\,[\,\overline{P}_{1cd}a \quad \overline{P}_{2cd} \quad -\overline{P}_{3cd}\,]/D_0(1-\nu^2)$, $D_0 = Eh_0^3/12(1-\nu^2)$ is the standard flexural rigidity of the plate, h_0 is standard thickness of the plate.

By integrating the above equation and applying the numerical integration in the same manner used in chapter 2, the discrete solution of the equivalent rectangular plate can be obtained from the equation (3.2) as follows:

$$X_{pij} = \sum_{d=1}^{6}\left(\sum_{k=0}^{i} a_{1pijkd}X_{rk0} + \sum_{l=0}^{j} a_{2pijld}X_{s0l}\right) + \overline{q}_{pij} + \sum_{f=1}^{3}\sum_{c=0}^{m}\sum_{d=0}^{n}\overline{q}_{fpijcd}P_{fcd} \tag{3.3}$$

The equation (3.2) and equation (3.3) are the simple forms of equations (2.2a) $\sim$ (2.2h) and (2.11), respectively.

By using the boundary conditions and the restrained conditions at the point supports, the quantities at any point of the equivalent rectangular plate can be obtained from equation (3.3).

For example, when an equivalent plate is a rectangular plate with SFFS, as shown in Figure 2.9, the boundary conditions of this plate are $Q_x = M_{xy} = M_x = 0$ along the edge $x = a$ and $Q_y = M_{xy} = M_y = 0$ along the edge $y = b$, and the integral constants are Q_x, M_{xy}, θ_x along the edge $x = 0$ and Q_y, M_{xy}, θ_y along the edge $y = 0$. Expressing these boundary conditions and integral constants in non-dimensional form and using the restrained conditions expressed in equation (2.20a) $\sim$ (2.20c), the following equation can be obtained from equation (3.3):

$$
\begin{bmatrix} X_{2mj} \\ X_{3mj} \\ X_{5mj} \\ X_{1in} \\ X_{3in} \\ X_{4in} \\ X_{Mc'd'} \\ X_{\theta c'd'} \\ X_{8c'd'} \end{bmatrix} =
\begin{bmatrix}
a_{12mjk1} & a_{12mjk2} & a_{12mjk4} & a_{22mjl1} & a_{22mjl2} & a_{22mjl5} \\
a_{13mjk1} & a_{13mjk2} & a_{13mjk4} & a_{23mjl1} & a_{23mjl2} & a_{23mjl5} \\
a_{15mjk1} & a_{15mjk2} & a_{15mjk4} & a_{25mjl1} & a_{25mjl2} & a_{25mjl5} \\
a_{11ink1} & a_{11ink2} & a_{11ink4} & a_{21inl1} & a_{21inl2} & a_{21inl5} \\
a_{13ink1} & a_{13ink2} & a_{13ink4} & a_{23inl1} & a_{23inl2} & a_{23inl5} \\
a_{14ink1} & a_{14ink2} & a_{14ink4} & a_{24inl1} & a_{24inl2} & a_{24inl5} \\
a'_{11c'd'k1} & a'_{11c'd'k2} & a'_{11c'd'k4} & a'_{12c'd'l1} & a'_{12c'd'l2} & a'_{12c'd'l5} \\
a'_{21c'd'k1} & a'_{21c'd'k2} & a'_{21c'd'k4} & a'_{22c'd'l1} & a'_{22c'd'l2} & a'_{22c'd'l5} \\
a_{18c'd'k1} & a_{18c'd'k2} & a_{18c'd'k4} & a_{28c'd'l1} & a_{28c'd'l2} & a_{28c'd'l5}
\end{bmatrix}
\begin{bmatrix}
\overline{q}_{12mjcd} & \overline{q}_{22mjcd} & \overline{q}_{32mjcd} \\
\overline{q}_{13mjcd} & \overline{q}_{23mjcd} & \overline{q}_{33mjcd} \\
\overline{q}_{15mjcd} & \overline{q}_{25mjcd} & \overline{q}_{35mjcd} \\
\overline{q}_{11incd} & \overline{q}_{21incd} & \overline{q}_{31incd} \\
\overline{q}_{13incd} & \overline{q}_{23incd} & \overline{q}_{33incd} \\
\overline{q}_{14incd} & \overline{q}_{24incd} & \overline{q}_{34incd} \\
q'_{11c'd'cd} & q'_{12c'd'cd} & q'_{13c'd'cd} \\
q'_{21c'd'cd} & q'_{22c'd'cd} & q'_{23c'd'cd} \\
\overline{q}_{18c'd'cd} & \overline{q}_{28c'd'cd} & \overline{q}_{38c'd'cd}
\end{bmatrix}
\times
\begin{bmatrix} X_{1k0} \\ X_{3k0} \\ X_{6k0} \\ X_{20l} \\ X_{30l} \\ X_{70l} \\ P_{1cd} \\ P_{2cd} \\ P_{3cd} \end{bmatrix}
+
\begin{bmatrix} \overline{q}_{2mj} \\ \overline{q}_{3mj} \\ \overline{q}_{5mj} \\ \overline{q}_{1in} \\ \overline{q}_{3in} \\ \overline{q}_{4in} \\ q'_{1c'd'} \\ q'_{2c'd'} \\ \overline{q}_{8c'd'} \end{bmatrix}
=
\begin{bmatrix} 0 \\ 0 \\ 0 \\ 0 \\ 0 \\ 0 \\ 0 \\ 0 \\ 0 \end{bmatrix}
\tag{3.4}
$$

where $X_{Mc'd'}, X_{\theta c'd'}$ and $X_{8c'd'}$ are the quantities of the point support at $(\eta_{c'}, \zeta_{d'})$,

$$a'_{11c'd'k1} = a_{15c'd'k1}\cos^2\alpha + a_{14c'd'k1}\sin^2\alpha + a_{13c'd'k1}\sin(2\alpha)$$

$$a'_{11c'd'k2} = a_{15c'd'k2}\cos^2\alpha + a_{14c'd'k2}\sin^2\alpha + a_{13c'd'k2}\sin(2\alpha)$$

$$a'_{11c'd'k4} = a_{15c'd'k4}\cos^2\alpha + a_{14c'd'k4}\sin^2\alpha + a_{13c'd'k4}\sin(2\alpha)$$

$$a'_{12c'd'l1} = a_{25c'd'l1}\cos^2\alpha + a_{24c'd'l1}\sin^2\alpha + a_{23c'd'l1}\sin(2\alpha)$$

$$a'_{12c'd'l2} = a_{25c'd'l2}\cos^2\alpha + a_{24c'd'l2}\sin^2\alpha + a_{23c'd'l2}\sin(2\alpha)$$

$$a'_{12c'd'l5} = a_{25c'd'l5}\cos^2\alpha + a_{24c'd'l5}\sin^2\alpha + a_{23c'd'l5}\sin(2\alpha)$$

$$q'_{11c'd'cd} = \overline{q}_{15c'd'cd}\cos^2\alpha + \overline{q}_{14c'd'cd}\sin^2\alpha + \overline{q}_{13c'd'cd}\sin(2\alpha)$$

$$q'_{12c'd'cd} = \overline{q}_{25c'd'cd}\cos^2\alpha + \overline{q}_{24c'd'cd}\sin^2\alpha + \overline{q}_{23c'd'cd}\sin(2\alpha)$$

$$q'_{13c'd'cd} = \overline{q}_{35c'd'cd}\cos^2\alpha + \overline{q}_{34c'd'cd}\sin^2\alpha + \overline{q}_{33c'd'cd}\sin(2\alpha)$$

$$a'_{21c'd'k1} = a_{17c'd'k1}\sin\alpha - a_{16c'd'k1}\cos\alpha \qquad a'_{21c'd'k2} = a_{17c'd'k2}\sin\alpha - a_{16c'd'k2}\cos\alpha$$

$$a'_{21c'd'k4} = a_{17c'd'k4}\sin\alpha - a_{16c'd'k4}\cos\alpha \qquad a'_{22c'd'l1} = a_{27c'd'l1}\sin\alpha - a_{26c'd'l1}\cos\alpha$$

$$a'_{22c'd'l2} = a_{27c'd'l2}\sin\alpha - a_{26c'd'l2}\cos\alpha \qquad a'_{22c'd'l5} = a_{27c'd'l5}\sin\alpha - a_{26c'd'l5}\cos\alpha$$

$$q'_{21c'd'cd} = \overline{q}_{17c'd'cd}\sin\alpha - \overline{q}_{16c'd'cd}\cos\alpha \qquad q'_{22c'd'cd} = \overline{q}_{27c'd'cd}\sin\alpha - \overline{q}_{26c'd'cd}\cos\alpha$$

$$q'_{23c'd'cd} = \overline{q}_{37c'd'cd}\sin\alpha - \overline{q}_{36c'd'cd}\cos\alpha \qquad q'_{2c'd'} = \overline{q}_{7c'd'}\sin\alpha - \overline{q}_{6c'd'}\cos\alpha$$

$$q'_{1c'd'} = \overline{q}_{5c'd'}\cos^2\alpha + \overline{q}_{4c'd'}\sin^2\alpha + \overline{q}_{3c'd'}\sin(2\alpha)$$

From equation (3.4), the integral constants and three reactions can be determined. By substituting these determined values into equation (3.3), the shearing forces, the twisting moment, the bending moments, the slopes and the deflection at every discrete point can be all obtained.

3.3 Numerical work

3.3.1 Circular plate, semi-circular plate and elliptic plate

Numerical solutions for deflections of a clamped circular plate, a semi-circular plate and an elliptic plate shown in Figure 3.1 are given in Table 3.1 for two cases of uniform load and concentrated load. The deflection of the point C is noted w_c. For the case of concentrated load, the load acts at this point. The numerical solutions are obtained by using Richardson's extrapolation formula for the two cases of divisional numbers $m(=n)$ of 8 and 12 for the one fourth part or a half part of each equivalent rectangular plate. Table 3.1 involves the theoretical values by Timoshenko and Krieger [37] or Saito *et al.* [38], and it shows the good convergency and adequate accuracy of the numerical solutions by the present method.

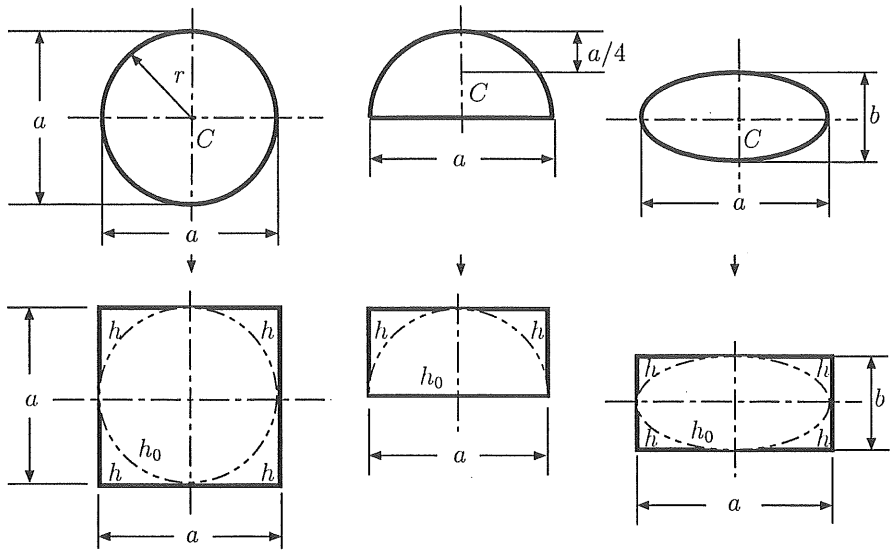

Figure 3.1: Clamped circular plate, semi-circular plate and elliptic plate

Table 3.1: Clamped circular, semi-circular and elliptic plates ($\nu = 0.3$)

	Circular plate $w_c D_0/q_0 a^4 \times 10^4$				Semi-circular plate $w_c D_0/q_0 a^4 \times 10^4$				Elliptic plate ($b/a = 0.5$) $w_c D_0/q_0 a^4 \times 10^4$			
	m		Nu.	Ref.	m		Nu.	Ref.	m		Nu.	Ref.
h/h_0	8	12	Solu.	[37]	8	12	Solu.	[37]	8	12	Solu.	[37]
4	7.96	8.73	9.35		1.06	1.16	1.24		1.16	1.24	1.30	
6	7.54	8.58	9.42		1.05	1.15	1.23		1.15	1.23	1.29	
8	7.32	8.54	9.52		1.04	1.14	1.22		1.15	1.23	1.29	
10	7.20	8.52	9.59	9.77	1.04	1.14	1.22	1.26 [1]	1.14	1.23	1.29	1.32
12	7.12	8.52	9.63		1.04	1.14	1.22		1.14	1.22	1.29	
20	6.98	8.51	9.73		1.04	1.14	1.22		1.14	1.23	1.29	
	Circular plate $w_c D_0/Pa^2 \times 10^3$				Semi-circular plate $w_c D_0/Pa^2 \times 10^4$				Elliptic plate ($b/a = 0.5$) $w_c D_0/Pa^2 \times 10^3$			
	m		Nu.	Ref.	m		Nu.	Ref.	m		Nu.	Ref.
h/h_0	8	12	Solu.	[37]	8	12	Solu.	[37]	8	12	Solu.	[38]
4	4.15	4.52	4.82		6.44	7.43	8.23		1.45	1.59	1.70	
6	4.04	4.49	4.84		6.40	7.41	8.21		1.45	1.59	1.70	
8	3.98	4.47	4.87		6.39	7.40	8.21		1.44	1.58	1.70	
10	3.95	4.47	4.89	4.97	6.38	7.39	8.20	–	1.44	1.58	1.70	1.71
12	3.93	4.47	4.90		6.38	7.39	8.20		1.44	1.58	1.70	
20	3.89	4.47	4.93		6.37	7.39	8.20		1.44	1.58	1.70	

1.26[1]: deflection at neighboring point, which is maximum deflection of the plate.

3.3.2 Isosceles right triangular plates

Numerical solutions for deflections of the right triangular plates with three types of boundary conditions shown in Figure 3.2 are given in Table 3.2. The numerical solutions are obtained by using the two cases of divisional numbers m $(=n)$ of 8 and 12 for the whole part of the equivalent plate. Table 3.2 involves the theoretical values by Fletcher [3], and it also shows the good convergency and adequate accuracy of the numerical solutions by the present method.

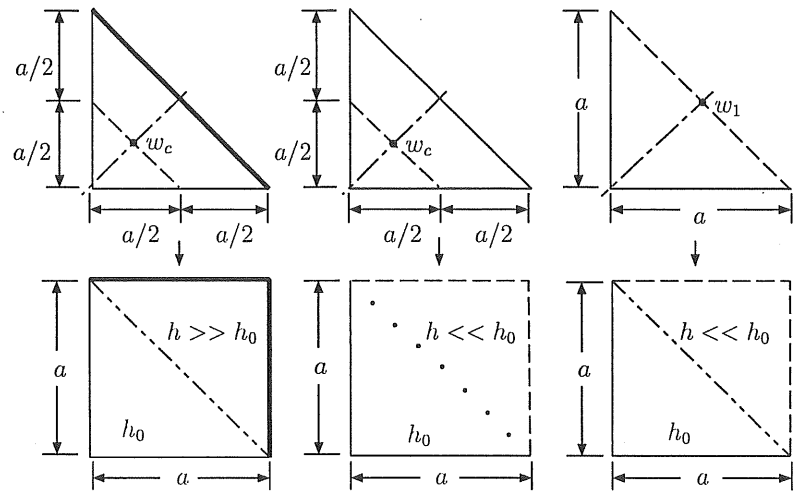

Figure 3.2: Isosceles right triangular plates

Table 3.2: Isosceles right triangular plates with clamped, simply supported or free diagonal edge and the other simply supported two edges ($\nu = 0.3$)

	Clamped diagonal $w_cD_0/q_0a^4 \times 10^4$					Simply supported diagonal $w_cD_0/q_0a^4 \times 10^4$				Free diagonal $w_1D_0/q_0a^4 \times 10^2$		
	m		Nu.	Ref.		m		Nu.	Ref.	m		Nu.
h/h_0	8	12	Solu.	[3]	h/h_0	8	12	Solu.	[3]	8	12	Solu.
4	3.74	3.97	4.16		1/4	4.78	5.42	5.93		2.61	2.04	1.95
6	3.18	3.54	3.82		1/6	4.80	5.42	5.92		2.20	2.07	1.97
8	3.02	3.41	3.72	3.69	1/8	4.81	5.42	5.91	6.07	2.23	2.08	1.97
10	2.95	3.35	3.66		1/10	4.81	5.42	5.91		2.25	2.09	1.96
12	2.91	3.31	3.62		1/12	4.81	5.42	5.91		2.27	2.09	1.95

3.3.3 Square plate with square opening

Numerical solutions for deflections and bending moments of rectangular plates with square opening at the center and two types of boundary conditions shown in Figure 3.3 are given in Tables 3.3 and 3.4. The numerical solutions are obtained by using the two cases of divisional numbers $m(=n)$ of 8 and 12 for the one fourth part of the equivalent plate. Tables 3.3 and 3.4 involve the theoretical values by Iwahara [39], and they show the good convergency and adequate accuracy of the numerical solutions for deflections and bending moments by the present method.

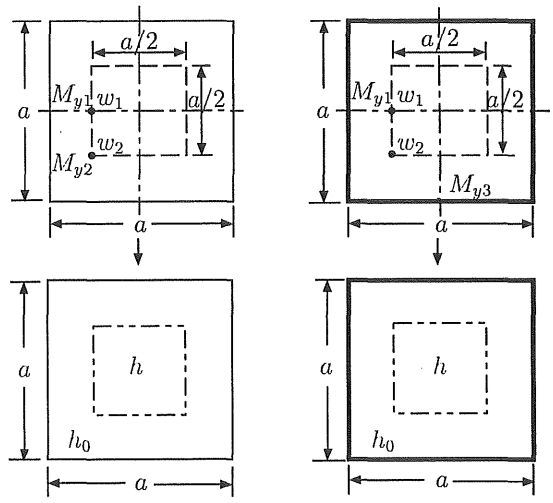

Figure 3.3: Square plate with square opening

Table 3.3: Simply supported square plate with square opening ($\nu = 0.3$)

	$w_1 D_0/q_0 a^4 \times 10^3$			$w_2 D_0/q_0 a^4 \times 10^3$			$M_{y1}/q_0 a^2 \times 10^2$			$M_{y2}/q_0 a^2 \times 10^2$		
	Nu.	[39]		Nu.	[39]		Nu.	[39]		Nu.	[39]	
h/h_0	Solu.	Map.[2]	FEM	Solu.	Map.	FEM	Solu.	Map.	FEM	Solu.	Map.	FEM
1/4	3.21			2.29			2.22			2.75		
1/6	3.27			2.33			2.23			2.81		
1/8	3.29	3.14	3.23	2.34	2.28	2.34	2.24	2.23	2.22	2.82	–	–
1/10	3.29			2.34			2.24			2.83		
1/12	3.29			2.34			2.24			2.83		

Map[2]: Mapping function method.

Table 3.4: Clamped square plate with square opening ($\nu = 0.3$)

	$w_1 D_0/q_0 a^4 \times 10^4$			$w_2 D_0/q_0 a^4 \times 10^4$			$M_{y1}/q_0 a^2 \times 10^3$			$-M_{y3}/q_0 a^2 \times 10^2$		
	Nu.	[39]		Nu.	[39]		Nu.	[39]		Nu.	[39]	
h/h_0	Solu.	Map.[3]	FEM	Solu.	Map.	FEM	Solu.	Map.	FEM	Solu.	Map.	FEM
1/4	3.68			2.55			3.01			2.73		
1/6	3.70			2.56			3.00			2.74		
1/8	3.70	3.56	3.80	2.56	2.50	2.67	3.00	3.60	2.7	2.74	2.76	2.75
1/10	3.70			2.56			3.00			2.74		
1/12	3.70			2.56			3.00			2.74		

Map[3]: Mapping function method.

3.3.4 Skew plate

Numerical solutions for deflections of skew plates with two simply and freely supported opposite sides shown in Figure 3.4 are given in Table 3.5. The numerical solutions for

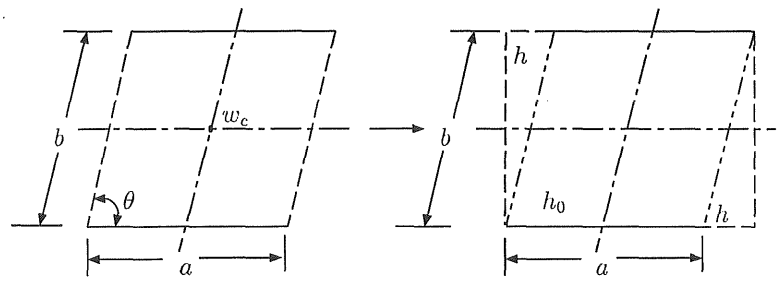

Figure 3.4: Simple-free skew plate

Table 3.5: Simple-free skew plates ($\nu = 0.3$)

	$\theta = 75^o$ $w_c D_0/q_0 a^4 \times 10^3$				$\theta = 60^o$ $w_c D_0/q_0 a^4 \times 10^3$				$\theta = 45^o$ $w_c D_0/q_0 a^4 \times 10^3$			
	m		Nu.	Ref.	m		Nu.	Ref.	m		Nu.	Ref.
h/h_0	12	14	Solu.	[37]	12	14	Solu.	[37]	12	14	Solu.	[37]
4	6.96	7.08	7.42		6.56	6.61	6.77		3.53	3.49	3.38	
6	7.18	7.40	8.00		6.93	7.02	7.27		3.73	3.69	3.56	
8	7.27	7.51	8.18	–	7.08	7.23	7.66	7.91	3.76	3.75	3.73	3.93
10	7.30	7.56	8.29		7.14	7.25	7.57		3.80	3.78	3.73	
12	7.32	7.58	8.32		7.17	7.29	7.65		3.82	3.80	3.74	

three cases of aspect angles are obtained by using the two cases of divisional numbers $m(=n)$ of 12 and 14 for the whole part of the equivalent plate. When $\theta = 75^o$, $\theta = 60^o$ and $\theta = 45^o$, b/a is 1, 1.663 and 1.414, respectively. Table 3.5 involves the theoretical values by Timoshenko and Krieger [37], and it shows the good convergency and adequate accuracy of the numerical solutions by the present method.

3.3.5 Rhombic plate

Numerical solutions for deflections of clamped rhombic plates shown in Figure 3.5 are given in Table 3.6 for three cases of aspect angles. The numerical solutions are obtained by using the two cases of divisional numbers $m(=n)$ of 8 and 12 for the one fourth part of the equivalent plate. Table 3.6 involves the theoretical values by Ota *et al.* [40], and it also shows the good convergency and adequate accuracy of the numerical solutions by the present method.

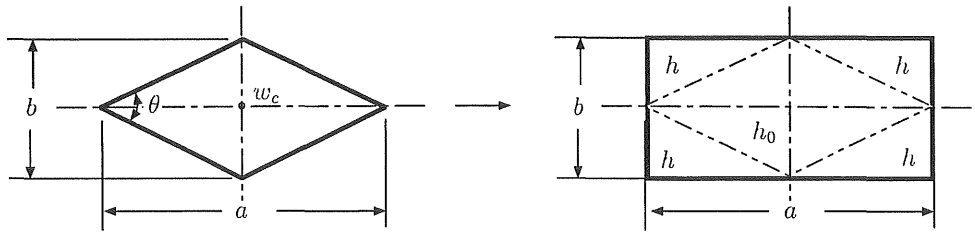

Figure 3.5: Clamped rhombic plate

Table 3.6: Clamped rhombic plates ($\nu = 0.3$)

	$\theta = 45^o$				$\theta = 60^o$				$\theta = 75^o$			
	$w_cD_0/q_0a^4 \times 10^5$				$w_cD_0/q_0a^4 \times 10^5$				$w_cD_0/q_0a^4 \times 10^4$			
	m		Nu.	Ref.	m		Nu.	Ref.	m		Nu.	Ref.
h/h_0	8	12	Solu.	[40]	8	12	Solu.	[40]	8	12	Solu.	[40]
4	3.05	3.25	3.40		8.21	8.69	9.08		1.74	1.83	1.91	
6	2.89	3.12	3.30		7.62	8.18	8.64		1.58	1.70	1.79	
8	2.83	3.07	3.26	3.24	7.41	8.02	8.50	8.54	1.53	1.65	1.75	1.77
10	2.80	3.05	3.25		7.31	7.94	8.45		1.51	1.63	1.74	
12	2.78	3.04	3.25		7.25	7.90	8.42		1.49	1.62	1.73	

3.3.6 Trapezoidal plate and regular triangular plate

Numerical solutions for deflections of clamped trapezoidal plates shown in Figure 3.6 are given in Table 3.7 with a clamped regular triangular plate and a clamped rectan-

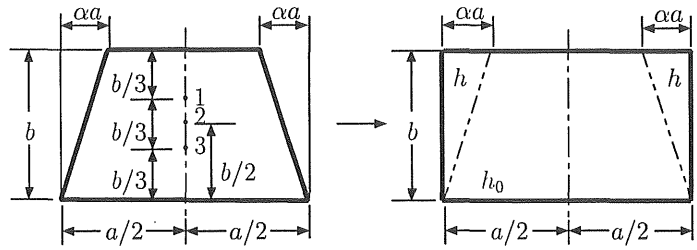

Figure 3.6: Clamped trapezoidal plate

Table 3.7: Clamped triangular, trapezoidal and rectangular plates ($\nu = 0.3$)

	$\alpha = 0.5$; regular triangular plate											
	$w_1 D_0/q_0 a^4 \times 10^4$				$w_2 D_0/q_0 a^4 \times 10^4$				$w_3 D_0/q_0 a^4 \times 10^4$			
	m		Nu.	Ref.	m		Nu.	Ref.	m		Nu.	Ref.
h/h_0	8	12	Solu.	[4]	8	12	Solu.	[4]	8	12	Solu.	[4]
4	0.428	0.508	0.571		1.15	1.33	1.47		1.62	1.77	1.90	
6	0.244	0.331	0.401		0.861	1.07	1.24		1.37	1.56	1.71	
8	0.189	0.279	0.352	–	0.766	0.991	1.17	–	1.28	1.49	1.66	1.67
10	0.166	0.258	0.332		0.726	0.957	1.14		1.25	1.46	1.64	
12	0.155	0.248	0.322		0.705	0.940	1.13		1.23	1.45	1.63	
	$\alpha = 0.25$; symmetric trapezoidal plate											
	$w_1 D_0/q_0 a^4 \times 10^4$				$w_2 D_0/q_0 a^4 \times 10^4$				$w_3 D_0/q_0 a^4 \times 10^4$			
	m		Nu.	Ref.	m		Nu.	Ref.	m		Nu.	Ref.
h/h_0	8	12	Solu.		8	12	Solu.		8	12	Solu.	
4	3.14	3.44	3.68		4.17	4.59	4.92		3.77	4.09	4.35	
6	2.88	3.24	3.52		3.84	4.36	4.77		3.52	3.93	4.27	
8	2.80	3.17	3.47	–	3.74	4.29	4.72	–	3.44	3.88	4.24	–
10	2.77	3.14	3.44		3.70	4.26	4.70		3.40	3.86	4.23	
12	2.76	3.13	3.43		3.67	4.24	4.69		3.38	3.85	4.23	
	$\alpha = 0$; rectangular plate											
	$w_1 D_0/q_0 a^4 \times 10^4$				$w_2 D_0/q_0 a^4 \times 10^4$				$w_3 D_0/q_0 a^4 \times 10^4$			
	m		Nu.	Ref.	m		Nu.	Ref.	m		Nu.	Ref.
	8	12	Solu.	[41]	8	12	Solu.	[41]	8	12	Solu.	[41]
	7.39	7.45	7.49	7.47	9.39	9.25	9.29	9.26	7.39	7.45	7.49	7.47

gular plate as two special cases of the trapezoidal plate. The numerical solutions are obtained by using the two cases of divisional numbers $m(=n)$ of 8 and 12 for the half part of the equivalent plate. Table 3.7 involves the theoretical values by Conway [4] or Sakiyama and Matsuda [41], and it shows the good convergency and adequate accuracy of the numerical solutions by the present method.

3.4 Conclusions

In this chapter, numerical results are obtained for the bending problem of various types of irregular-shaped plates by using the concept of the equivalent rectangular plate. The main conclusions of the work are summarized as follows:

1. The concept of the equivalent rectangular plate is proper. The irregular-shaped plates such as plate with opening, circular plate, semi-circular plate, elliptic plate, triangular plate, skew plate, rhombic plate, trapezoidal plate or the other polygonal plates can be finally considered as a kind of rectangular plate with non-uniform thickness.

2. By using the discrete method proposed in chapter 2, the numerical results are obtained. It is shown that the numerical solutions have the good convergency and adequate accuracy for various types of irregular-shaped plates even if the divisional numbers m, n are not large. With the increase of divisional numbers, the solutions can have more adequate accuracy.

3. Although the numerical results are shown mainly for the case of uniform load, they can be obtained similarly by the proposed method for the other cases of external loads such as concentrated loads or non-uniform loads.

Chapter 4

Free vibration analysis of irregular-shaped plates

4.1 Free vibration analysis of rectangular plates with variable thickness

4.1.1 Introduction

In previous chapters, a discrete method for analyzing elastic bending problems of irregular-shaped plates has been proposed and the accuracy of the numerical solutions has been investigated. In this section, the discrete method is extended to analyze the free vibration of rectangular plates with variable thickness by using the Green function. The discrete-form solution for deflection of the plate with a concentrated load gives the discrete-type Green function of the plate. The characteristic equation of free vibration of rectangular plate with variable thickness is obtained and expressed in matrix form. The convergency and accuracy of the numerical solutions for the natural frequency parameter obtained by the proposed method are investigated, and the lowest sixteen values of the frequency parameters and their modes of free vibration are shown for some rectangular plates.

4.1.2 Discrete Green function of a plate with variable thickness

The Green function of a plate bending problem is given by the displacement function of the plate with a unit concentrated load, so the Green function $G(x, y, x_q, y_r) = w(x, y, x_q, y_r)/\overline{P}$ of a plate with variable thickness can be obtained from the fundamental differential equations of the plate with a concentrated load $\overline{P}$ at a point (x_q, y_r) as shown in Figure 4.1, which are given by the following equations.

$$\frac{\partial Q_x}{\partial x} + \frac{\partial Q_y}{\partial y} + \overline{P}\delta(x - x_q)\delta(y - y_r) = 0 \tag{4.1a}$$

$$\frac{\partial M_{xy}}{\partial x} + \frac{\partial M_y}{\partial y} - Q_y = 0 \tag{4.1b}$$

$$\frac{\partial M_x}{\partial x} + \frac{\partial M_{xy}}{\partial y} - Q_x = 0 \tag{4.1c}$$

$$\frac{\partial \theta_x}{\partial x} + \nu\frac{\partial \theta_y}{\partial y} = \frac{M_x}{D} \tag{4.1d}$$

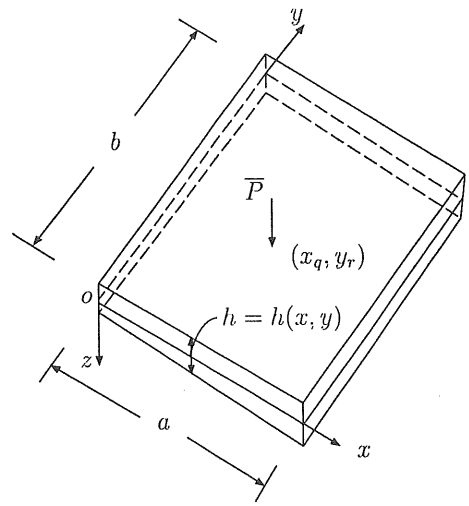

Figure 4.1: Rectangular plate with a concentrated load

$$\frac{\partial \theta_y}{\partial y} + \nu \frac{\partial \theta_x}{\partial x} = \frac{M_y}{D} \tag{4.1e}$$

$$\frac{\partial \theta_x}{\partial y} + \frac{\partial \theta_y}{\partial x} = \frac{2}{(1-\nu)} \frac{M_{xy}}{D} \tag{4.1f}$$

$$\frac{\partial w}{\partial x} + \theta_x = \frac{Q_x}{G t_s} \tag{4.1g}$$

$$\frac{\partial w}{\partial y} + \theta_y = \frac{Q_y}{G t_s} \tag{4.1h}$$

where Q_x, Q_y are the shearing forces, M_{xy} is the twisting moment, M_x, M_y are the bending moments, θ_x, θ_y are the slopes, w is the deflection, $D = Eh^3/12(1-\nu^2)$ is the flexural rigidity of the plate, E is the modulus of elasticity, G is the shear modulus of elasticity, ν is Poisson's ratio, $h = h(x, y)$ is the thickness of the plate, $t_s = h/1.2$, $\delta(x - x_q)$ and $\delta(x - x_r)$ are Dirac's delta functions.

By introducing the following non-dimensional expressions,

$$[\, X_1 \quad X_2 \,] = \frac{a^2}{D_0(1-\nu^2)} [\, Q_y \quad Q_x \,], [\, X_6 \quad X_7 \quad X_8 \,] = [\, \theta_y \quad \theta_x \quad w/a \,]$$

$$[\, X_3 \quad X_4 \quad X_5 \,] = \frac{a}{D_0(1-\nu^2)} [\, M_{xy} \quad M_y \quad M_x \,], [\, \eta \quad \zeta \,] = [\, x/a \quad y/b \,]$$

the differential equations (4.1a) $\sim$ (4.1h) can be rewritten as follows:

$$\sum_{e=1}^{8} [F_{1te} \frac{\partial X_e}{\partial \zeta} + F_{2te} \frac{\partial X_e}{\partial \eta} + F_{3te} X_e] + P\delta(\eta - \eta_q)\delta(\zeta - \zeta_r)\delta_{1t} = 0 \tag{4.2}$$

where F_{111}=F_{123}=F_{134}=F_{146}=F_{167}=F_{178}=F_{188}=1, F_{212}=F_{225}=F_{233}=F_{257}=F_{266}=μ, $F_{156}=\nu$, $F_{247}=\nu\mu$, $F_{322}=F_{331}=-\mu$, $F_{344}=F_{355}=-I$, $F_{363}=-J$, $F_{372}=-K$, $F_{377}=1$, $F_{381}=-\mu K$, $F_{386}=\mu$, other $F_{1te}=0$, $F_{2te}=0$, $F_{3te}=0$, $t=1\sim 8$, a and b are the length of the sides of the rectangular plate, $\mu=b/a$, $P=\overline{P}a/D_0(1-\nu^2)$, δ_{ft} is Kronecker's delta, $I=\mu(1-\nu^2)[h_0/h(x,y)]^3$, $J=2\mu(1+\nu)[h_0/h(x,y)]^3$, $K=Eh_0^3/(10Ga^2h)$, h_0 is standard thickness of the plate.

By integrating the above equation and applying the numerical integration in the same manner used in chapter 2, the following equation can be obtained:

$$\begin{aligned} X_{pij}=&\sum_{k=0}^{i}\Big\{a_{1pijk1}(Q_y)_{k0}+a_{1pijk2}(M_{xy})_{k0}+a_{1pijk3}(M_y)_{k0}\\ &+a_{1pijk4}(\theta_y)_{k0}+a_{1pijk5}(\theta_x)_{k0}+a_{1pijk6}(w)_{k0}\Big\}\\ &+\sum_{l=0}^{j}\Big\{a_{2pijl1}(Q_x)_{0l}+a_{2pijl2}(M_{xy})_{0l}+a_{2pijl3}(M_x)_{0l}\\ &+a_{2pijl4}(\theta_y)_{0l}+a_{2pijl5}(\theta_x)_{0l}+a_{2pijl6}(w)_{0l}\Big\}+\overline{q}_{pij}P \end{aligned} \tag{4.3}$$

where $(Q_y)=X_1$, $(Q_x)=X_2$, $(M_{xy})=X_3$, $(M_y)=X_4$, $(M_x)=X_5$, $(\theta_y)=X_6$, $(\theta_x)=X_7$, $(w)=X_8$, and

$$\begin{aligned} a_{1pijuv}=&\sum_{e=1}^{8}\Big\{\sum_{k=0}^{i}\beta_{ik}A_{pe}[a_{1ek0uv}-a_{1ekjuv}(1-\delta_{ki})]\\ &+\sum_{l=0}^{j}\beta_{jl}B_{pe}[a_{1e0luv}-a_{1eiluv}(1-\delta_{lj})]\\ &+\sum_{k=0}^{i}\sum_{l=0}^{j}\beta_{ik}\beta_{jl}C_{pekl}a_{1ekluv}(1-\delta_{ki}\delta_{lj})\Big\} \end{aligned}$$

$$\begin{aligned} a_{2pijuv}=&\sum_{e=1}^{8}\Big\{\sum_{k=0}^{i}\beta_{ik}A_{pe}[a_{2ek0uv}-a_{2ekjuv}(1-\delta_{ki})]\\ &+\sum_{l=0}^{j}\beta_{jl}B_{pe}[a_{2e0luv}-a_{2eiluv}(1-\delta_{lj})]\\ &+\sum_{k=0}^{i}\sum_{l=0}^{j}\beta_{ik}\beta_{jl}C_{pekl}a_{2ekluv}(1-\delta_{ki}\delta_{lj})\Big\} \end{aligned}$$

$$\overline{q}_{pij} = \sum_{e=1}^{8} \Big\{ \sum_{k=0}^{i} \beta_{ik} A_{pe} [\overline{q}_{ek0} - \overline{q}_{ekj}(1 - \delta_{ki})]$$
$$+ \sum_{l=0}^{j} \beta_{jl} B_{pe} [\overline{q}_{e0l} - \overline{q}_{eil}(1 - \delta_{lj})]$$
$$+ \sum_{k=0}^{i} \sum_{l=0}^{j} \beta_{ik} \beta_{jl} C_{pekl} \overline{q}_{ekl} (1 - \delta_{ki}\delta_{lj}) \Big\}$$
$$- \gamma_{p1} u_{iq} u_{jr}$$

where $u = 0, 1, \cdots, i\,(h = 1),\ 0, 1, \cdots, j(h = 2),\quad v = 1, 2, \cdot, 6.$

The equation (4.3) gives the discrete solution of the fundamental differential equation (4.2), and the discrete Green function $G(x_i, y_i, x_q, y_r)$ of the plate is obtained from X_{8ij}=$G(x_i, y_j, x_q, y_r)[\overline{P}/a]$, which is the displacement at point (x_i, y_j) of the plate with a concentrated load $\overline{P}$ at point (x_q, y_r).

4.1.3 Characteristic equation of free vibration of rectangular plate with variable thickness

During the free vibration, there is inertial force $-\rho h \partial^2 \hat{w}(x, y)/\partial t^2 dxdy$ at every point (x, y) of the rectangular plate, in which ρ is the mass density of the plate material and $\hat{w}(x, y)$ is the displacement at point (x, y). Supposing the displacement $\hat{w}(x, y)$ can be expressed in term of sin and cosin functions, that is, $\hat{w}(x, y) = A\sin(\omega t) + B\cos(\omega t)$, then, the inertial force $-\rho h \partial \hat{w}(x, y)/\partial t^2 dxdy$ can be written as $\rho h \omega^2 \hat{w}(x, y)dxdy$. Considering the inertial force $\rho h \omega^2 \hat{w}(x, y)dxdy$ as a concentrated load at point (x, y), it can be concluded that the free vibration problem of a rectangular plate will correspond to the bending problem of the rectangular plate with a concentrated load $\rho h \omega^2 \hat{w}(x, y)dxdy$ at any point (x, y). By applying the Green function $w(x_0, y_0, x, y)/\overline{P}$, which is the displacement at point (x_0, y_0) of a plate with a unit concentrated load at point (x, y), and using the method of superposition, the displacement at point (x_0, y_0) of the plate with a concentrated $\rho h \omega^2 \hat{w}(x, y)dxdy$ at every point (x, y) will be obtained as :

$$\hat{w}(x_0, y_0) = \int_0^b \int_0^a \rho h \omega^2 \hat{w}(x, y)[w(x_0, y_0, x, y)/\overline{P}]dxdy \tag{4.4}$$

The above equation (4.4) gives the displacement amplitude $\hat{w}(x_0, y_0)$ at a point (x_0, y_0) of the rectangular plate during the free vibration.

By using the non-dimensional expressions:

$$\lambda^4 = \frac{\rho_0 h_0 \omega^2 a^4}{D_0(1-\nu^2)}, \qquad H(\eta,\zeta) = \frac{\rho(x,y)}{\rho_0}\frac{h(x,y)}{h_0},$$
$$W(\eta,\zeta) = \frac{\hat{w}(x,y)}{a}, \qquad G(\eta_0,\zeta_0,\eta,\zeta) = \frac{w(x_0,y_0,x,y)}{a}\frac{D_0(1-\nu^2)}{\overline{P}a}$$

ρ_0 is standard mass density.

The integral equation (4.4) can be rewritten as follows:

$$W(\eta_0,\zeta_0) = \int_0^1\int_0^1 \mu\lambda^4 H(\eta,\zeta)G(\eta_0,\zeta_0,\eta,\zeta)W(\eta,\zeta)d\eta d\zeta \tag{4.5}$$

By applying the numerical integration method mentioned in chapter 2, equation (4.5) is discretely expressed as

$$\Lambda W_{kl} = \sum_{i=0}^{m}\sum_{j=0}^{n}\beta_{mi}\beta_{nj}H_{ij}G_{klij}W_{ij}, \quad \Lambda = 1/(\mu\lambda^4) \tag{4.6}$$

From equation (4.6) homogeneous linear equations in $(m+1)\times(n+1)$ unknowns W_{00},W_{01},$\cdots$,W_{0n}, W_{10},W_{11} $\cdots$,W_{1n},$\cdots$ W_{m0},W_{m1},$\cdots$,W_{mn} are obtained as follows:

$$\sum_{i=0}^{m}\sum_{j=0}^{n}(\beta_{mi}\beta_{nj}H_{ij}G_{klij} - \Lambda\delta_{ik}\delta_{jl})W_{ij} = 0, (k = 0,1,\cdots,m, l = 0,1,\cdots,n) \tag{4.7}$$

The characteristic equation of the free vibration of a rectangular plate with variable thickness is obtained from the equation (4.7):

$$\begin{vmatrix} K_{00} & K_{01} & K_{02} & \cdots & K_{0m} \\ K_{10} & K_{11} & K_{12} & \cdots & K_{1m} \\ K_{20} & K_{21} & K_{22} & \cdots & K_{2m} \\ \vdots & \vdots & \vdots & \ddots & \vdots \\ K_{m0} & K_{m1} & K_{m2} & \cdots & K_{mm} \end{vmatrix} = 0 \tag{4.8}$$

where

$$\mathbf{K_{ij}} = \beta_{mj}\begin{bmatrix} \beta_{n0}H_{j0}G_{i0j0} - \Lambda\delta_{ij} & \beta_{n1}H_{j1}G_{i0j1} & \cdots & \beta_{nn}H_{jn}G_{i0jn} \\ \beta_{n0}H_{j0}G_{i1j0} & \beta_{n1}H_{j1}G_{i1j1} - \Lambda\delta_{ij} & \cdots & \beta_{nn}H_{jn}G_{i1jn} \\ \vdots & \vdots & \ddots & \vdots \\ \beta_{n0}H_{j0}G_{inj0} & \beta_{n1}H_{j1}G_{inj1} & \cdots & \beta_{nn}H_{jn}G_{injn} - \Lambda\delta_{ij} \end{bmatrix}$$

4.1.4 Numerical work

The convergency and accuracy of numerical solutions have been investigated for the free vibration problems of some rectangular plates with uniform thickness or with variable thickness.

The convergent values of numerical solutions of frequency parameter for these plates have been obtained by using Richardson's extrapolation formula for two cases of combinations of divisional numbers m and n.

[1] Simply supported square plate and rectangular plate with uniform thickness

Numerical solutions for the lowest sixteen values of the natural frequency parameter λ of a simply supported square plate and a rectangular plate of aspect ratio b/a=2 are shown in Table 4.1. The thickness ratio h_0/a of these plates is 0.01. The convergent

Table 4.1: Natural frequency parameter λ for a simple rectangular plate; $\nu = 0.3$

	b/a=1				b/a=2			
	m		Nu.	Ref.	m		Nu.	Ref.
Mode	12	16	Solu.	[42]	12	16	Solu.	[42]
1	4.574	4.563	4.548	4.549	3.617	3.608	3.596	3.596
2	7.333	7.270	7.188	7.192	4.615	4.585	4.547	4.549
3	9.306	9.211	9.089	9.098	6.029	5.924	5.789	5.799
4	10.672	10.442	10.146	–	6.778	6.712	6.627	6.631
5	10.672	10.442	10.146	–	7.793	7.511	7.148	7.192
6	12.110	11.873	11.569	11.597	7.359	7.284	7.187	7.192
7	14.530	13.931	13.161	13.262	8.318	8.192	8.030	8.041
8	14.374	14.037	13.603	13.647	9.961	9.326	8.511	8.661
9	15.614	15.032	14.282	–	9.672	9.403	9.056	9.098
10	15.614	15.032	14.282	–	12.691	11.402	9.745	10.172
11	17.424	16.789	15.972	16.083	10.299	10.062	9.798	9.782
12	19.083	17.769	16.079	–	10.689	10.451	10.146	10.172
13	19.083	17.769	16.079	–	11.489	10.906	10.156	10.298
14	19.918	18.642	17.001	17.322	11.370	11.102	10.757	10.789
15	20.009	19.145	18.033	18.196	13.921	12.725	11.187	11.597
16	21.360	20.081	18.436	–	12.393	12.022	11.545	11.597

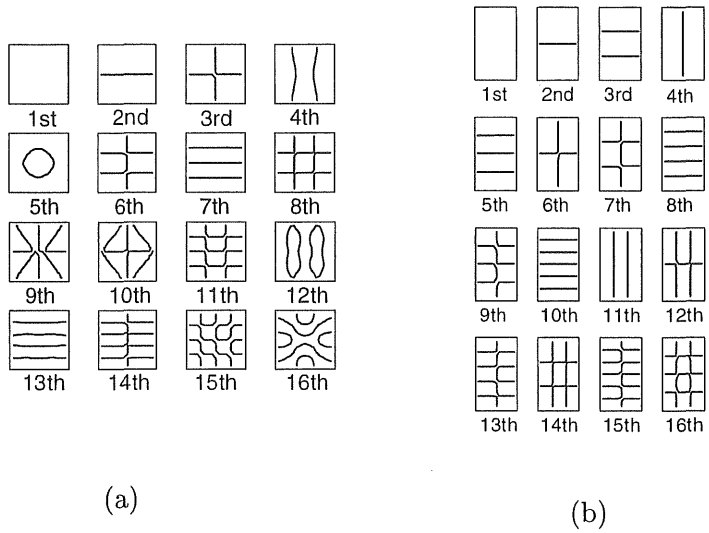

(a) (b)

Figure 4.2: Nodal patterns for a simply supported plate. (a) square plate; (b) rectangular plate ($b/a = 2$)

values of numerical solutions are obtained by using Richardson's extrapolation formula for the two cases of divisional numbers $m(= n)$ of 12 and 16 for the whole part of the rectangular plate. Table 4.1 includes the past theoretical values of Leissa [42], and it shows the good convergency and adequate accuracy of the numerical solutions obtained by the present method. The nodal lines of sixteen modes of free vibration of the two plates are shown in Figure 4.2

[2] Clamped square plate and rectangular plate with uniform thickness

Numerical solutions for the lowest sixteen values of the natural frequency parameter λ of a clamped square plate and a clamped rectangular plate of aspect ratio b/a=2 are shown in Table 4.2. The thickness ratio h_0/a of these plates is 0.01. The convergent values of numerical solutions are obtained by using Richardson's extrapolation formula for the two cases of divisional numbers $m(= n)$ of 12 and 16 for the whole part of the plate. Table 4.2 includes the other theoretical values by Claassen and Thorne [43] and Bolotin [44]. The numerical solutions obtained by the present method have the good convergency and adequate accuracy. The nodal lines of sixteen modes of free vibration of the two plates are shown in Figure 4.3.

Table 4.2: Natural frequency parameter λ for a clamped rectangular plate; $\nu = 0.3$

	b/a=1					b/a=2			
	m		Nu.	Ref.		m		Nu.	Ref.
Mode	12	16	Solu.	[43]	[44]	12	16	Solu.	[43]
1	6.205	6.175	6.138	6.142	6.066	5.133	5.107	5.073	5.076
2	9.030	8.911	8.756	8.771	8.742	5.883	5.834	5.771	5.776
3	10.985	10.829	10.629	10.651	10.614	7.175	7.024	6.829	6.851
4	12.533	12.162	11.686	11.745	11.747	8.970	8.573	8.064	8.148
5	12.563	12.191	11.714	11.772	–	8.475	8.344	8.176	8.190
6	13.910	13.552	13.091	13.152	13.127	8.923	8.789	8.617	8.632
7	16.690	15.803	14.663	14.856	14.849	11.305	10.430	9.305	9.564
8	16.194	15.717	15.105	–	15.163	9.743	9.558	9.320	9.343
9	17.655	16.817	15.741	15.933	15.934	11.023	10.667	10.209	10.279
10	17.697	16.856	15.744	–	–	14.372	12.611	10.347	–
11	19.421	18.551	17.432	–	17.606	18.600	15.193	10.813	11.044
12	21.676	19.825	17.446	–	–	12.892	12.134	11.160	–
13	21.684	19.833	17.454	–	–	12.196	11.808	11.309	–
14	22.409	20.633	18.351	–	–	12.505	11.123	11.632	–
15	22.063	20.929	19.471	–	19.712	15.565	13.992	11.970	–
16	23.707	21.982	19.765	–	–	13.074	12.672	12.155	–

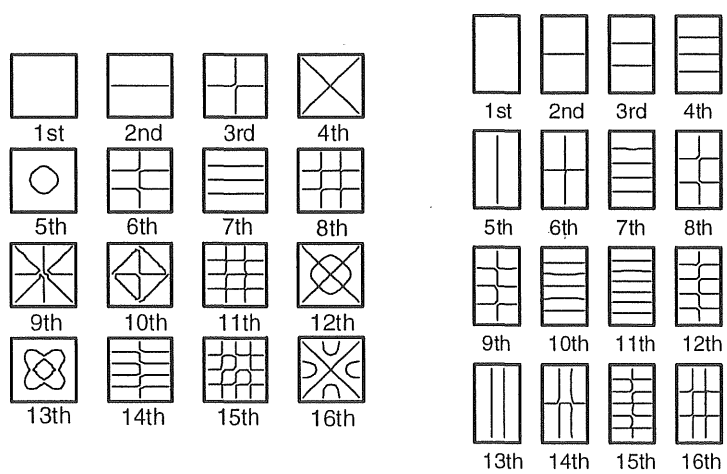

(a) (b)

Figure 4.3: Nodal patterns for a clamped plate. (a) square plate; (b) rectangular plate (b/a=2).

[3] Cantilever square plate and rectangular plate with uniform thickness

Numerical solutions for the lowest sixteen values of the natural frequency parameter λ of a cantilever square plate and a rectangular plate of aspect ratio b/a=2 are shown in Table 4.3. The thickness ratio h_0/a of these plates is 0.01. The convergent values are obtained for the two cases of divisional numbers $m(=n)$ of 12 and 16 for the whole part of the plate. Table 4.3 involves the other theoretical values by Claassen and Thorne [45] and Young [46]. The nodal lines of sixteen modes of free vibration of the two plates are shown in Figure 4.4.

Table 4.3: Natural frequency parameter λ for a cantilever rectangular plate; $\nu = 0.3$

	b/a=1					b/a=2			
	m		Nu.	Ref.		m		Nu.	Ref.
Mode	12	16	Solu.	[45]	[46]	12	16	Solu.	[45]
1	1.909	1.908	1.906	1.908	1.914	1.915	1.914	1.913	1.914
2	2.990	2.987	2.982	2.994	2.993	2.372	2.370	2.366	2.375
3	4.783	4.756	4.721	4.724	4.741	3.294	3.281	3.264	3.273
4	5.399	5.372	5.337	5.340	5.365	4.605	4.543	4.465	4.463
5	5.756	5.724	5.684	5.710	5.716	4.849	4.820	4.783	4.791
6	7.640	7.588	7.521	7.545	–	5.155	5.122	5.080	5.099
7	8.305	8.171	7.999	8.016	–	5.846	5.800	5.741	5.746
8	8.478	8.354	8.195	8.204	–	6.354	6.173	5.939	5.979
9	8.913	8.776	8.601	8.633	–	6.907	6.818	6.705	6.729
10	10.179	10.027	9.830	–	–	8.310	7.912	7.400	–
11	10.389	10.244	10.059	–	–	8.192	8.011	7.779	–
12	11.999	11.614	11.119	–	–	8.333	8.190	8.007	–
13	12.259	11.863	11.355	–	–	8.531	8.345	8.107	–
14	12.404	12.043	11.578	–	–	8.943	8.803	8.623	–
15	12.606	12.348	12.016	–	–	10.764	9.938	8.876	–
16	13.338	12.952	12.457	–	–	9.704	9.445	9.111	–

[4] Moderately thick square plate with uniform thickness

Numerical solutions for the lowest sixteen values of the natural frequency parameter λ of a simply supported square plate and a clamped square plate of thickness ratio h_0/a=0.2 are shown in Table 4.4. The convergent values are obtained for the two cases of divisional numbers $m(=n)$ of 12 and 16 for the whole part of the plate. Table 4.4 involves the other theoretical values by Liew *et al.* [47] The nodal lines are the same

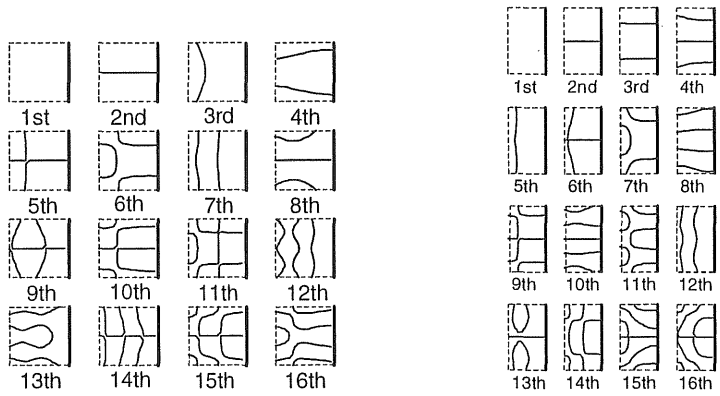

(a) (b)

Figure 4.4: Nodal patterns for a cantilever plate. (a) square plate; (b) rectangular plate (b/a=2).

as those in Figure 4.2 (a) or Figure 4.3 (a).

Table 4.4: Natural frequency parameter λ for a moderately thick square plate; $\nu = 0.3$

	Simple plate				Clamped plate			
	m		Nu.	Ref.	m		Nu.	Ref.
Mode	12	16	Solu.	[47]	12	16	Solu.	[47]
1	4.346	4.336	4.323	4.274	5.349	5.332	5.310	5.266
2	6.536	6.490	6.431	6.318	7.177	7.121	7.048	6.954
3	7.885	7.832	7.744	7.593	8.341	8.273	8.185	8.057
4	8.727	8.589	8.413	8.251	9.077	8.932	8.747	8.600
5	8.727	8.589	8.413	8.251	9.119	8.975	8.789	8.659
6	9.545	9.415	9.247	9.068	9.836	9.700	9.526	9.367
7	10.789	10.495	10.117	–	10.995	10.698	10.316	–
8	10.713	10.547	10.334	–	10.921	10.751	10.532	–
9	11.302	11.030	10.679	–	11.463	11.188	10.835	–
10	11.302	11.030	10.679	–	11.494	11.218	10.863	–
11	12.109	11.832	11.477	–	12.248	11.969	11.610	–
12	12.800	12.256	11.556	–	12.910	12.366	11.667	–
13	12.800	12.256	11.556	–	12.918	12.375	11.676	–
14	13.133	12.620	11.960	–	13.237	12.724	12.064	–
15	13.169	12.824	12.382	–	13.273	12.927	12.481	–
16	13.688	13.197	12.565	–	13.769	13.278	12.647	–

[5] Simply supported square plate and rectangular plate with variable thickness

A simply supported rectangular plate with linear thickness variation in the η direction given by $h(\eta, \zeta) = h_0(1 + \alpha\eta)$ is shown in Figure 4.5. Numerical solutions for the lowest sixteen values of the natural frequency parameter λ of this plate with aspect ratio b/a=1 and 2 are shown in Table 4.5 and 4.6 for two cases of $\alpha = 0.1$ and 0.8. The thickness ratio h_0/a of these plates is 0.01. The convergent values of numerical solution are obtained for the two cases of divisional numbers $m(= n)$ of 12 and 16 for the whole part of the plate. Tables 4.5 and 4.6 involve the other theoretical values of the fundamental frequency by Apple and Byers [48]. The nodal lines of sixteen modes of free vibration of the four plates of $b/a = 1, 2$ and $\alpha = 0.1, 0.8$ are shown in Figures 4.6 and 4.7

Table 4.5: Natural frequency parameter λ for a simple square plate with variable thickness ($b/a = 1$); $\nu = 0.3$

	α=0.1				α=0.8			
	m		Nu.	Ref.	m		Nu.	Ref.
Mode	12	16	Solu.	[48]	12	16	Solu.	[48]
1	4.687	4.675	4.660	4.661	5.386	5.372	5.354	5.355
2	7.512	7.446	7.363	–	8.576	8.501	8.404	–
3	7.513	7.447	7.363	–	8.612	8.535	8.437	–
4	9.534	9.436	9.311	–	10.944	10.829	10.680	–
5	10.927	10.692	10.389	–	12.342	12.080	11.742	–
6	10.932	10.696	10.393	–	12.512	12.238	11.886	–
7	12.405	12.162	11.851	–	14.210	13.926	13.560	–
8	12.407	12.164	11.852	–	14.265	13.977	13.607	–
9	14.870	14.269	13.496	–	16.581	15.918	15.066	–
10	14.724	14.258	13.659	–	16.889	16.308	15.562	–
11	14.883	14.378	13.729	–	17.018	16.481	15.791	–
12	15.993	15.396	14.628	–	18.294	17.602	16.712	–
13	15.997	15.400	14.631	–	18.402	17.701	16.799	–
14	17.846	17.195	16.358	–	20.428	19.670	18.695	–
15	17.848	17.197	16.360	–	20.513	19.742	18.752	–
16	19.514	18.174	16.451	–	21.467	20.047	18.222	–

Table 4.6: Natural frequency parameter λ for a simple rectangular plate with variable thickness ($b/a = 2$); $\nu = 0.3$

	α=0.1				α=0.8			
	m		Nu.	Ref.	m		Nu.	Ref.
Mode	12	16	Solu.	[48]	12	16	Solu.	[48]
1	3.705	3.696	3.684	3.684	4.245	4.234	4.220	4.221
2	4.728	4.698	4.659	–	5.433	5.398	5.353	–
3	6.176	6.069	5.930	–	7.078	6.955	6.797	–
4	6.944	6.876	6.789	–	7.955	7.876	7.775	–
5	7.982	7.693	7.322	–	9.100	8.776	8.359	–
6	7.539	7.462	7.362	–	8.641	8.552	8.436	–
7	8.521	8.392	8.226	–	9.775	9.624	9.430	–
8	10.200	9.633	8.903	–	11.547	10.831	9.910	–
9	9.909	9.551	9.091	–	11.377	11.055	10.641	–
10	10.549	10.307	9.995	–	14.574	13.145	11.308	–
11	12.695	11.673	10.360	–	12.072	11.791	11.430	–
12	10.949	10.706	10.393	–	12.533	12.250	11.886	–
13	11.647	11.173	10.565	–	13.529	12.833	11.938	–
14	11.770	11.373	10.862	–	13.336	13.017	12.813	–
15	12.992	12.315	11.445	–	16.407	14.984	13.154	–
16	14.193	13.036	11.550	–	14.545	14.102	13.532	–

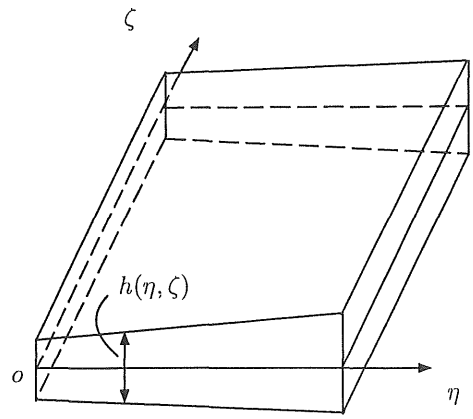

Figure 4.5: A simply supported rectangular plate with variable thickness in one direction

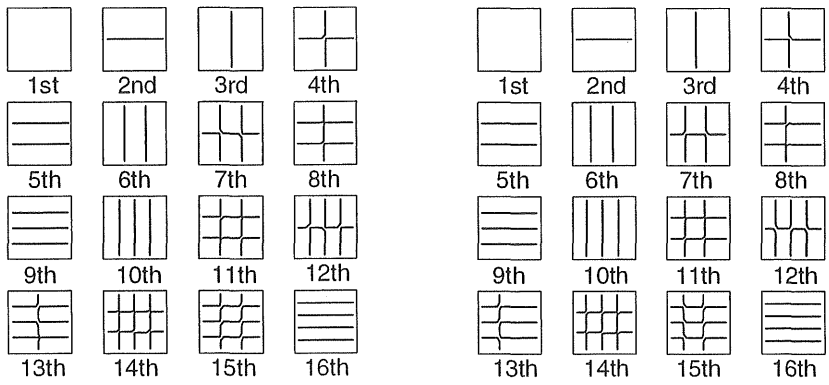

(a) (b)

Figure 4.6: Nodal patterns for a simply supported square plate with variable thickness ($b/a = 1$). (a) α=0.1; (b) α=0.8.

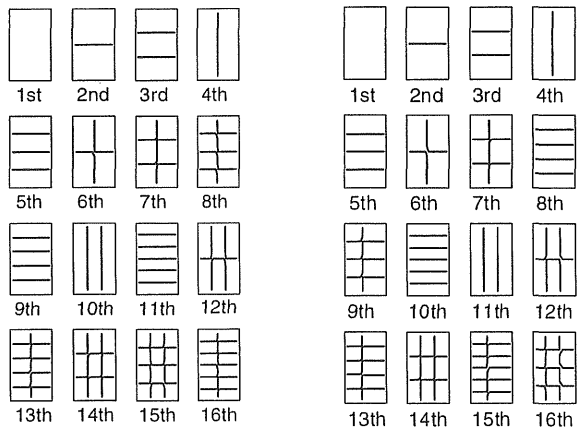

(a) (b)

Figure 4.7: Nodal patterns for a simply supported rectangular plate with variable thickness (b/a=2). (a) α=0.1; (b) α=0.8.

[6] Clamped square plate with variable thickness

A clamped square with a sinusoidal thickness variation in the η, ζ directions given by $h(\eta, \zeta) = h_0(1 - \alpha sin\pi\eta)(1 - \alpha sin\pi\zeta)$ is shown in Figure 4.8. Numerical solutions for the lowest sixteen values of the natural frequency parameter λ of this plate are shown in Table 4.7 for two cases of $\alpha = 0.3$ and 0.5. The thickness ratio h_0/a of these plates is 0.01. The convergent values of numerical solutions are obtained for the two cases of

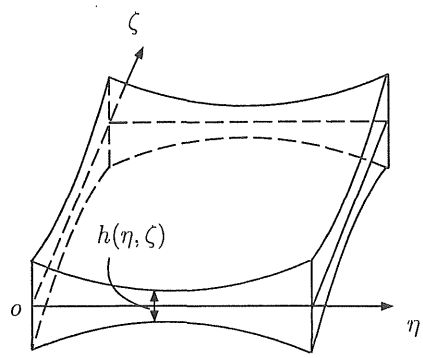

Figure 4.8: A clamped square plate with variable thickness in two directions

Table 4.7: Natural frequency parameter λ for a clamped square plate with variable thickness; $\nu = 0.3$

	α=0.3			α=0.5		
	m		Nu.	m		Nu.
Mode	12	16	Solu.	12	16	Solu.
1	1.990	1.989	1.988	2.166	2.164	2.162
2	2.799	2.794	2.789	2.675	2.671	2.665
3	4.324	4.300	4.270	3.745	3.720	3.687
4	4.603	4.576	4.540	4.033	4.006	3.971
5	5.014	4.985	4.948	4.337	4.307	4.269
6	6.523	6.476	6.415	5.148	5.046	4.914
7	6.860	6.747	6.601	5.378	5.323	5.254
8	7.274	7.153	6.997	6.178	6.062	5.914
9	7.694	7.575	7.421	6.671	6.422	6.103
10	8.675	8.538	8.361	6.446	6.331	6.183
11	8.868	8.734	8.562	6.992	6.842	6.650
12	9.591	9.281	8.884	7.328	7.188	7.009
13	10.464	10.115	9.665	8.433	7.904	7.224
14	10.662	10.378	10.013	8.701	8.378	7.963
15	10.790	10.520	10.172	8.941	8.596	8.154
16	11.373	11.032	10.593	8.765	8.521	8.207

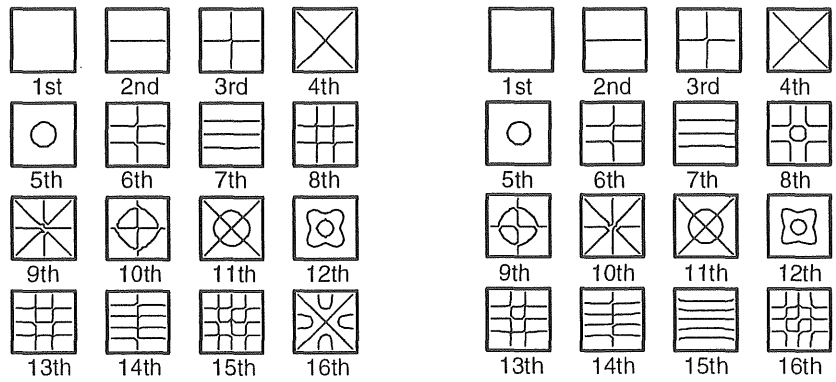

(a) (b)

Figure 4.9: Nodal patterns for a clamped square plate with variable thickness. (a) α=0.3; (b) α=0.5.

divisional numbers $m(=n)$ of 12 and 16 for the whole part of the plate. The nodal lines of sixteen modes of free vibration of the two plates of α=0.3, 0.5 are shown in Figure 4.9. There are some changes of mode order in the 9th, 10th, 15th and 16th modes.

[7] Cantilever square plate with variable thickness

A cantilever square plate with a linear thickness variation in the η direction given by $h(\eta,\zeta) = h_0[\alpha + (1-\alpha)\eta]$ is shown in Figure 4.10. Numerical solutions for the lowest sixteen values of the natural parameter λ of this plate are shown in Table 4.8 for two

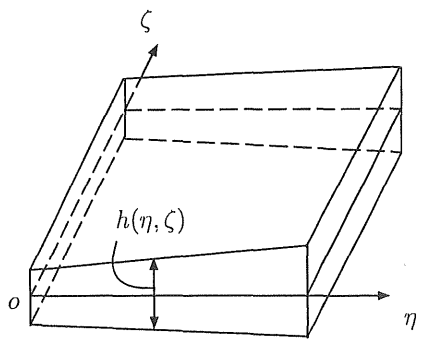

Figure 4.10: A cantilever square plate with variable thickness in one direction

Table 4.8: Natural frequency parameter λ for a cantilever square plate with variable thickness; $\nu = 0.3$

	α=1/2			α=1/8		
	m		Nu.	m		Nu.
Mode	12	16	Solu.	12	16	Solu.
1	1.743	1.742	1.741	1.541	1.540	1.540
2	2.459	2.456	2.451	1.886	1.883	1.880
3	3.866	3.846	3.819	2.579	2.561	2.537
4	4.096	4.070	4.037	3.057	3.035	3.006
5	4.532	4.506	4.472	3.266	3.229	3.182
6	5.990	5.891	5.764	3.472	3.411	3.333
7	5.918	5.873	5.816	4.079	4.005	3.909
8	6.655	6.542	6.396	4.391	4.243	4.052
9	7.032	6.919	6.775	4.867	4.755	4.610
10	7.897	7.768	7.602	5.230	5.003	5.712
11	8.064	7.902	7.695	5.067	4.944	4.784
12	8.352	8.121	7.825	5.544	5.271	4.921
13	9.615	9.286	8.862	6.563	6.038	5.363
14	9.782	9.525	9.195	5.801	5.655	5.467
15	9.889	9.617	9.266	6.850	6.401	5.825
16	10.339	10.022	9.614	7.018	6.680	6.245

cases of $\alpha = 1/2$ and $1/8$. The thickness ratio h_0/a of these plates is 0.01. The convergent values of numerical solutions are obtained for the two cases of divisional numbers $m(= n)$ of 12 and 16 for the whole part of the plate. The nodal lines of sixteen modes of free vibration of the two plates of α=1/2 and 1/8 are shown in Figure 4.11. There are some differences of mode shape and mode order between these two cantilever plates.

[8] Moderately thick simple square plate with variable thickness

A moderately thick simply supported square plate with a linear thickness variation in the η direction given by $h(\eta, \zeta) = h_0(1 - \eta)$ is shown in Figure 4.12. Numerical solutions for the lowest sixteen values of the natural parameter λ of this plate are shown in Table 4.9 for two cases of thickness ratio h_0/a=0.1 and 0.2. The convergent

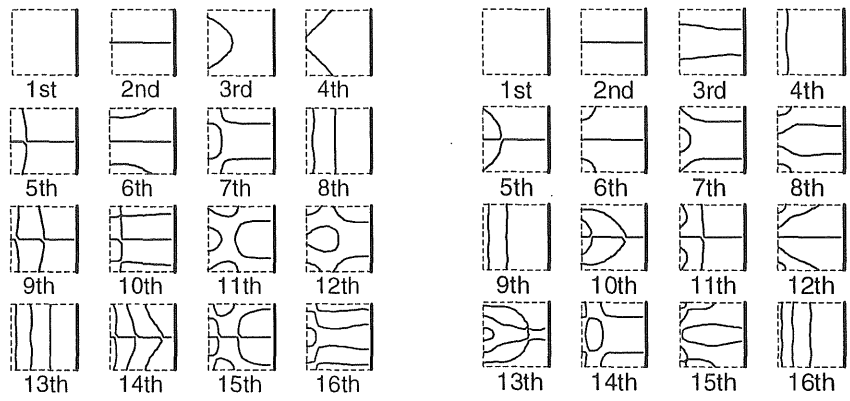

(a) (b)

Figure 4.11: Nodal patterns for a cantilever square plate with variable thickness. $\alpha = 1/2$; (b) $\alpha = 1/8$.

values of numerical solutions are obtained by using Richardson's extrapolation formula for the two cases of divisional numbers $m(= n)$ of 12 and 16 for the whole part of the plate. Table 4.9 involves the other theoretical values by Aksu and Al-Kaabi [10] and it shows good convergency and adequate accuracy of the numerical solutions by the present method. The nodal lines of free vibration of these two moderately thick plates with variable thickness are shown in Figure 4.13.

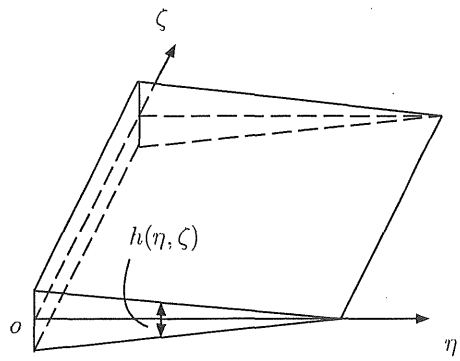

Figure 4.12: A moderately thick simple square plate with variable thickness in one direction

Table 4.9: Natural frequency parameter λ for a moderately thick simple square plate with variable thickness; $\nu = 0.3$

	h_0/a=0.1				h_0/a=0.2			
	m		Nu.	Ref.	m		Nu.	Ref.
Mode	12	16	Solu.	[10]	12	16	Solu.	[10]
1	5.327	5.314	5.298	5.238	4.828	4.818	4.806	4.758
2	8.054	7.995	7.920	7.975	6.791	6.751	6.700	6.873
3	8.056	7.998	7.922	7.994	6.802	6.762	6.711	6.882
4	9.761	9.683	9.582	9.649	7.916	7.866	7.801	8.048
5	10.835	10.658	10.431	10.654	8.615	8.501	8.355	8.671
6	10.852	10.673	10.444	–	8.618	8.507	8.364	–
7	11.879	11.712	11.497	–	9.285	9.177	9.039	–
8	11.882	11.715	11.502	–	9.292	9.183	9.044	–
9	13.487	13.105	12.244	–	10.247	10.016	9.719	–
10	13.540	13.156	12.291	–	10.315	10.069	9.753	–
11	13.381	13.166	12.511	–	10.254	10.115	9.936	–
12	14.148	13.793	13.337	–	10.742	10.512	10.217	–
13	14.150	13.796	13.340	–	10.766	10.534	10.236	–
14	15.191	14.832	14.371	–	11.806	11.381	10.834	–
15	15.191	14.832	14.371	–	11.420	11.185	10.882	–
16	16.097	15.386	14.472	–	11.435	11.197	10.891	–

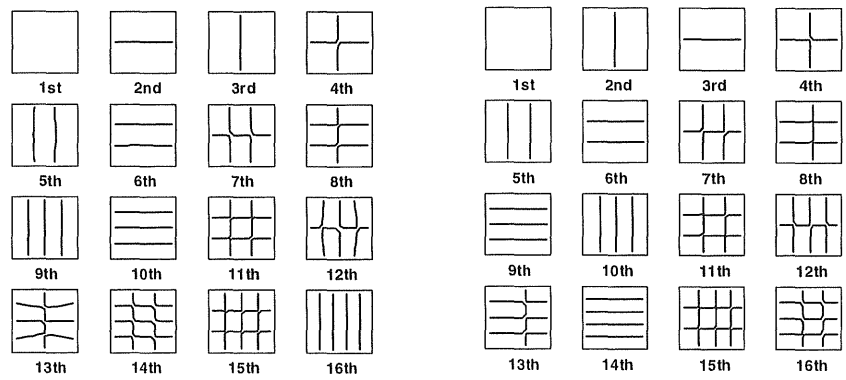

(a) (b)

Figure 4.13: Nodal patterns for a moderately thick simple square plate with variable thickness. (a) $h_0/a = 0.1$; (b) $h_0/a = 0.2$.

4.1.5 Conclusions

In this section, the discrete method is extended for the free vibration problems of rectangular plates with variable thickness. In order to confirm the efficiency of this method, free vibration analysis of rectangular plates with different boundary conditions and variable thickness is carried out. The main conclusions are summarized as follows

1. Based on Green function, a discrete method has been proposed for analyzing the free vibration problem of various types of rectangular plates with uniform or non-uniform thickness.

2. The numerical results compared with other published ones show that the numerical solutions by the discrete method have good convergency and adequate accuracy.

3. The effects of the boundary conditions on the natural frequency parameters and nodal lines of modes of free vibration are illustrated in tables and figures. It is observed that the frequency parameters increase as the constraints of the plate increase.

4. The thickness of the plates also influences the natural frequency parameters and nodal lines of mode shape. There are some changes of mode order for some plates with different thickness.

4.2 Free vibration analysis of rectangular plates with various-shaped holes

4.2.1 Introduction

In previous section, the discrete method has been proposed for free vibration analysis of rectangular plates with various thickness. In this section, by using the concept of equivalent rectangular plates, which is the plates with hole can be considered finally as a kind of rectangular plate with non-uniform thickness, the discrete solutions obtained in previous section are extended for free vibration analysis of rectangular plates with

various-shaped and arbitrary-located holes. Here, the shapes of hole are circular, semi-circular, elliptic, square, rectangular, triangular and rhombic *etc.* The convergency and accuracy of numerical solutions are investigated.

4.2.2 Equivalent rectangular plate of a rectangular plate with various-shaped hole

Rectangular plates with various-shaped hole such as circular, semi-crcular, elliptic, square, rectangular, triangular or rhombic hole can be translated into their equivalent rectangular plates with non-uniform thickness by considering the hole as an extremely thin part of the plate. An example of translation from an original plate with hole to its equivalent rectangular plate with non-uniform thickness is shown in Figure 4.14.

4.2.3 Numerical work

After the equivalent rectangular plate is obtained, the numerical work is carried out in the equivalent rectangular plate. The numerical solutions of the natural frequency parameter λ are obtained by using the equation (4.8) and Richardson's extrapolation formula for two cases of divisional numbers $m(= n)$. The convergency and accuracy of numerical solutions have been investigated for the free vibration problem of some rectangular plates with various-shaped hole such as circular, semi-circular, elliptic, square, rectangular, triangular or rhombic hole as shown in Figure 4.15.

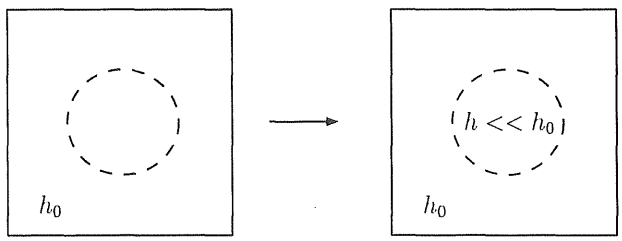

Figure 4.14: Example of equivalent plate

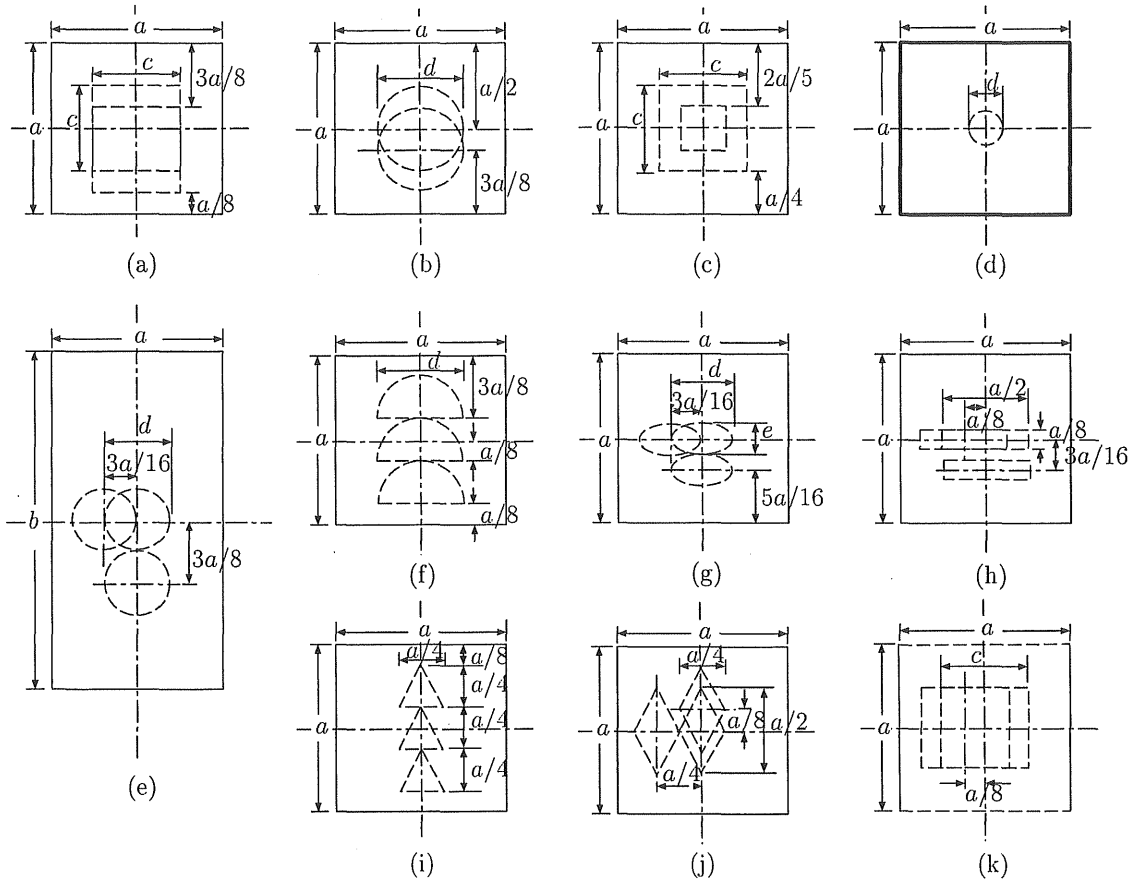

Figure 4.15: Rectangular plates with various-shaped opening holes

[1] Thin SSSS square plate with square hole

In order to examine the convergency of numerical values for the natural frequency parameter λ and determine the suitable values of divisional numbers m and n, the lowest twelve values of the natural frequency parameter for SSSS square plates with square hole of size ratio c/a=0.5 at the central or lower part shown in Figure 4.15 (a) are analyzed. The thickness ratio h_0/a of these plates is 0.01. The results are shown in Figure 4.16. They show the good convergency of numerical solutions by the proposed method. After studying the curves of Figure 4.16, the divisional numbers $m = (n)$ in Richardson's extrapolation formula are chosen to be 12 and 16.

The lowest twelve numerical values of the natural frequency parameter λ of these plates are given in Table 4.10. Table 4.10 involves the other theoretical values by Ali

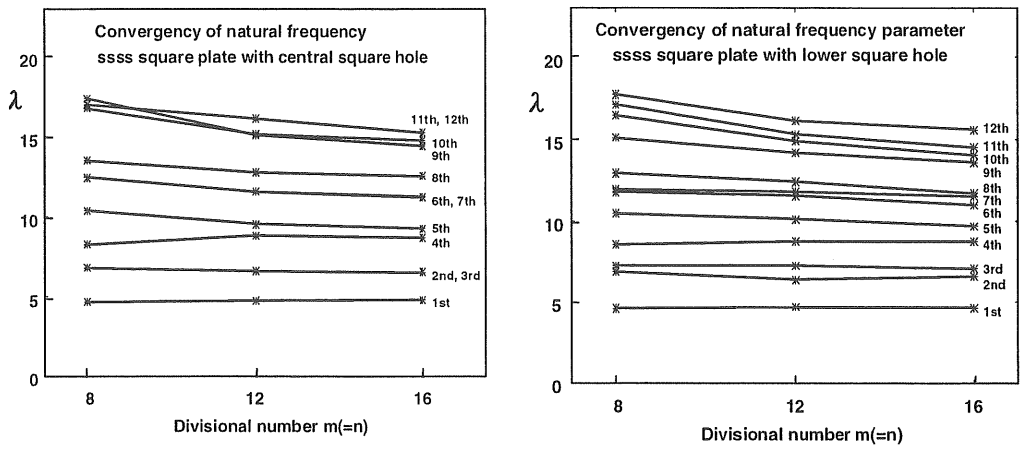

(a) (b)

Figure 4.16: Convergency of the natural frequency parameter.(a) central hole; (b) lower hole.

Table 4.10: Natural frequency parameter λ for SSSS square plates with square hole

	central hole				lower hole		
	m		Nu.	Ref.	m		Nu.
Mode	12	16	Solu.	[21]	12	16	Solu.
1	4.731	4.779	4.839	4.936	4.713	4.663	4.600
2	6.595	6.525	6.435	6.502	6.377	6.591	6.867
3	6.595	6.527	6.440	6.502	7.234	7.078	6.878
4	8.818	8.676	8.492	8.525	8.751	8.745	8.738
5	9.531	9.244	8.875	8.813	10.080	9.668	9.138
6	11.552	11.225	10.805	–	11.526	10.952	10.213
7	11.552	11.237	10.831	–	12.387	11.682	10.776
8	12.757	12.553	12.291	–	11.781	11.519	11.182
9	15.112	14.422	13.534	–	14.181	13.555	12.749
10	16.136	15.249	14.108	–	14.875	14.020	12.920
11	15.174	14.763	14.234	–	15.268	14.494	13.499
12	15.174	14.769	14.247	–	16.113	15.559	14.848

and Atwal [21], and it shows the adequate accuracy of the numerical solutions by the present method. The nodal patterns of the twelve modes of the two plates are shown in Figure 4.17

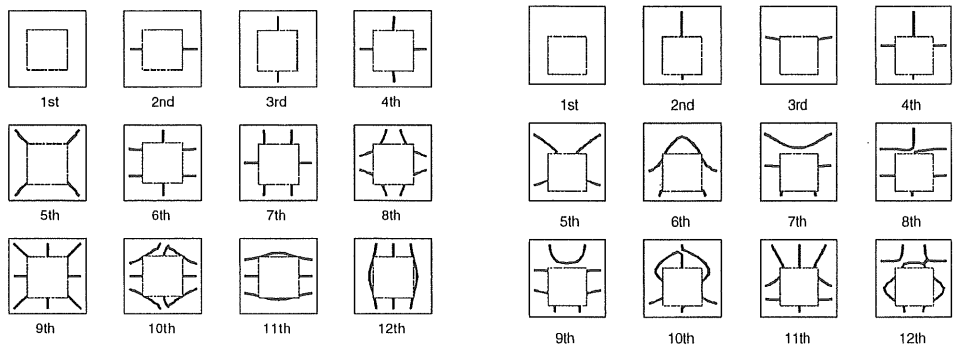

(a) (b)

Figure 4.17: Nodal patterns for SSSS square plates with square hole. (a) central hole; (b) lower hole.

[2] Thin SSSS square plate with circular hole

The lowest twelve numerical values of the natural frequency parameter λ of SSSS square plates with circular hole of size ratio $d/a = 0.5$ at the central or lower part shown in Figure 4.15 (b) are given in Table 4.11. The thickness ratio h_0/a of these plates is 0.01. Table 4.11 involves the other theoretical value by Rao and Pickett [49]. The nodal

Table 4.11: Natural frequency parameter λ for SSSS square plates with circular hole; $d/a = 1/2$

	central hole				lower hole		
	m		Nu.	Ref.	m		Nu.
Mode	12	16	Solu.	[49]	12	16	Solu.
1	4.731	4.772	4.824	4.852	4.688	4.639	4.575
2	6.595	6.661	6.746	–	6.578	6.734	6.936
3	6.595	6.668	6.762	–	7.276	7.162	7.014
4	8.776	8.531	8.214	–	8.742	8.769	8.804
5	9.530	9.597	9.683	–	10.181	9.776	9.256
6	11.552	11.401	11.206	–	11.525	11.024	10.381
7	11.552	11.449	11.316	–	12.600	11.907	11.016
8	12.757	12.587	12.368	–	11.534	11.578	11.635
9	15.208	14.419	13.405	–	14.465	13.668	12.643
10	15.174	14.457	13.537	–	13.415	13.786	14.263
11	15.174	14.458	13.537	–	14.790	14.681	14.541
12	15.112	14.487	13.683	–	16.179	15.633	14.931

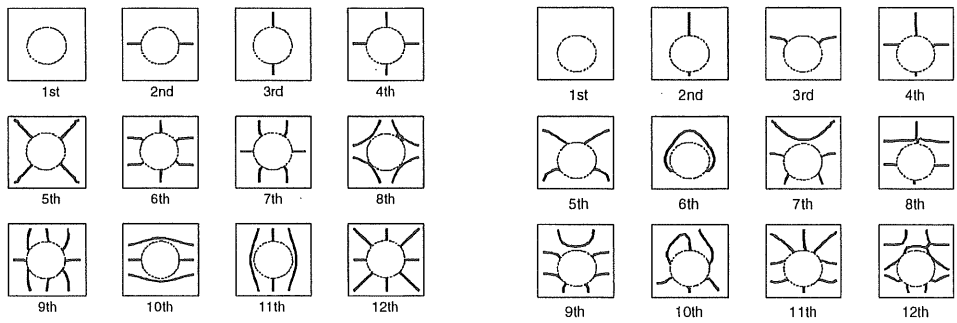

(a) (b)

Figure 4.18: Nodal patterns for SSSS square plates with circular hole. (a) central hole; (b) lower hole.

pattens of the twelve modes of the two plates are shown in Figure 4.18.

[3] Moderately thick SSSS square plate with square hole

The lowest twelve numerical values of the natural frequency parameter λ of SSSS square plates with moderate thickness ratio of $h_0/a = 0.2$ and square hole of size ratio $c/a = 0.5, 0.2$ at the central part shown in Figure 4.15 (c) are given in Table 4.12.

Table 4.12: Natural frequency parameter λ for SSSS moderately thick square plates with central square hole; $h_0/a = 0.2$

	c/a=0.5				c/a=0.2			
	m		Nu.	Ref.	m		Nu.	Ref.
Mode	12	16	Solu.	[50]	12	16	Solu.	[50]
1	4.533	4.574	4.628	4.753	4.313	4.289	4.258	4.277
2	5.775	5.792	5.814	–	6.157	6.291	6.462	–
3	5.775	5.792	5.814	–	6.158	6.293	6.468	–
4	7.731	7.486	7.329	–	7.761	7.692	7.603	–
5	7.579	7.501	7.401	–	9.335	8.872	8.278	–
6	9.065	8.964	8.833	–	8.473	8.479	8.488	–
7	9.065	8.964	8.833	–	9.346	9.276	9.185	–
8	10.032	9.884	9.694	–	9.346	9.282	9.199	–
9	10.866	10.601	10.235	–	10.539	10.197	9.756	–
10	11.341	11.105	10.802	–	10.539	10.197	9.758	–
11	11.341	11.105	10.802	–	11.129	10.738	10.235	–
12	12.249	11.691	11.333	–	11.287	11.028	10.695	–

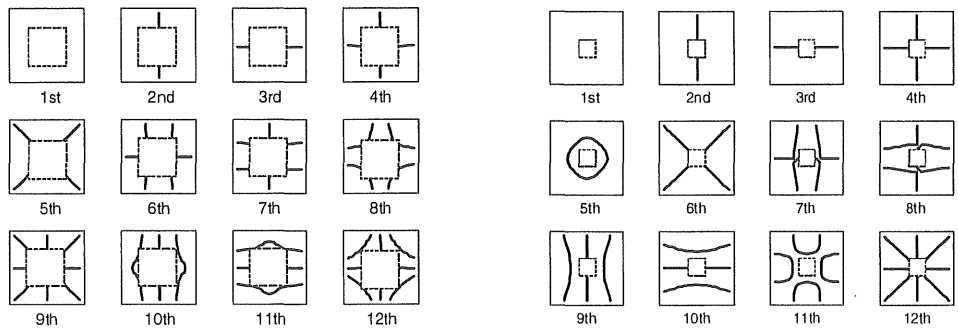

(a) (b)

Figure 4.19: Nodal patterns for SSSS moderately thick square plates with square hole. (a) larger hole; (b) smaller hole.

Table 4.12 involves the other theoretical value by Reddy [50]. The nodal patterns of the twelve modes of the two plates are shown in Figure 4.19.

[4] CCCC square plate with circular hole

Table 4.13 gives the lowest twelve numerical values of the natural frequency parameter λ of CCCC square plates with circular hole of size ratio $d/a = 0.2$ at the central part

Table 4.13: Natural frequency parameter λ for CCCC square plates with central circular hole; $d/a = 0.2$

	ν=0.3				ν=0.5			
	m		Nu.	Ref.	m		Nu.	Ref.
Mode	12	16	Solu.	[51]	12	16	Solu.	[52]
1	6.188	6.211	6.240	6.099	6.338	6.363	6.395	6.428
2	8.943	8.731	8.457	8.396	9.304	9.040	8.702	–
3	8.940	8.731	8.462	–	9.302	9.040	8.704	–
4	11.033	10.683	10.233	–	11.402	11.196	10.932	–
5	12.157	11.965	11.719	–	12.758	12.586	12.365	–
6	12.747	12.551	12.299	12.008	13.076	12.941	12.767	–
7	13.718	13.420	13.037	–	14.314	13.961	13.507	–
8	13.715	13.420	13.041	–	14.309	13.962	13.516	–
9	16.459	16.007	15.426	–	17.125	15.703	13.875	–
10	16.505	15.215	13.556	–	17.108	15.705	13.901	–
11	16.503	15.215	13.560	–	17.182	16.710	16.102	–
12	17.626	16.802	15.741	–	18.479	17.619	16.512	–

shown in Figure 4.15 (d) for $\nu = 0.3$ and $\nu = 0.5$. The thickness ratio h_0/a of these plates is 0.01. Table 4.13 involves the other theoretical values by Kumai [51] and Hegarty and Ariman [52], and it shows the adequate accuracy of the numerical solutions by the present method. The nodal patterns of the twelve modes of the two plates are shown in Figure 4.20.

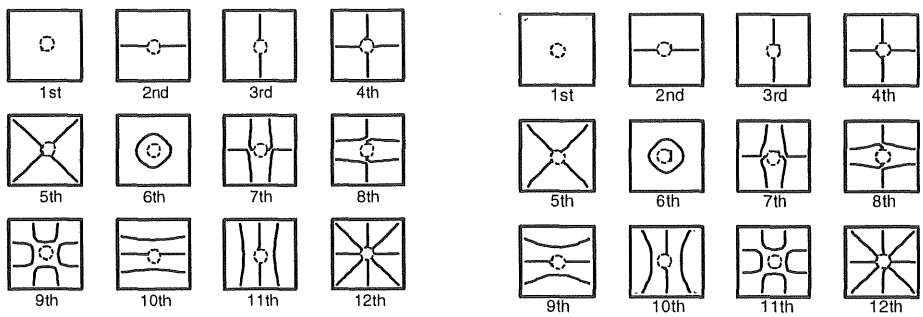

(a) (b)

Figure 4.20: Nodal patterns for CCCC square plates with circular hole ($d/a = 0.2$). (a) $\nu = 0.3$; (b) $\nu = 0.5$.

[5] SSSS rectangular plate with circular hole

The lowest twelve numerical values of the natural frequency parameter λ of SSSS rectangular plates with aspect ratio $b/a = 2$ and circular hole of size ratio $d/a = 3/8$ at the central, lower or left-side part shown in Figure 4.15 (e) are given in Table 4.14. The thickness ratio h_0/a of these plates is 0.01. The nodal patterns of the twelve modes of the three plates are shown in Figure 4.21.

[6] SSSS square plate with semi-circular hole

The lowest twelve numerical values of the natural frequency parameter λ of SSSS square plates with semi-circular hole of size ratio $d/a = 1/2$ at the central, upper or lower part shown in Figure 4.15 (f) are given in Table 4.15. The thickness ratio h_0/a of these plates is 0.01. The nodal patterns of the twelve modes of the three plates are shown in Figure 4.22.

Table 4.14: Natural frequency parameter λ for SSSS rectangular plates with circular hole; $b/a = 2$

	central hole			lower hole			left-side hole		
	m		Nu.	m		Nu.	m		Nu.
Mode	12	16	Solu.	12	16	Solu.	12	16	Solu.
1	2.961	2.965	2.970	3.005	2.983	2.953	2.932	2.962	3.001
2	3.796	3.803	3.810	3.865	3.853	3.838	3.823	3.792	3.753
3	5.183	5.046	4.870	4.947	4.848	4.722	5.012	4.982	4.943
4	5.171	5.303	5.472	5.539	5.333	5.067	5.602	5.622	5.648
5	6.342	6.080	5.743	6.075	5.922	5.725	6.449	6.145	5.754
6	6.027	5.992	5.946	6.376	6.250	6.088	6.097	6.040	5.967
7	6.729	6.718	6.704	6.878	6.544	6.114	7.058	6.956	6.824
8	8.114	7.661	7.079	7.990	7.594	7.086	8.017	7.759	7.428
9	8.011	7.779	7.482	8.266	7.775	7.143	8.417	8.001	7.466
10	10.663	9.307	7.563	8.746	8.553	8.306	10.637	9.383	7.771
11	9.045	8.694	8.244	10.190	9.404	8.393	7.635	7.860	8.149
12	8.927	8.728	8.472	9.567	9.106	8.513	8.857	8.743	8.598

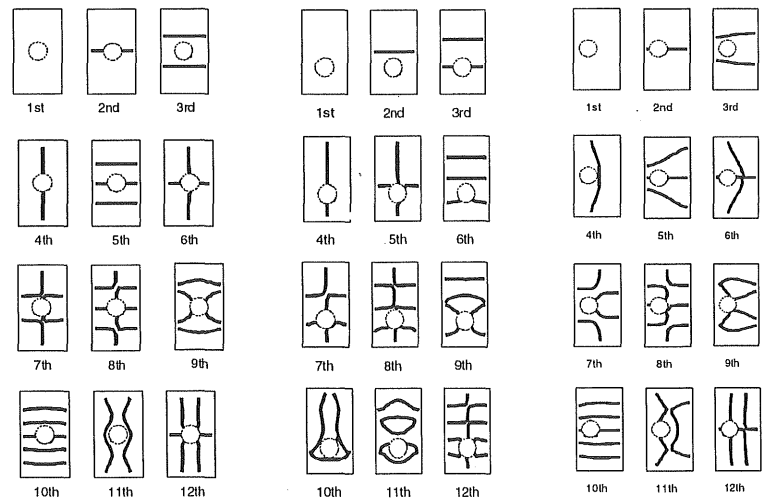

(a) (b) (c)

Figure 4.21: Nodal patterns for SSSS rectangular plates with circular hole ($b/a = 2$). (a) central hole; (b) lower hole; (c) left-side hole.

Table 4.15: Natural frequency parameter λ for SSSS square plates with semi-circular hole

	central hole			upper hole			lower hole		
	m		Nu.	m		Nu.	m		Nu.
Mode	12	16	Solu.	12	16	Solu.	12	16	Solu.
1	4.522	4.532	4.545	4.474	4.442	4.402	4.460	4.421	4.730
2	6.686	6.568	6.416	7.363	7.173	6.928	7.352	7.189	6.980
3	7.027	7.005	6.977	7.121	7.111	7.100	7.124	7.166	7.221
4	8.988	8.947	8.893	9.491	9.193	8.810	9.773	9.268	8.619
5	10.194	9.927	9.584	9.070	9.074	9.079	9.128	9.041	8.929
6	11.568	11.083	10.459	10.853	10.531	10.117	10.854	10.488	10.018
7	11.904	11.578	11.160	13.123	12.256	11.141	12.312	11.790	11.119
8	11.630	11.559	11.466	12.522	11.996	11.319	11.892	11.671	11.386
9	13.188	13.048	12.868	11.622	11.552	11.461	12.911	12.316	11.551
10	14.159	13.719	13.154	14.433	13.898	13.209	14.325	13.806	13.137
11	14.924	14.481	13.910	14.552	13.982	13.245	14.545	13.987	13.270
12	15.480	14.844	14.027	14.919	14.380	13.686	14.993	14.275	13.351

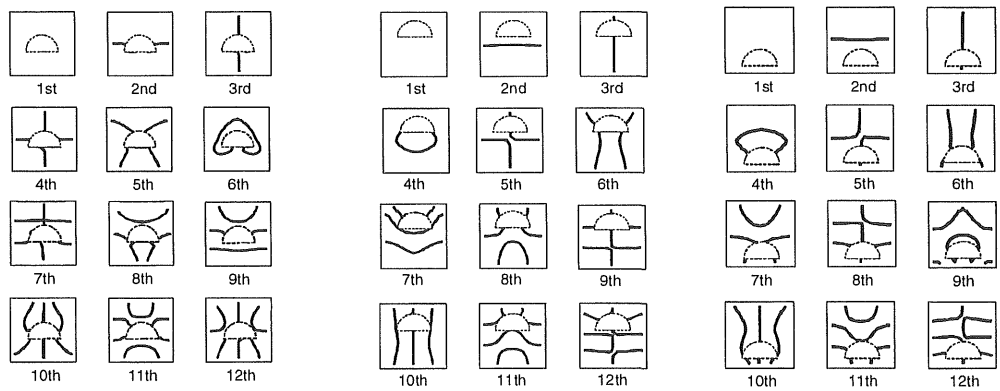

(a) (b) (c)

Figure 4.22: Nodal patterns for SSSS square plates with semi-circular hole. (a) central hole; (b) upper hole; (c) lower hole

[7] SSSS square plate with elliptic hole

The lowest twelve numerical values of the natural frequency parameter λ of SSSS square plates with elliptic hole of size ratio $d/a = 3/8$ and $d/e = 2$ at the central, lower or left-side part shown in Figure 4.15 (g) are given in Table 4.16. The thickness ratio h_0/a of these plates is 0.01. The nodal patterns of the twelve modes of the three plates are

Table 4.16: Natural frequency parameter λ for SSSS square plates with elliptic hole

	central hole			lower hole			left-side hole		
	m		Nu.	m		Nu.	m		Nu.
Mode	12	16	Solu.	12	16	Solu.	12	16	Solu.
1	4.510	4.482	4.447	4.469	4.483	4.502	4.499	4.496	4.491
2	6.980	6.912	6.824	7.214	7.118	6.994	7.204	6.979	6.690
3	7.086	7.103	7.125	7.173	7.147	7.114	7.301	7.265	7.219
4	9.056	8.721	8.295	9.223	9.090	8.920	9.189	8.907	8.544
5	10.233	10.200	10.159	9.946	9.545	9.028	10.190	10.142	10.081
6	11.451	10.889	10.167	10.701	10.489	10.216	10.702	10.503	10.247
7	11.754	11.457	11.074	11.932	11.626	11.232	14.062	12.735	11.029
8	13.698	12.777	11.593	12.146	11.923	11.638	11.994	11.645	11.197
9	11.823	11.780	11.724	14.403	13.762	12.939	12.303	12.088	11.813
10	14.095	13.720	13.238	13.313	13.245	13.157	14.470	14.003	13.403
11	14.942	14.381	13.659	14.417	14.050	13.578	15.238	14.569	13.709
12	15.404	14.794	14.010	15.239	14.795	14.224	13.786	13.793	13.802

shown in Figure 4.23.

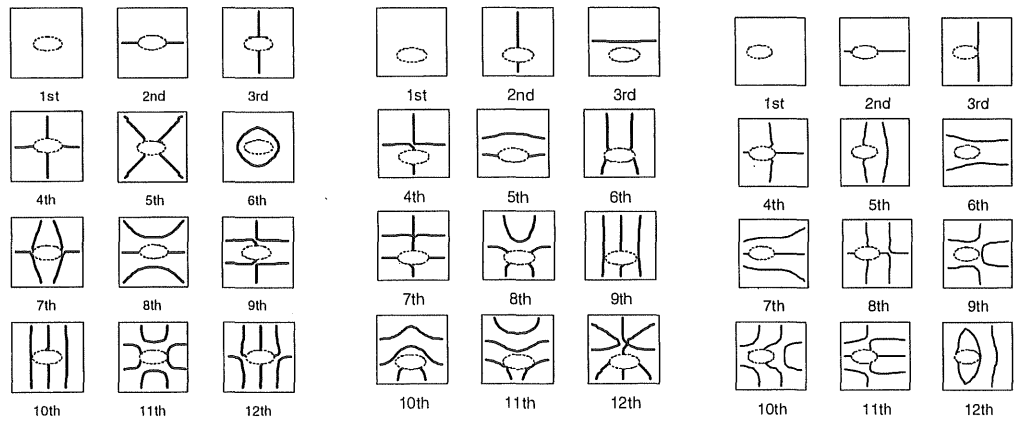

(a) (b) (c)

Figure 4.23: Nodal patterns for SSSS square plates with elliptic hole. (a) central hole; (b) lower hole; (c) left-side hole.

[8] SSSS square plate with thin rectangular hole

The lowest twelve numerical values of the natural frequency parameter λ of SSSS square plates with thin rectangular hole at the central, lower or left-side part shown in Figure 4.15 (h) are given in Table 4.17. The thickness ratio h_0/a of these plates is 0.01. The nodal patterns of the twelve modes of the three plates are shown in Figure 4.24.

Table 4.17: Natural frequency parameter λ for SSSS square plates with thin rectangular hole

	central hole			lower hole			left-side hole		
	m		Nu.	m		Nu.	m		Nu.
Mode	12	16	Solu.	12	16	Solu.	12	16	Solu.
1	4.407	4.374	4.332	4.437	4.417	4.393	4.393	4.399	4.407
2	7.279	7.225	7.156	7.063	6.919	6.733	7.276	7.216	7.139
3	7.324	7.263	7.185	7.284	7.224	7.148	7.295	7.254	7.201
4	9.272	9.177	9.054	9.243	9.140	9.007	9.190	9.157	9.113
5	10.227	9.879	9.432	10.667	10.416	10.093	10.196	9.949	9.631
6	10.654	10.397	10.067	10.644	10.407	10.101	10.622	10.387	10.084
7	12.014	11.765	11.445	12.083	11.834	11.515	11.990	11.733	11.401
8	12.031	11.797	11.496	12.034	11.810	11.521	12.043	11.826	11.546
9	14.525	13.901	13.099	14.214	13.625	12.868	14.422	13.859	13.135
10	14.380	13.923	13.335	14.492	13.941	13.233	14.516	13.914	13.140
11	14.510	14.024	13.399	14.248	13.930	13.522	14.373	13.968	13.447
12	15.483	14.988	14.352	15.687	14.975	14.059	15.505	14.935	14.202

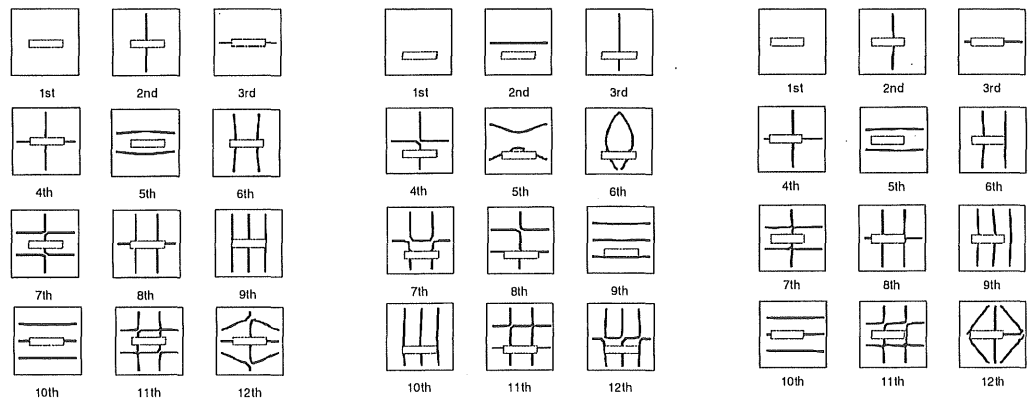

(a) (b) (c)

Figure 4.24: Nodal patterns for SSSS square plates with thin rectangular hole. (a) central hole; (b) lower hole; (c) left-side hole

[9] SSSS square plate with triangular hole

The lowest twelve numerical values of the natural frequency parameter λ of SSSS square plates with triangular hole at the central, upper or lower part shown in Figure 4.15 (i) are given in Table 4.18. The thickness ratio h_0/a of these plates is 0.01. The nodal patterns of the twelve modes of the three plates are shown in Figure 4.25.

Table 4.18: Natural frequency parameter λ for SSSS square plates with triangular hole

	central hole			upper hole			lower hole		
	m		Nu.	m		Nu.	m		Nu.
Mode	12	16	Solu.	12	16	Solu.	12	16	Solu.
1	4.455	4.482	4.517	4.498	4.517	4.542	4.510	4.523	4.540
2	7.311	7.265	7.207	7.234	7.171	7.090	7.214	7.171	7.115
3	7.254	7.241	7.225	7.268	7.228	7.176	7.294	7.248	7.190
4	9.191	9.161	9.122	9.269	9.200	9.110	9.259	9.195	9.111
5	10.684	10.367	9.959	10.597	10.389	10.121	10.581	10.351	10.055
6	10.462	10.298	10.088	10.642	10.414	10.122	10.411	10.296	10.147
7	12.061	11.850	11.579	12.064	11.794	11.447	12.073	11.809	11.470
8	12.031	11.860	11.640	12.000	11.852	11.662	12.026	11.830	11.578
9	14.478	13.888	13.129	14.136	13.751	13.256	14.505	13.906	13.136
10	14.212	13.770	13.202	14.347	13.882	13.283	14.228	13.764	13.168
11	14.434	14.024	13.497	14.361	13.974	13.477	14.461	14.046	13.512
12	15.527	14.860	14.002	15.483	14.913	14.180	15.539	14.970	14.238

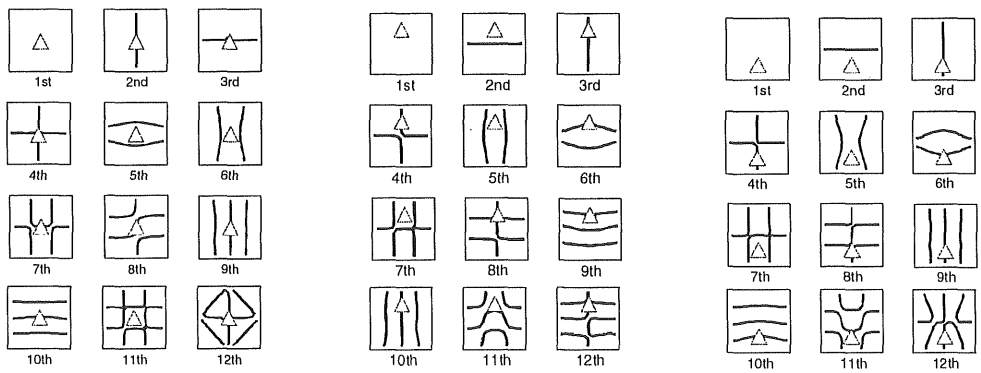

(a) (b) (c)

Figure 4.25: Nodal patterns for SSSS square plates with triangular hole. (a) central hole; (b) upper hole; (c) lower hole.

[10] SSSS square plate with rhombic hole

The lowest twelve numerical values of the natural frequency parameter λ of SSSS square plates with rhombic hole at the central, upper or left-side part shown in Figure 4.15 (j) are given in Table 4.19. The thickness ratio h_0/a of these plates is 0.01. The nodal patterns of the twelve modes of the three plates are shown in Figure 4.26.

Table 4.19: Natural frequency parameter λ for SSSS square plates with rhombic hole

	central hole			upper hole			left-side hole		
	m		Nu.	m		Nu.	m		Nu.
Mode	12	16	Solu.	12	16	Solu.	12	16	Solu.
1	4.628	4.547	4.442	4.433	4.541	4.679	4.593	4.523	4.432
2	7.332	7.138	6.889	7.142	7.165	7.195	7.472	7.263	6.994
3	7.442	7.276	7.062	7.191	7.324	7.495	7.355	7.203	7.007
4	9.176	9.145	9.106	9.090	9.054	9.008	9.439	9.212	8.919
5	10.467	10.239	9.947	10.250	10.390	10.569	10.582	10.162	9.621
6	11.565	10.996	10.264	10.532	10.707	10.933	11.034	10.634	10.120
7	11.982	11.651	11.225	11.899	11.733	11.520	12.777	12.184	11.422
8	12.232	11.888	11.446	12.023	12.110	12.221	12.172	11.894	11.536
9	14.778	13.502	11.862	13.970	13.459	12.802	14.708	13.322	11.539
10	14.925	14.076	12.983	14.636	14.005	13.194	14.719	13.929	12.913
11	15.195	14.456	13.505	15.294	14.711	13.960	14.988	14.168	13.114
12	15.496	14.950	14.249	15.544	14.994	14.288	15.620	15.030	14.271

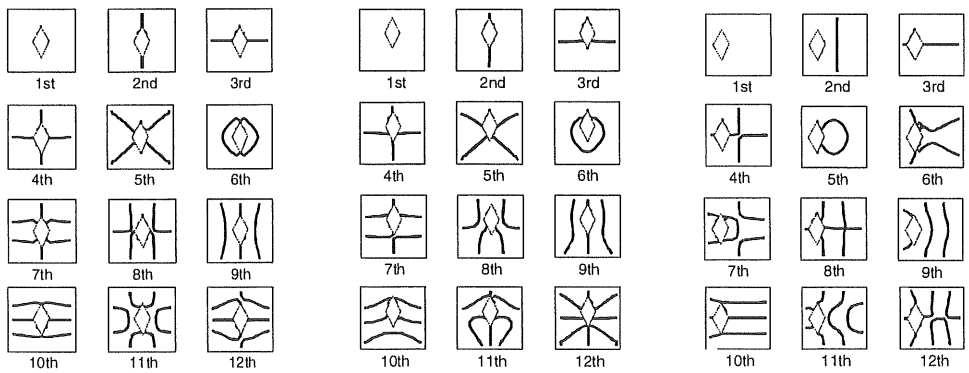

Figure 4.26: Nodal patterns for SSSS square plates with rhombic hole. (a) central hole; (b) upper hole; (c) left-side hole.

[11] FSFS square plate with square hole

The lowest twelve numerical values of the natural frequency λ of FSFS square plates with square hole of size ratio $c/a = 0.5$ at the central or left-side part shown in Figure 4.15 (k) are given in Table 4.20. The thickness ratio h_0/a of these plates is 0.01. The nodal patterns of the twelve modes of the two plates are shown in Figure 4.27.

Table 4.20: Natural frequency parameter λ for FSFS square plates with square hole

	central hole			left-side hole		
	m		Nu.	m		Nu.
Mode	12	16	Solu.	12	16	Solu.
1	3.299	3.036	2.699	3.307	3.032	2.680
2	4.308	4.233	4.137	4.200	4.198	4.196
3	6.231	5.880	5.428	6.435	5.998	5.437
4	6.975	6.865	6.724	7.419	6.999	6.459
5	7.263	7.096	6.881	7.205	7.107	6.981
6	9.257	8.849	8.324	9.837	9.188	8.355
7	9.124	8.793	8.367	9.135	8.904	8.606
8	10.523	9.745	8.745	10.576	9.821	8.849
9	10.728	10.356	9.877	10.807	10.474	10.045
10	11.936	11.301	10.485	12.042	11.391	10.554
11	12.274	11.713	10.992	12.248	11.578	10.717
12	14.675	13.612	12.246	13.392	12.283	10.857

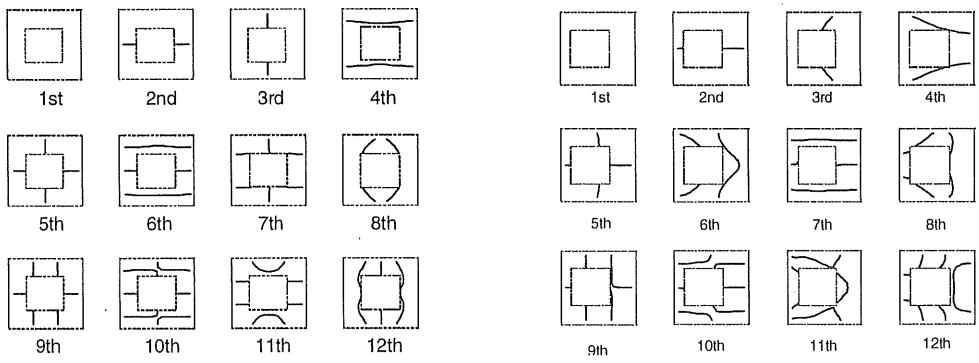

(a) (b)

Figure 4.27: Nodal patterns for FSFS square plates with square hole. (a) central hole; (b) left-side hole.

4.2.4 Conclusions

In this section, the discrete method has been extended for the free vibration analysis of rectangular plates with various-shaped and arbitrary-located hole. The main conclusions are summarized as follows:

1. Under the concept that the plates with hole can be considered finally as a kind of rectangular plates with non-uniform thickness, the discrete method used in preceding section is applicable to the free vibration problem of rectangular plates with a various-shaped and arbitrary-located hole.

2. The effects of the shape, the size and the position of the hole on the vibration characteristics are investigated and illustrated in tables and figures.

4.3 Free vibration analysis of right triangular plates with variable thickness

4.3.1 Introduction

In previous two sections, the discrete method with Green function has been used for solving the free vibration problems of rectangular plates with variable thickness and various-shaped holes. In this section, under the concept of an equivalent rectangular plate (see chapter 2), the same method is also used for the free vibration analysis of right triangular plates. In previous sections, the Green function is obtained by using the solution for the deflection of the plate with a concentrated load, and in this section, the Green function is obtained by using the solution for the deflection of the plate with not only a concentrated load but also point supports. The characteristic equation of free vibration of rectangular plate with variable thickness and point supports is obtained and expressed in matrix form. The convergency and accuracy of the numerical solutions for the natural frequency parameter obtained by the proposed method are investigated, and the lowest eight frequency parameters and their modes of free vibration are shown for some right triangular plates.

4.3.2 Discrete Green function of a rectangular plate with non-uniform thickness and point supports

The Green function of a plate bending problem in this section is given by the displacement function of the plate with a unit concentrated load and point supports, so the Green function $G(x, y, x_q, y_r) = w(x, y, x_q, y_r)/\overline{P}$ can be obtained from the fundamental differential equations of rectangular plates with a concentrated load $\overline{P}$ at a point (x_q, y_r), non-uniform thickness and point supports at each discrete point (x_c, y_d) shown in Figure 4.28, which are given by following equations.

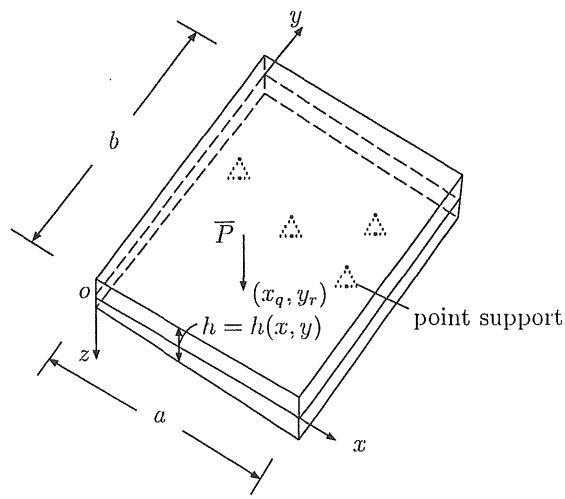

Figure 4.28: Rectangular plate with a concentrated load and point supports

$$\frac{\partial Q_x}{\partial x} + \frac{\partial Q_y}{\partial y} + \sum_{c=0}^{m}\sum_{d=0}^{n} \overline{P}_{1cd}\delta(x - x_c)\delta(y - y_d) + \overline{P}\delta(x - x_q)\delta(y - y_r) = 0 \quad (4.9a)$$

$$\frac{\partial M_{xy}}{\partial x} + \frac{\partial M_y}{\partial y} - Q_y + \sum_{c=0}^{m}\sum_{d=0}^{n} \overline{P}_{2cd}\delta(x - x_c)\delta(y - y_d) = 0 \quad (4.9b)$$

$$\frac{\partial M_x}{\partial x} + \frac{\partial M_{xy}}{\partial y} - Q_x - \sum_{c=0}^{m}\sum_{d=0}^{n} \overline{P}_{3cd}\delta(x - x_c)\delta(y - y_d) = 0 \quad (4.9c)$$

$$\frac{\partial \theta_x}{\partial x} + \nu\frac{\partial \theta_y}{\partial y} = \frac{M_x}{D} \quad (4.9d)$$

$$\frac{\partial \theta_y}{\partial y} + \nu\frac{\partial \theta_x}{\partial x} = \frac{M_y}{D} \quad (4.9e)$$

$$\frac{\partial \theta_x}{\partial y} + \frac{\partial \theta_y}{\partial x} = \frac{2}{(1-\nu)} \frac{M_{xy}}{D} \tag{4.9f}$$

$$\frac{\partial w}{\partial x} + \theta_x = \frac{Q_x}{G t_s} \tag{4.9g}$$

$$\frac{\partial w}{\partial y} + \theta_y = \frac{Q_y}{G t_s} \tag{4.9h}$$

where Q_x, Q_y are the shearing forces, M_{xy} is the twisting moment, M_x, M_y are the bending moments, θ_x, θ_y are the slopes, w is the deflection, $D = Eh^3/12(1-\nu^2)$ is the flexural rigidity of the plate, E is the modulus of elasticity, G is the shear modulus of elasticity, ν is Poisson's ratio, $h = h(x,y)$ is the thickness of the plate, $t_s = h/1.2$, $\overline{P}_{1cd}$ is vertical reaction of the point support at (x_c, y_d), $\overline{P}_{2cd}$ and $\overline{P}_{3cd}$ are moment reactions around x- and y-axis, respectively, $\delta(x-x_c)$, $\delta(y-y_d)$, $\delta(x-x_q)$ and $\delta(y-y_r)$ are Dirac's delta functions.

By introducing the following non-dimensional expressions,

$$[\,X_1 \quad X_2\,] = \frac{a^2}{D_0(1-\nu^2)}[\,Q_y \quad Q_x\,], [\,X_6 \quad X_7 \quad X_8\,] = [\,\theta_y \quad \theta_x \quad w/a\,]$$

$$[\,X_3 \quad X_4 \quad X_5\,] = \frac{a}{D_0(1-\nu^2)}[\,M_{xy} \quad M_y \quad M_x\,], [\,\eta \quad \zeta\,] = [\,x/a \quad y/b\,]$$

the differential equations (4.9a) $\sim$ (4.9h) are rearranged together as follows:

$$\sum_{e=1}^{8}[F_{1te}\frac{\partial X_e}{\partial \zeta} + F_{2te}\frac{\partial X_e}{\partial \eta} + F_{3te}X_e] + \sum_{f=1}^{3}\sum_{c=0}^{m}\sum_{d=0}^{n} P_{fcd}\delta(\eta-\eta_c)\delta(\zeta-\zeta_d)\delta_{ft} + P\delta(\eta-\eta_q)\delta(\zeta-\zeta_r)\delta_{1t} = 0 \tag{4.10}$$

where $t = 1 \sim 8, \mu = b/a, D_0 = Eh_0^3/12(1-\nu^2)$ is standard flexural rigidity of the plate, h_0 is the standard thickness of the plate, a and b are the length of the sides of the rectangular plate, $[P, P_{1cd}, P_{2cd}, P_{3cd}] = \nu a^2[\overline{P}a, \overline{P}_{1cd}a, \overline{P}_{2cd}, -\overline{P}_{3cd}]/D_0(1-\nu^2)$, δ_{ft} is Kronecker's delta, F_{1te}, F_{2te} and F_{3te} are expressed in section 1 of this chapter.

By integrating the above equation and applying the numerical integration in the same manner used in chapter 2, the following equation can be obtained:

$$X_{pij} = \sum_{k=0}^{i}\Big\{a_{1pijk1}(Q_y)_{k0} + a_{1pijk2}(M_{xy})_{k0} + a_{1pijk3}(M_y)_{k0} + a_{1pijk4}(\theta_y)_{k0} + a_{1pijk5}(\theta_x)_{k0} + a_{1pijk6}(w)_{k0}\Big\}$$

$$+ \sum_{l=0}^{j}\Big\{a_{2pijl1}(Q_x)_{0l} + a_{2pijl2}(M_{xy})_{0l} + a_{2pijl3}(M_x)_{0l}$$

$$+ a_{2pijl4}(\theta_y)_{0l} + a_{2pijl5}(\theta_x)_{0l} + a_{2pijl6}(w)_{0l}\Big\}$$

$$+ \sum_{f=1}^{3}\sum_{c=0}^{m}\sum_{d=0}^{n} \overline{q}_{fpijcd} P_{fcd} + \overline{q}_{pij} P \tag{4.11}$$

where $(Q_y) = X_1$, $(Q_x) = X_2$, $(M_{xy}) = X_3$, $(M_y) = X_4$, $(M_x) = X_5$, $(\theta_y) = X_6$, $(\theta_x) = X_7$, $(w) = X_8$, a_{1pijuv}, a_{2pijuv} and $\overline{q}_{fpijcd}$ are expressed in chapter 2, $\overline{q}_{pij}$ is shown in section 1 of this chapter.

The equation (4.11) gives the discrete solution of the fundamental differential equation (4.10) of a rectangular plate with a concentrated load and point supports. The discrete Green function $G(x_i, y_j, x_q, y_r)$ of the plate is obtained from X_{8ij}=$G(x_i, y_j, x_q, y_r)[\overline{P}/a]$ which is the displacement at a point (x_i, y_j) of the plate with a concentrated load $\overline{P}$ at a point (x_q, y_r).

4.3.3 Equivalent rectangular plate of right triangular plate

In chapter 2, equivalent rectangular plates have been obtained by translating the original irregular-shaped plates into rectangular plates with non-uniform thickness and intermediate point supports. Typical translations from some original right triangular plates into their equivalent rectangular plates are shown in Figure 4.29. In order to get more precise values, in this section, a clamped diagonal edge of an original plate shown in Figure 4.29 is translated into a line with some equally arranged point supports and an equally thick part with two clamped edges. The values of three reactions P_{1cd}, P_{2cd}, P_{3cd} at each point support of the equivalent plate are determined by three conditions, namely, $\theta_n = 0$, $\theta_t = 0$, $w = 0$. The first condition $\theta_n = 0$ means that the slope θ_n around the tangential axis of the line of point supports is zero. The second condition $\theta_t = 0$ means that the slope θ_t around the normal axis of the line of point supports is zero and the third condition $w = 0$ means the deflection w is zero. According to equations (2.12) and (2.13), the following equations can be obtained:

$$\theta_n = \theta_x \cos\alpha + \theta_y \sin\alpha \tag{4.12}$$

$$\theta_t = \theta_x \sin\alpha - \theta_y \cos\alpha \tag{4.13}$$

where $\alpha = tan^{-1}(a/b)$. Thus, the three restrained conditions can be expressed as

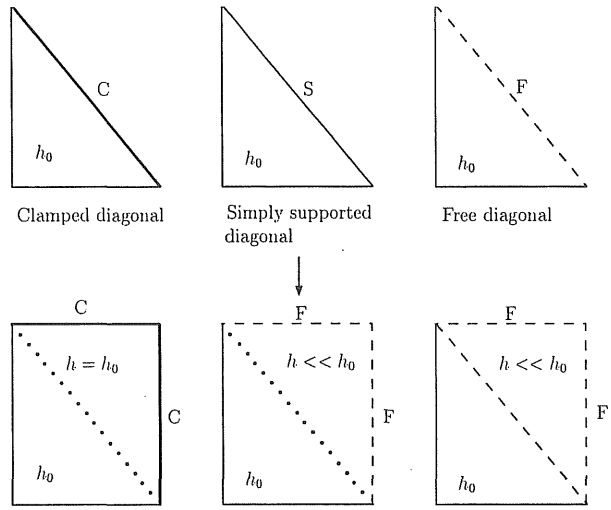

Figure 4.29: Triangular plates and their equivalent rectangular plates

follows:

$$\theta_n = \theta_x \sin\alpha + \theta_y \cos\alpha = 0 \tag{4.14a}$$

$$\theta_t = \theta_x \cos\alpha - \theta_y \sin\alpha = 0 \tag{4.14b}$$

$$w = 0 \tag{4.14c}$$

From the above equations, the following restrained conditions in non-dimensional form can be obtained:

$$X_6 = X_7 = X_8 = 0 \tag{4.15}$$

In Figure 4.29, the simply supported diagonal edge of an original plate is translated into a line with some equally arranged point supports and an additional extremely thin part with two free edges. According to equations (2.20a) $\sim$ (2.20c), the restrained conditions at point supports are as follows:

$$X_M = X_5 \cos^2\alpha + X_4 \sin^2\alpha + 2X_3 \sin\alpha\cos\alpha = 0 \tag{4.16a}$$

$$X_\theta = X_7 \sin\alpha - X_6 \cos\alpha = 0 \tag{4.16b}$$

$$X_8 = 0 \tag{4.16c}$$

In Figure 4.29, a free diagonal edge of original plate is translated into an additional extremely thin part with two free edges.

4.3.4 Characteristic equation of free vibration of rectangular plate with non-uniform thickness and point supports

By applying the Green function $w(x_0, y_0, x, y)/\overline{P}$ which is the displacement at a point (x_0, y_0) of the plate with a unite concentrated load at a point (x, y), the displacement amplitude $\hat{w}(x_0, y_0)$ at a point (x_0, y_0) of the equivalent rectangular plate during the free vibration is given as follows:

$$\hat{w}(x_0, y_0) = \int_0^b \int_0^a \rho h \omega^2 \hat{w}(x, y)[w(x_0, y_0, x, y)/\overline{P}]dxdy \tag{4.17}$$

where ρ is the mass density of the plate material. By using the non-dimensional expressions,

$$\lambda^4 = \frac{\rho_0 h_0 \omega^2 a^4}{D_0(1-\nu^2)}, \quad H(\eta, \zeta) = \frac{\rho(x, y)}{\rho_0}\frac{h(x, y)}{h_0},$$
$$W(\eta, \zeta) = \frac{\hat{w}(x, y)}{a}, \quad G(\eta_0, \zeta_0, \eta, \zeta) = \frac{w(x_0, y_0, x, y)}{a}\frac{D_0(1-\nu^2)}{\overline{P}a}$$

where ρ_0 is standard mass density.

The integral equation (4.17) can be rewritten as follows:

$$W(\eta_0, \zeta_0) = \int_0^1 \int_0^1 \mu\lambda^4 H(\eta, \zeta) G(\eta_0, \zeta_0, \eta, \zeta) W(\eta, \zeta) d\eta d\zeta \tag{4.18}$$

By applying the numerical integration method mentioned in chapter 2, equation (4.18) is discretely expressed as

$$\Lambda W_{kl} = \sum_{i=0}^{m}\sum_{j=0}^{n} \beta_{mi}\beta_{nj} H_{ij} G_{klij} W_{ij}, \quad \Lambda = 1/(\mu\lambda^4) \tag{4.19}$$

From equation (4.19), homogeneous linear equations in $(m+1) \times (n+1)$ unknowns $W_{00}, W_{01}, \cdots, W_{0n}$, $W_{10}, W_{11}, \cdots, W_{1n}, \cdots W_{m0}, W_{m1}, \cdots, W_{mn}$ are obtained as follows.

$$\sum_{i=0}^{m}\sum_{j=0}^{n}(\beta_{mi}\beta_{nj} H_{ij} G_{klij} - \Lambda\delta_{ik}\delta_{jl})W_{ij} = 0, (k = 0, 1, \cdots, m, l = 0, 1, \cdots, n) \tag{4.20}$$

The characteristic equation of the free vibration of a rectangular plate with variable thickness and point supports obtained from equation (4.20) is given by

$$\begin{vmatrix} K_{00} & K_{01} & K_{02} & \dots & K_{0m} \\ K_{10} & K_{11} & K_{12} & \dots & K_{1m} \\ K_{20} & K_{21} & K_{22} & \dots & K_{2m} \\ \vdots & \vdots & \vdots & \ddots & \vdots \\ K_{m0} & K_{m1} & K_{m2} & \dots & K_{mm} \end{vmatrix} = 0 \tag{4.21}$$

where

$$\mathbf{K_{ij}} = \beta_{mj} \begin{bmatrix} \beta_{n0}H_{j0}G_{i0j0} - \Lambda\delta_{ij} & \beta_{n1}H_{j1}G_{i0j1} & \cdots & \beta_{nn}H_{jn}G_{i0jn} \\ \beta_{n0}H_{j0}G_{i1j0} & \beta_{n1}H_{j1}G_{i1j1} - \Lambda\delta_{ij} & \cdots & \beta_{nn}H_{jn}G_{i1jn} \\ \vdots & \vdots & \ddots & \vdots \\ \beta_{n0}H_{j0}G_{inj0} & \beta_{n1}H_{j1}G_{inj1} & \cdots & \beta_{nn}H_{jn}G_{injn} - \Lambda\delta_{ij} \end{bmatrix}$$

From equation (4.21), the values of the natural frequency parameter λ can be obtained.

4.3.5 Numerical work

Numerical solutions for the natural frequency parameter λ and the mode have been investigated for right triangular plates with four kinds of boundary conditions SCS, SSS, SFC and CFF, as shown in Figure 4.30. The symbolism used for the boundary conditions will identify a right triangle plate with the edge $y = 0$ ($\zeta = 0$), the diagonal

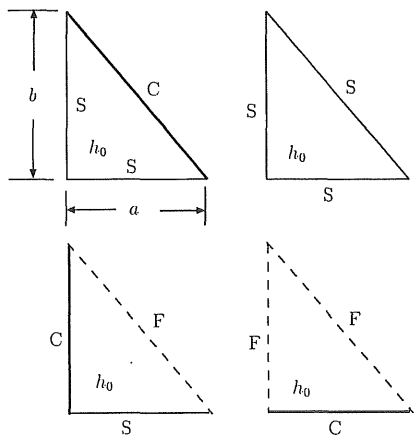

Figure 4.30: Right triangular plates with various boundary conditions

edge and the edge $x = 0$ ($\eta = 0$). The convergent values for the natural frequency parameter λ have been obtained by using Richardson's extrapolation formula for two cases of combinations of divisional numbers m and n.

[1] Convergency and accuracy of numerical results for right triangular plates with uniform or linearly varying thickness

In order to examine the convergency of numerical values for the natural frequency parameter λ and determine the suitable divisional numbers m and n, the analysis is carried out for isosceles right triangular plate with uniform thickness and four boundary conditions shown in Figure 4.30. The lowest eight values of the natural frequency parameter λ are shown in Figures 4.31. These results show the good convergency of

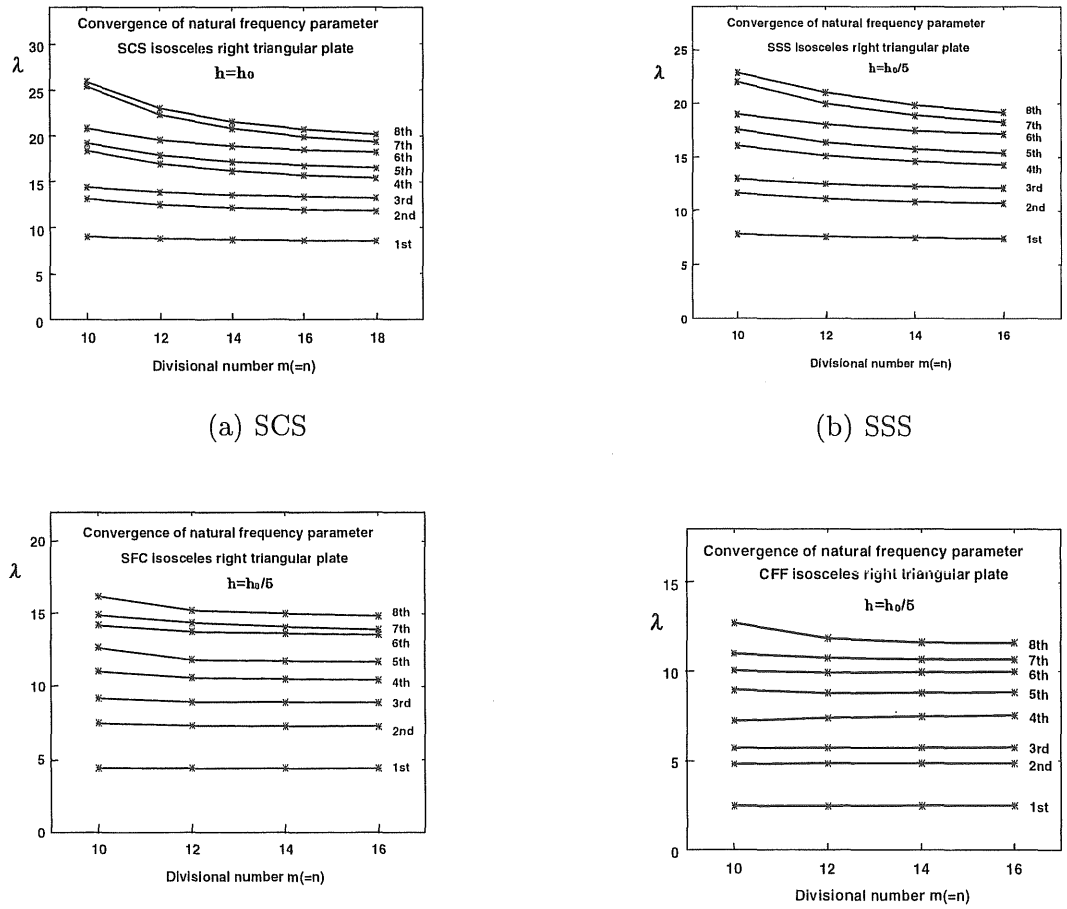

(a) SCS

(b) SSS

(c) SFC

(d) CFF

Figure 4.31: Convergence of natural frequency parameter λ of isosceles right triangular plates with different boundary conditions.

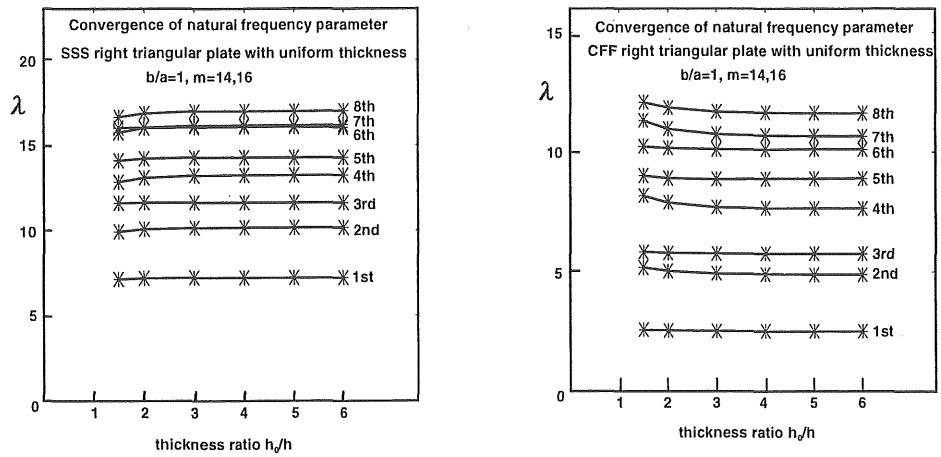

(a) SSS (b) CFF

Figure 4.32: Convergence of natural frequency parameter of right triangular plates with different boundary conditions.

numerical solutions by the proposed method. After studying the curves of Figure 4.31, the divisional numbers m and n are chosen to be 16 and 18 for SCS right triangular plates and to be 14 and 16 for SSS, SFC and CFF right triangular plates. In order to determine the suitable values of the thickness ratio h_0/h, the lowest eight values of the natural frequency parameter λ for isosceles right triangular plates with SSS and CFF are shown in Figure 4.32. After studying the curves of Figure 4.32, the thickness ratio is chosen to be 1/5 for the right triangular plate with simply supported or free diagonal edge. In order to demonstrate the accuracy of numerical results for the natural frequency parameter λ obtained by the proposed method, the lowest eight natural frequency parameters for the four right triangular plates with two aspect ratios, b/a=1 and 1.5 are presented in Tables 4.21 $\sim$ 4.24 and compared with previously published results by Kim and Dickinson [13] for the uniform thickness plates and by Liew, Lim and Lim [53] for the linearly varying thickness plates. The thickness ratio h_0/a of these plates is 0.01. In these examples, the SSS and CFF plates with the aspect ratio $b/a = 1$ have linearly varying thickness, the other plates have uniform thickness. The thickness variations of the two plates are as follows:

$$\text{SSS plate} : h(\eta, \zeta) = h_0(1 - 0.5\zeta) \tag{4.22}$$

$$\text{CFF plate} : h(\eta, \zeta) = h_0(1 - \zeta) \tag{4.23}$$

Table 4.21: Natural frequency parameters λ for SCS right triangular plates

	$b/a = 1$, uniform				$b/a = 1.5$, uniform			
	m		Nu.	Ref.	m		Nu.	Ref.
Mode	16	18	Solu.	[13]	16	18	Solu.	[13]
1	8.602	8.548	8.343	8.305	7.196	7.149	6.973	6.940
2	11.945	11.804	11.272	11.267	9.785	9.669	9.233	9.230
3	13.374	13.246	12.766	12.726	11.356	11.238	10.796	10.768
4	15.697	15.396	14.261	14.378	12.598	12.365	11.486	11.556
5	16.758	16.483	15.446	15.575	14.177	13.924	12.973	13.080
6	18.492	18.220	17.198	17.288	15.616	15.227	13.762	13.915
7	19.902	19.334	17.193	–	15.828	15.547	14.489	–
8	20.709	20.176	18.170	–	17.363	16.898	15.146	–

Table 4.22: Natural frequency parameters λ for SSS right triangular plates

	$b/a = 1$, variable (eq. (4.22))				$b/a = 1.5$, uniform			
	m		Nu.	Ref.	m		Nu.	Ref.
Mode	14	16	Solu.	[53]	14	16	Solu.	[13]
1	6.914	6.826	6.539	6.592	6.291	6.211	5.952	5.995
2	9.923	9.705	8.992	9.162	8.981	8.793	8.180	8.298
3	11.405	11.229	10.652	10.693	10.492	10.312	9.726	9.820
4	13.187	12.881	11.882	11.887	11.855	11.525	10.447	10.640
5	14.590	14.149	12.709	13.074	13.397	13.071	12.007	12.153
6	16.303	15.918	14.662	14.623	14.929	14.478	13.008	13.028
7	16.763	16.327	14.905	14.830	15.134	14.693	13.254	-
8	18.155	17.565	15.641	15.746	16.614	16.069	14.289	-

Table 4.23: Natural frequency parameters λ for SFC right triangular plates

	$b/a = 1$, uniform				$b/a = 1.5$, uniform			
	m		Nu.	Ref.	m		Nu.	Ref.
Mode	14	16	Solu.	[13]	14	16	Solu.	[13]
1	4.390	4.385	4.372	4.340	3.839	3.834	3.817	3.798
2	7.280	7.253	7.163	7.090	6.104	6.079	5.995	5.940
3	8.910	8.886	8.808	8.786	7.614	7.588	7.503	7.465
4	10.511	10.438	10.202	10.089	8.617	8.551	8.333	8.281
5	11.751	11.685	11.470	11.378	9.927	9.858	9.631	9.532
6	13.659	13.569	13.279	13.195	11.269	11.131	10.681	10.621
7	14.090	13.913	13.336	–	11.666	11.597	11.373	–
8	15.017	14.850	14.312	–	12.622	12.494	12.074	–

Table 4.24: Natural frequency parameters λ for CFF right triangular plates

	$b/a = 1$, variable (eq. (4.23))				$b/a = 1.5$, uniform			
	m		Nu.	Ref.	m		Nu.	Ref.
Mode	14	16	Solu.	[53]	14	16	Solu.	[13]
1	2.714	2.722	2.748	2.763	1.682	1.687	1.705	1.736
2	4.193	4.196	4.205	4.217	3.488	3.492	3.506	3.563
3	4.889	4.908	4.971	5.048	4.190	4.204	4.250	4.322
4	5.768	5.765	5.765	5.729	5.505	5.506	5.509	5.576
5	6.617	6.584	6.476	6.598	6.522	6.537	6.588	6.695
6	7.504	7.470	7.361	7.353	7.656	7.632	7.555	7.660
7	8.027	7.973	7.793	7.894	8.289	8.270	8.210	–
8	8.883	8.848	8.733	8.775	9.071	9.041	8.941	–

The effects of boundary conditions and aspect ratios can be seen from the Tables 4.21 $\sim$ 4.24. For these four kinds of plates with uniform and $b/a = 1.5$, the lowest fundamental frequency parameter is found for the CFF plate and the highest one for SCS plate. By comparing the values in Tables 4.21 and 4.23, it can be found the vibration frequency parameters tend to decrease as the aspect ratio b/a increases for SCS and SFC plates. Tables 4.21 $\sim$ 4.24 show that a close agreement is achieved. In figures 4.33 $\sim$ 4.36, the corresponding nodal patterns are presented, and these are also confirmed to agree with the nodal patterns given by Refs,[13] and [53].

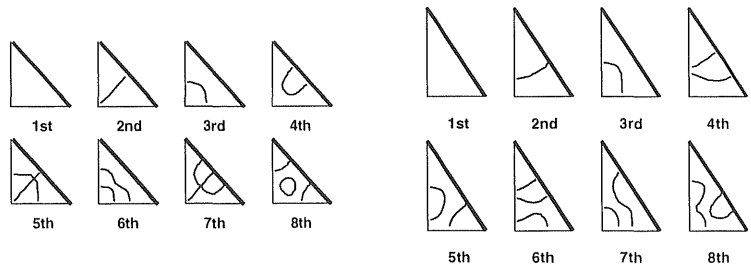

(a) (b)

Figure 4.33: Nodal patterns for SCS right triangular plate. (a) b/a=1; (b) b/a=1.5.

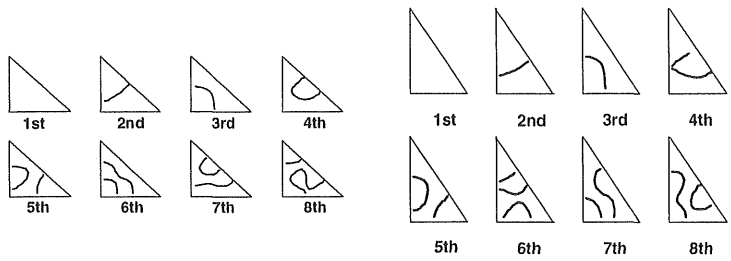

(a) (b)

Figure 4.34: Nodal patterns for SSS right triangular plate. (a) b/a=1; (b) b/a=1.5.

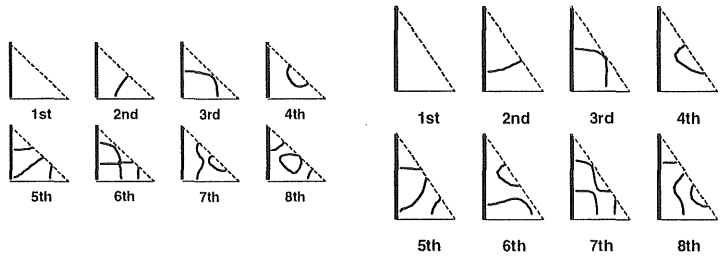

(a) (b)

Figure 4.35: Nodal patterns for SFC right triangular plate. (a) b/a=1; (b) b/a=1.5.

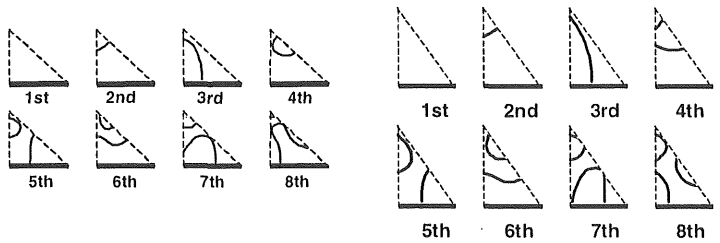

(a) (b)

Figure 4.36: Nodal patterns for CFF right triangular plate. (a) b/a=1; (b) b/a=1.5.

[2] Numerical results for right triangular plates with variable thickness

Tables 4.25 and 4.26 present the lowest eight numerical values of the natural frequency parameter λ of SCS and CFF right triangular plates with variable thickness and two aspect ratios, b/a=1 and 1.5. The thickness variations of these plates are each as

follows:

$$\text{SCS plate:} \quad h(\eta,\zeta) = h_0[1 + \sin 0.5\pi(\eta+\zeta)] \tag{4.24}$$

$$\text{CFF plate:} \quad h(\eta,\zeta) = h_0[1 - 0.5(\eta^2+\zeta^2)] \tag{4.25}$$

Table 4.25: Natural frequency parameters λ for SCS right triangular plates with variable thickness (eq.(4.24))

	$b/a = 1$			$b/a = 1.5$		
	m		Nu.	m		Nu.
Mode	16	18	Solu.	16	18	Solu.
1	11.340	11.272	11.014	9.486	9.440	9.269
2	15.920	15.756	15.139	13.016	12.880	12.371
3	17.268	17.126	16.593	14.750	14.590	13.988
4	20.818	20.468	19.151	16.665	16.390	15.357
5	21.953	21.631	20.420	18.729	18.435	17.328
6	23.634	23.288	21.985	20.582	20.077	18.178
7	26.181	25.536	23.105	20.176	19.919	18.953
8	26.982	26.389	24.156	22.957	22.407	20.336

Table 4.26: Natural frequency parameters λ for CFF right triangular plates with variable thickness (eq:(4.25))

	$b/a = 1$			$b/a = 1.5$		
	m		Nu.	m		Nu.
Mode	14	16	Solu.	14	16	Solu.
1	2.479	2.487	2.513	1.673	1.679	1.699
2	4.504	4.514	4.545	3.243	3.249	3.270
3	5.459	5.473	5.520	3.978	3.992	4.037
4	6.724	6.767	6.908	4.990	4.992	4.997
5	7.885	7.933	8.092	5.913	5.929	5.980
6	9.051	9.075	9.154	6.924	6.912	6.870
7	9.787	9.749	9.632	7.430	7.414	7.363
8	10.357	10.331	10.248	8.353	8.333	8.268

The thickness ratio h_0/a of these plates is 0.01. The corresponding nodal patterns are presented in Figures 4.37 and 4.38.

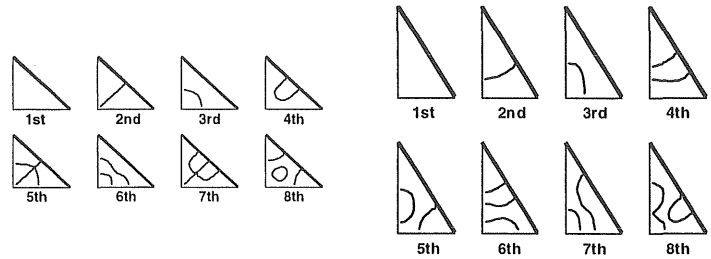

(a) (b)

Figure 4.37: Nodal patterns for SCS right triangular plate with variable thickness. (a) b/a=1; (b) b/a=1.5.

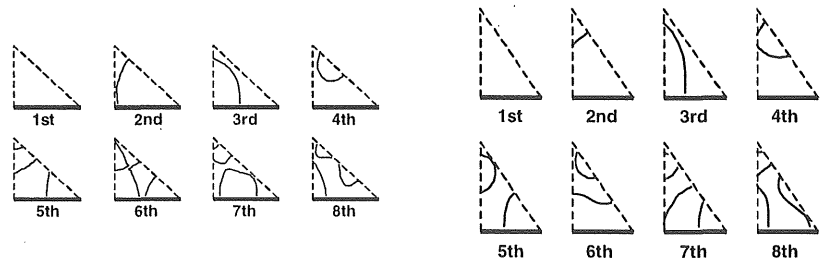

(a) (b)

Figure 4.38: Nodal patterns for CFF right triangular plate with variable thickness. (a) b/a=1; (b) b/a=1.5.

[3] Numerical results for right triangular plates with moderate thickness

The lowest eight numerical values of the natural frequency parameter λ are shown in Table 4.27 and Table 4.28 for SSS and SFC moderately thick right triangular plates with two aspect ratios, b/a=1 and 1.5. The thickness ratio h_0/a of these plates is 0.2. The corresponding nodal patterns are shown in Figure 4.39 and Figure 4.40.

Table 4.27: Natural frequency parameters λ for SSS right triangular plates with moderate thickness

	$b/a = 1$			$b/a = 1.5$		
	m		Nu.	m		Nu.
Mode	14	16	Solu.	14	16	Solu.
1	6.632	6.589	6.477	5.694	5.660	5.558
2	8.793	8.716	8.465	7.530	7.483	7.252
3	9.606	9.534	9.299	8.543	8.473	8.245
4	10.788	10.644	10.174	9.269	9.138	8.711
5	11.304	11.171	10.737	10.117	9.984	9.552
6	12.102	11.969	11.537	10.857	10.656	9.998
7	12.674	12.429	11.626	10.958	10.811	10.331
8	13.017	12.785	12.028	11.670	11.445	10.712

Table 4.28: Natural frequency parameters λ for SFC right triangular plates with moderate thickness

	$b/a = 1$			$b/a = 1.5$		
	m		Nu.	m		Nu.
Mode	14	16	Solu.	14	16	Solu.
1	4.124	4.119	4.102	3.644	3.640	3.626
2	6.402	6.381	6.311	5.513	5.494	5.433
3	7.539	7.523	7.468	6.602	6.588	6.542
4	8.520	8.468	8.300	7.314	7.267	7.112
5	9.314	9.268	9.119	8.49	8.108	7.976
6	10.293	10.241	10.073	8.985	8.890	8.580
7	10.531	10.432	10.107	9.177	9.134	8.995
8	11.037	10.946	10.646	9.750	9.663	9.381

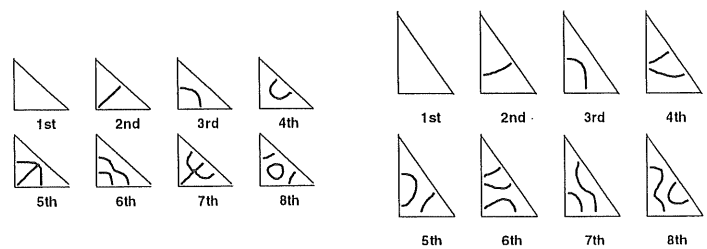

(a) (b)

Figure 4.39: Nodal patterns for SSS right triangular plate with moderate thickness. (a) b/a=1; (b) b/a=1.5.

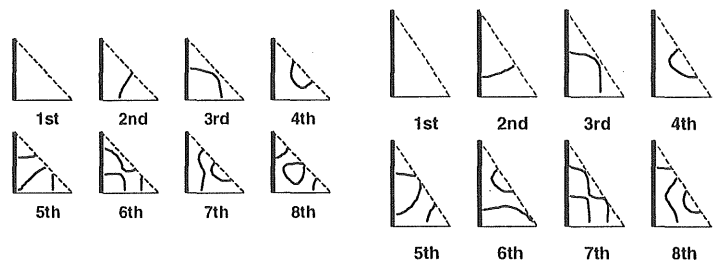

(a) (b)

Figure 4.40: Nodal patterns for SFC right triangular plate with moderate thickness. (a) b/a=1; (b) b/a=1.5.

4.3.6 Conclusions

In this section, the discrete method has been proposed for the free vibration analysis of right triangular plates with variable thickness. The main conclusions are summarized as follows:

1. Under the concept that a right triangular plate can be considered finally as a kind of rectangular plates with non-uniform thickness, the discrete method is used to analyze the free vibration problems of right triangular plates. Green function is obtained by the displacement function of the equivalent rectangular plate with a unit concentrated load and point supports. Characteristic equation of free vibration of right triangular plates has been established.

2. Frequency parameters and modes of free vibration have been presented for plates with various thickness, different boundary conditions, aspect ratios and thickness ratios. The effects of these conditions on the natural frequency parameters and nodal lines of modes of free vibration are discussed and illustrated in tables and figures.

3. The numerical results compared with previously published ones show that the numerical solutions by the discrete method have good convergency and adequate accuracy.

Chapter 5

Elasto-plastic analysis of rectangular plates with hole

5.1 Introduction

In previous chapters, the discrete method has been proposed for the elastic analysis of bending and free vibration problems of irregular-shaped plates. All these plates are in elastic state and Hook's law can be used. In this chapter, the same method is extended for the elasto-plastic bending analysis of square plates with various-shaped holes. In plastic region, the strain depends on not only the final state of stress, but also the loading history, so the stress-strain relationships are no more unique. In order to analyze this kind of problem, the stress-strain relationships in incremental form and stress yield criteria are used.

In this chapter, by adding a thin part, a rectangular plate with hole can be considered as an equivalent rectangular plate with variable thickness shown in Figure 5.1. Therefore the elasto-plastic bending problem of a rectangular plate with hole can be replaced by the elasto-plastic bending problem of the equivalent rectangular plate. The Prandtle-Reuss's law and von Mises yield criteria are used. Under the assumptions that the increments are infinitesimal and all the governing equations may be linearized in each increment, the fundamental differential equations of elasto-plastic bending problem of rectangular plates with various thickness and point supports are derived. Then, the discrete solutions are obtained by translating the differential equations into integral equations and applying numerical integration. In order to consider the expansion of the yield regions in the direction of the thickness of the plate, the thickness of the plate is divided into many layers. Numerical results are carried out for square plates with square, triangular or circular hole and compared with previously published results.

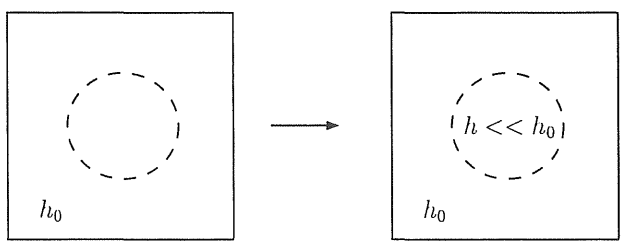

Figure 5.1: Example of equivalent plate

The convergency and accuracy of the solutions obtained by the proposed method are investigated.

5.2 Fundamental differential equations and discrete solutions

5.2.1 Stress-strain relationships

The stress-strain relationships of plane stress problems proposed in Ref. [54] can be expressed as follows:

$$\begin{bmatrix} \Delta\sigma_x \\ \Delta\sigma_y \\ \Delta\tau_{xy} \end{bmatrix} = \frac{E}{1-\nu^2} \begin{bmatrix} 1 & \nu & 0 \\ \nu & 1 & 0 \\ 0 & 0 & (1-\nu)/2 \end{bmatrix} \begin{bmatrix} \Delta\varepsilon_x \\ \Delta\varepsilon_y \\ \Delta\gamma_{xy} \end{bmatrix} - \frac{1}{S} \begin{bmatrix} S_1^2 & S_1S_2 & S_1S_3 \\ S_1S_2 & S_2^2 & S_2S_3 \\ S_1S_3 & S_2S_3 & S_3^2 \end{bmatrix} \begin{bmatrix} \Delta\varepsilon_x \\ \Delta\varepsilon_y \\ \Delta\gamma_{xy} \end{bmatrix} \tag{5.1}$$

where

$$S_1 = \frac{E}{1-\nu^2}(\sigma_x' + \nu\sigma_y'), \quad S_2 = \frac{E}{1-\nu^2}(\nu\sigma_x' + \sigma_y')$$
$$S_3 = \frac{E}{1+\nu}\tau_{xy}', \quad S = S_1\sigma_x' + S_2\sigma_y' + 2S_3\tau_{xy}' \tag{5.2}$$

Substituting equation (5.2) into equation (5.1), the following equation can be obtained:

$$\begin{bmatrix} \Delta\sigma_x \\ \Delta\sigma_y \\ \Delta\tau_{xy} \end{bmatrix} = \frac{E}{1-\nu^2} \begin{bmatrix} 1 & \nu & 0 \\ \nu & 1 & 0 \\ 0 & 0 & (1-\nu)/2 \end{bmatrix} \begin{bmatrix} \Delta\varepsilon_x \\ \Delta\varepsilon_y \\ \Delta\gamma_{xy} \end{bmatrix} - \frac{E}{1-\nu^2}\frac{1}{d} \begin{bmatrix} a^2 & ab & ac \\ ab & b^2 & bc \\ ac & bc & c^2 \end{bmatrix} \begin{bmatrix} \Delta\varepsilon_x \\ \Delta\varepsilon_y \\ \Delta\gamma_{xy} \end{bmatrix} \tag{5.3}$$

where $a = \sigma_x' + \nu\sigma_y'$, $b = \nu\sigma_x' + \sigma_y'$, $c = (1-\nu)\tau_{xy}'$, $d = a\sigma_x' + b\sigma_y' + 2c\tau_{xy}'$.

σ_x', σ_y' and τ_{xy}' are deviatoric stresses and expressed as follows:

$$\sigma_x' = \frac{2\sigma_x - \sigma_y}{3}, \quad \sigma_y' = \frac{2\sigma_y - \sigma_x}{3}, \quad \tau_{xy}' = \tau_{xy}$$

5.2.2 Moment-displacement relationships

Rewriting the equation (5.3), the following equation can be obtained:

$$\begin{bmatrix} \Delta\sigma_x \\ \Delta\sigma_y \\ \Delta\tau_{xy} \end{bmatrix} = \frac{E}{1-\nu^2} \begin{bmatrix} \alpha_{11} & \alpha_{12} & \alpha_{13} \\ \alpha_{11} & \alpha_{12} & \alpha_{13} \\ \alpha_{11} & \alpha_{12} & \alpha_{13} \end{bmatrix} \begin{bmatrix} \Delta\varepsilon_x \\ \Delta\varepsilon_y \\ \Delta\gamma_{xy} \end{bmatrix}$$
$$= \frac{Ez}{1-\nu^2} \begin{bmatrix} \alpha_{11} & \alpha_{12} & \alpha_{13} \\ \alpha_{11} & \alpha_{12} & \alpha_{13} \\ \alpha_{11} & \alpha_{12} & \alpha_{13} \end{bmatrix} \begin{bmatrix} \Delta\beta_x \\ \Delta\beta_y \\ \Delta\beta_{xy} \end{bmatrix} \tag{5.4}$$

where $\Delta\varepsilon_x = z\Delta\beta_x \quad \Delta\varepsilon_y = z\Delta\beta_y \quad \Delta\tau_{xy} = z\Delta\beta_{xy}$

$$\Delta\beta_x = \frac{\partial\Delta\theta_x}{\partial x} \quad \Delta\beta_y = \frac{\partial\Delta\theta_y}{\partial y} \quad \Delta\beta_{xy} = \frac{\partial\Delta\theta_x}{\partial y} + \frac{\partial\Delta\theta_y}{\partial x}$$

Considering moment-stress relationships,

$$\Delta M_x = \int_{-\frac{h}{2}}^{\frac{h}{2}} z\Delta\sigma_x dz \tag{5.5a}$$

$$\Delta M_y = \int_{-\frac{h}{2}}^{\frac{h}{2}} z\Delta\sigma_y dz \tag{5.5b}$$

$$\Delta M_{xy} = \int_{-\frac{h}{2}}^{\frac{h}{2}} z\Delta\tau_{xy} dz \tag{5.5c}$$

moment-displacement relationships can be obtained as:

$$\Delta M_x = \frac{E}{1-\nu^2} \int_{-\frac{h}{2}}^{\frac{h}{2}} z^2(\alpha_{11}\Delta\beta_x + \alpha_{12}\Delta\beta_y + \alpha_{13}\Delta\beta_{xy})dz$$
$$= \frac{Eh^3}{12(1-\nu^2)} \left[(\frac{12}{h^3} \int_{-\frac{h}{2}}^{\frac{h}{2}} \alpha_{11} z^2 dz)\Delta\beta_x \right.$$
$$\left. + (\frac{12}{h^3} \int_{-\frac{h}{2}}^{\frac{h}{2}} \alpha_{12} z^2 dz)\Delta\beta_x + (\frac{12}{h^3} \int_{-\frac{h}{2}}^{\frac{h}{2}} \alpha_{13} z^2 dz)\Delta\beta_x \right]$$

Introducing the notations $\xi = z/h$ and

$$a_{ij} = \frac{12}{h^3} \int_{-\frac{h}{2}}^{\frac{h}{2}} \alpha_{ij} z^2 dz = 12 \int_{-\frac{1}{2}}^{\frac{1}{2}} \alpha_{ij} \xi^2 d\xi$$

the above equation is represented as

$$\Delta M_x = D[a_{11}\Delta\beta_x + a_{12}\Delta\beta_y + a_{13}\Delta\beta_{xy}] \tag{5.6}$$

where $D = Eh^3/[12(1-\nu^2)]$.

In the same manner, the following two equations can be obtained:

$$\Delta M_y = D[a_{21}\Delta\beta_x + a_{22}\Delta\beta_y + a_{23}\Delta\beta_{xy}] \tag{5.7}$$

$$\Delta M_{xy} = D[a_{31}\Delta\beta_x + a_{32}\Delta\beta_y + a_{33}\Delta\beta_{xy}] \tag{5.8}$$

Rewriting equations (5.6) $\sim$ (5.8) in matrix form:

$$\begin{bmatrix} \Delta M_x \\ \Delta M_y \\ \Delta M_{xy} \end{bmatrix} = D \begin{bmatrix} a_{11} & a_{12} & a_{13} \\ a_{21} & a_{22} & a_{23} \\ a_{31} & a_{32} & a_{33} \end{bmatrix} \begin{bmatrix} \Delta\beta_x \\ \Delta\beta_y \\ \Delta\beta_{xy} \end{bmatrix} \tag{5.9}$$

5.2.3 Fundamental differential equations

In order to obtain the fundamental differential equations of plates with variable thickness and point supports, the rectangular Cartesian coordinates (x, y, z) are used. The xy plane is taken as the middle plane of the plate. The positive direction of the z axis is downward and the origin o is at the corner of the plate, as shown in Figure 5.2. The fundamental differential equations in incremental forms are presented as follows.

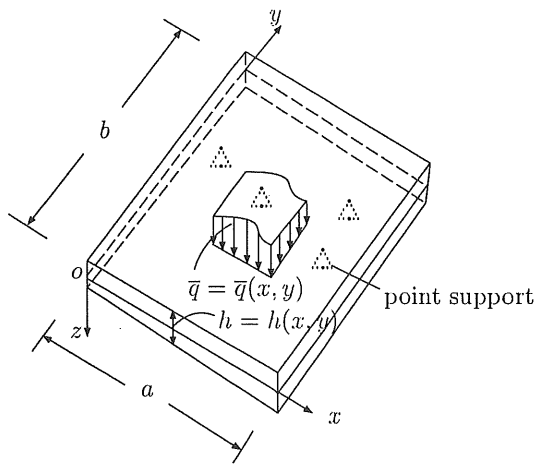

Figure 5.2: Rectangular Plate and Coordinate System

$$\frac{\partial\Delta Q_x}{\partial x} + \frac{\partial\Delta Q_y}{\partial y} + \Delta\overline{q} + \sum_{c=0}^{m}\sum_{d=0}^{n}\Delta\overline{P}_{1cd}\delta(x - x_c)\delta(y - y_d) = 0 \tag{5.10a}$$

$$\frac{\partial\Delta M_{xy}}{\partial x} + \frac{\partial\Delta M_y}{\partial y} - \Delta Q_y + \sum_{c=0}^{m}\sum_{d=0}^{n}\Delta\overline{P}_{2cd}\delta(x - x_c)\delta(y - y_d) = 0 \tag{5.10b}$$

$$\frac{\partial\Delta M_x}{\partial x} + \frac{\partial\Delta M_{xy}}{\partial y} - \Delta Q_x - \sum_{c=0}^{m}\sum_{d=0}^{n}\Delta\overline{P}_{3cd}\delta(x - x_c)\delta(y - y_d) = 0 \tag{5.10c}$$

$$\frac{\partial \Delta\theta_x}{\partial x} = \frac{1}{D}(b_{11}\Delta M_x + b_{12}\Delta M_y + b_{13}\Delta M_{xy}) \tag{5.10d}$$

$$\frac{\partial \Delta\theta_y}{\partial y} = \frac{1}{D}(b_{21}\Delta M_x + b_{22}\Delta M_y + b_{23}\Delta M_{xy}) \tag{5.10e}$$

$$\frac{\partial \Delta\theta_x}{\partial y} + \frac{\partial \Delta\theta_y}{\partial x} = \frac{1}{D}(b_{31}\Delta M_x + b_{32}\Delta M_y + b_{33}\Delta M_{xy}) \tag{5.10f}$$

$$\frac{\partial \Delta w}{\partial x} + \Delta\theta_x = \frac{\Delta Q_x}{Gt_s} \tag{5.10g}$$

$$\frac{\partial \Delta w}{\partial y} + \Delta\theta_y = \frac{\Delta Q_y}{Gt_s} \tag{5.10h}$$

where $\Delta Q_x, \Delta Q_y$ are increments of the shearing forces Q_x, Q_y, ΔM_{xy} is increment of the twisting moment M_{xy}, $\Delta M_x, \Delta M_y$ are increments of the bending moments M_x, M_y, $\Delta\theta_x, \Delta\theta_y$ are increments of the slopes θ_x, θ_y, Δw is increment of the deflection w, Δq is increment of the load q, $\Delta\overline{P}_{1cd}$ is increment of the vertical reaction $\overline{P}_{1cd}$ of the point support at (x_c, y_d), $\Delta\overline{P}_{2cd}$ and $\Delta\overline{P}_{3cd}$ are the increments of the moment reactions around x- and y-axis, respectively; $D = Eh^3/12(1-\nu^2)$ is the flexural rigidity of the plate, E is modulus of elasticity, G is shear modulus of elasticity, ν is Poisson's ratio, $h = h(x, y)$ is the thickness of the plate, $t_s = h/1.2$, $[b_{ij}]$=$[a_{ij}]^{-1}$.

5.2.4 Discrete solutions of fundamental differential equations

By introducing the following non-dimensional expressions,

$$[X_1 \quad X_2] = \frac{a^2}{D_0(1-\nu^2)}[Q_y \quad Q_x], [X_6 \quad X_7 \quad X_8] = [\theta_y \quad \theta_x \quad w/a]$$

$$[X_3 \quad X_4 \quad X_5] = \frac{a}{D_0(1-\nu^2)}[M_{xy} \quad M_y \quad M_x], [\eta \quad \zeta] = [x/a \quad y/b]$$

the differential equations (5.10a) $\sim$ (5.10h) can be rewritten as follows:

$$\sum_{e=1}^{8}[F_{1te}\frac{\partial \Delta X_e}{\partial \zeta} + F_{2te}\frac{\partial \Delta X_e}{\partial \eta} + F_{3te}\Delta X_e] + \delta_{1t}\Delta q + \sum_{f=1}^{3}\sum_{c=0}^{m}\sum_{d=0}^{n}\Delta P_{fcd}\delta(\eta-\eta_c)\delta(\zeta-\zeta_d)\delta_{ft} = 0 \tag{5.11}$$

where $t = 1 \sim 8, \mu = b/a, D_0 = Eh_0^3/12(1-\nu^2)$ is the standard flexural rigidity of the plate, h_0 is the standard thickness of the plate, a, b are the length and width of the rectangular plate, respectively, $\Delta q = \mu\Delta q_0 a^3/D_0(1-\nu^2)[\Delta\overline{q}(x,y)/\Delta q_0]$, Δq_0 is the standard load intensity, δ_{ft} is Kronecker's delta,

$$[\Delta P_{1cd} \quad \Delta P_{2cd} \quad \Delta P_{3cd}] = \mu a^2 [\Delta \overline{P}_{1cd} a \quad \Delta \overline{P}_{2cd} \quad -\Delta \overline{P}_{3cd}] / D_0(1-\nu^2)$$

$$F_{111} = F_{123} = F_{134} = F_{156} = F_{167} = F_{188} = F_{278} = F_{377} = 1.0,$$

$$F_{212} = F_{225} = F_{233} = F_{247} = F_{266} = F_{386} = -F_{322} = -F_{331} = \mu,$$

$$F_{345} = -b_{11}I,\ F_{344} = -b_{12}I,\ F_{343} = -b_{13}I,\ F_{355} = -b_{21}I,$$

$$F_{354} = -b_{22}I,\ F_{353} = -b_{23}I,\ F_{365} = -b_{31}I,\ F_{364} = -b_{32}I,\ F_{363} = -b_{33}I,$$

$$F_{372} = -K,\ F_{381} = -\mu K,\ \text{other } F_{ijk} = 0,\ I = \mu(1-\nu^2)(h_0/h)^3,$$

$$K = (1/10)(E/G)(h_0/a)^2(h_0/h)$$

By transforming differential equations into integral equations and applying numerical integration used in chapter 2, the discrete solutions of equation (5.11) are given by

$$\begin{aligned}
\Delta X_{pij} = &\sum_{k=0}^{i} \Big\{ a_{1pijk1}(\Delta Q_y)_{k0} + a_{1pijk2}(\Delta M_{xy})_{k0} + a_{1pijk3}(\Delta M_y)_{k0} \\
&\quad + a_{1pijk4}(\Delta \theta_y)_{k0} + a_{1pijk5}(\Delta \theta_x)_{k0} + a_{1pijk6}(\Delta w)_{k0} \Big\} \\
&+ \sum_{l=0}^{j} \Big\{ a_{2pijl1}(\Delta Q_x)_{0l} + a_{2pijl2}(\Delta M_{xy})_{0l} + a_{2pijl3}(\Delta M_x)_{0l} \\
&\quad + a_{2pijl4}(\Delta \theta_y)_{0l} + a_{2pijl5}(\Delta \theta_x)_{0l} + a_{2pijl6}(\Delta w)_{0l} \Big\} \\
&+ \Delta \overline{q}_{pij} + \sum_{f=1}^{3} \sum_{c=0}^{m} \sum_{d=0}^{n} \overline{q}_{fpijcd} \Delta P_{fcd}
\end{aligned} \tag{5.12}$$

where

$$\begin{aligned}
a_{hpijuv} = &\sum_{e=1}^{8} \Big\{ \sum_{k=0}^{i} \beta_{ik} A_{pe} [a_{hek0uv} - a_{hekjuv}(1-\delta_{ki})] \\
&\quad + \sum_{l=0}^{j} \beta_{jl} B_{pe} [a_{he0luv} - a_{heiluv}(1-\delta_{lj})] \\
&\quad + \sum_{k=0}^{i} \sum_{l=0}^{j} \beta_{ik}\beta_{jl} C_{pekl} a_{hekluv}(1-\delta_{ki}\delta_{lj}) \Big\} \\
\Delta \overline{q}_{pij} = &\sum_{e=1}^{8} \Big\{ \sum_{k=0}^{i} \beta_{ik} A_{pe} [\Delta \overline{q}_{ek0} - \Delta \overline{q}_{ekj}(1-\delta_{ki})] \\
&\quad + \sum_{l=0}^{j} \beta_{jl} B_{pe} [\Delta \overline{q}_{e0l} - \Delta \overline{q}_{eil}(1-\delta_{lj})] \\
&\quad + \sum_{k=0}^{i} \sum_{l=0}^{j} \beta_{ik}\beta_{jl} C_{pekl} \Delta \overline{q}_{ekl}(1-\delta_{ki}\delta_{lj}) \Big\}
\end{aligned}$$

$$
\begin{aligned}
&- \sum_{k=0}^{i}\sum_{l=0}^{j} \beta_{ik}\beta_{jl}\gamma_{p1}\Delta q_{kl} \\
\Delta\overline{q}_{fpijcd} = &\sum_{e=1}^{8}\Big\{\sum_{k=0}^{i} \beta_{ik}A_{pe}[\Delta\overline{q}_{fek0cd} - \Delta\overline{q}_{fekjcd}(1-\delta_{ki})] \\
&+ \sum_{l=0}^{j} \beta_{jl}B_{pe}[\Delta\overline{q}_{fe0lcd} - \Delta\overline{q}_{feilcd}(1-\delta_{lj})] \\
&+ \sum_{k=0}^{i}\sum_{l=0}^{j} \beta_{ik}\beta_{jl}C_{pekl}\Delta\overline{q}_{feklcd}(1-\delta_{ki}\delta_{lj})\Big\} \\
&- \gamma_{pf}u_{ic}u_{jd}\overline{u}_{fcd}
\end{aligned}
$$

Here $h = 1, 2, \quad p = 1, 2, \cdots, 8, \quad i = 1, 2, \cdots, m, \quad j = 1, 2, \cdots, n, \quad v = 1, 2, \cdots, 6$

$$
u = \begin{cases} 0, 1, \cdots, i & (h = 1) \\ 0, 1, \cdots, j & (h = 2) \end{cases}
\qquad
\overline{u}_{fcd} = \begin{cases} 0 : \text{not existing point support} \\ 1 : \text{existing point support} \end{cases}
$$

$A_{p1} = \gamma_{p1}$	$B_{p1} = 0$	$C_{p1kl} = \mu(\gamma_{p3} + k_{kl}\gamma_{p8})$
$A_{p2} = 0$	$B_{p2} = \mu\gamma_{p1}$	$C_{p2kl} = \mu\gamma_{p2} + k_{kl}\gamma_{p7}$
$A_{p3} = \gamma_{p2}$	$B_{p3} = \mu\gamma_{p3}$	$C_{p3kl} = I_{kl}(\gamma_{p4}b_{13kl} + \gamma_{p5}b_{23kl} + \gamma_{p6}b_{33kl})$
$A_{p4} = \gamma_{p3}$	$B_{p4} = 0$	$C_{p4kl} = I_{kl}(\gamma_{p4}b_{12kl} + \gamma_{p5}b_{22kl} + \gamma_{p6}b_{32kl})$
$A_{p5} = 0$	$B_{p5} = \mu\gamma_{p2}$	$C_{p5kl} = I_{kl}(\gamma_{p4}b_{11kl} + \gamma_{p5}b_{21kl} + \gamma_{p6}b_{31kl})$
$A_{p6} = \gamma_{p5}$	$B_{p6} = \mu\gamma_{p6}$	$C_{p6kl} = -\mu\gamma_{p8}$
$A_{p7} = \gamma_{p6}$	$B_{p7} = \gamma_{p4}$	$C_{p7kl} = -\gamma_{p7}$
$A_{p8} = \gamma_{p8}$	$B_{p8} = \gamma_{p7}$	$C_{p8kl} = 0$

$[\gamma_{pe}] = [\rho_{ep}]^{-1}$

$\rho_{11} = \beta_{ii}$	$\rho_{12} = \mu\beta_{jj}$	$\rho_{22} = -\mu\beta_{ij}$
$\rho_{23} = \beta_{ii}$	$\rho_{25} = \mu\beta_{jj}$	$\rho_{31} = -\mu\beta_{ij}$
$\rho_{33} = \mu\beta_{jj}$	$\rho_{34} = \beta_{ii}$	$\rho_{43} = -I_{ij}\beta_{ij}b_{13ij}$
$\rho_{44} = -I_{ij}\beta_{ij}b_{12ij}$	$\rho_{45} = -I_{ij}\beta_{ij}b_{11ij}$	$\rho_{45} = -I_{ij}\beta_{ij}b_{11ij}$
$\rho_{47} = \mu\beta_{jj}$	$\rho_{53} = -I_{ij}\beta_{ij}b_{23ij}$	$\rho_{54} = -I_{ij}\beta_{ij}b_{22ij}$
$\rho_{55} = -I_{ij}\beta_{ij}b_{21ij}$	$\rho_{56} = \beta_{ii}$	$\rho_{63} = -I_{ij}\beta_{ij}b_{33ij}$
$\rho_{64} = -I_{ij}\beta_{ij}b_{32ij}$	$\rho_{65} = -I_{ij}\beta_{ij}b_{31ij}$	$\rho_{66} = \mu\beta_{jj}$
$\rho_{67} = \beta_{ii}$	$\rho_{72} = -\beta_{ij}k_{ij}$	$\rho_{77} = \beta_{ij}$
$\rho_{78} = \beta_{jj}$	$\rho_{81} = -\mu\beta_{ij}k_{ij}$	$\rho_{86} = \mu\beta_{ij}$
$\rho_{88} = \beta_{ii}$	other $\rho_{pk} = 0$	$\beta_{ij} = \beta_{ii}\beta_{jj}$

5.3 Computational procedure

In this chapter, the main assumptions are: a) the displacement of the mid-surface of the plate is small compared with the plate thickness; b) the transverse stresses are negligible; c) the normal to the mid-surface remain straight after deformation but not necessarily normal; d) Prandtl-Reuss's law obeying the von Mises yield criterion is assumed; e) the plate is made of non-hardening elasto-plastic material.

In order to consider the expansion of the yield regions in the directions of the thickness of the plate, the thickness of the plate is divided into many layers shown in Figure 5.3.

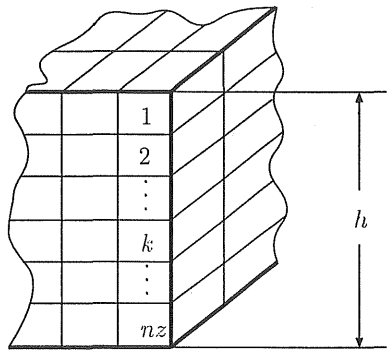

Figure 5.3: Subdivision of the thickness

If the data σ_x/σ_0, σ_y/σ_0, τ_{xy}/σ_0, $\overline{\sigma}$ in the [n-1]-th load incremental step can be obtained, in which $\overline{\sigma} = (\sigma_x^2 + \sigma_y^2 - \sigma_x\sigma_y + 3\tau_{xy}^2)^{\frac{1}{2}}$ is the equivalent stress and σ_0 is the yield stress, then, the results of σ_x/σ_0, σ_y/σ_0, τ_{xy}/σ_0, $\overline{\sigma}$ in the [n]-th load incremental step can also be obtained by using the following computational procedure.

1. Non-dimensional deviatoric stress:

$$\overline{\sigma}'_x = \frac{1}{3}(2\frac{\sigma_x}{\sigma_0} - \frac{\sigma_y}{\sigma_0}),\ \overline{\sigma}'_y = \frac{1}{3}(2\frac{\sigma_y}{\sigma_0} - \frac{\sigma_x}{\sigma_0}),\ \overline{\tau}'_{xy} = \frac{\tau_{xy}}{\sigma_0}$$

$$\overline{\sigma}'_x = \sigma'_x/\sigma_0,\ \overline{\sigma}'_y = \sigma'_y/\sigma_0,\ \overline{\tau}'_{xy} = \tau'_{xy}/\sigma_0$$

2. When $\overline{\sigma}$ is not greater than σ_0,

$$\begin{bmatrix} \alpha_{11} & \alpha_{12} & \alpha_{13} \\ \alpha_{21} & \alpha_{22} & \alpha_{23} \\ \alpha_{31} & \alpha_{32} & \alpha_{33} \end{bmatrix} = \begin{bmatrix} 1 & \nu & 0 \\ \nu & 1 & 0 \\ 0 & 0 & (1-\nu)/2 \end{bmatrix}$$

When $\overline{\sigma}$ is greater than σ_0,

$$a = \overline{\sigma}'_x + \nu\overline{\sigma}'_y, \quad b = \nu\overline{\sigma}'_x + \overline{\sigma}'_y, \quad c = (1-\nu)\overline{\tau}'_{xy}, \quad d = a\overline{\sigma}'_x + b\overline{\sigma}'_y + 2c\overline{\tau}'_{xy}$$

$$\begin{bmatrix} \alpha_{11} & \alpha_{12} & \alpha_{13} \\ \alpha_{21} & \alpha_{22} & \alpha_{23} \\ \alpha_{31} & \alpha_{32} & \alpha_{33} \end{bmatrix} = \begin{bmatrix} 1 & \nu & 0 \\ \nu & 1 & 0 \\ 0 & 0 & (1-\nu)/2 \end{bmatrix} - \frac{1}{d} \begin{bmatrix} a^2 & ab & ac \\ ab & b^2 & bc \\ ac & bc & c^2 \end{bmatrix}$$

3.

$$a_{ij} = 12 \int_{-\frac{1}{2}}^{\frac{1}{2}} \alpha_{ij} \xi^2 d\xi, \quad [b_{ij}] = [a_{ij}]^{-1}$$

4. The incremental moments ΔM_y, ΔM_y, ΔM_{xy} are calculated by the discrete solutions.

5.

$$\begin{bmatrix} \Delta\beta_x \\ \Delta\beta_y \\ \Delta\beta_{xy} \end{bmatrix} = \frac{1}{D} \begin{bmatrix} a_{11} & a_{12} & a_{13} \\ a_{21} & a_{22} & a_{23} \\ a_{31} & a_{32} & a_{33} \end{bmatrix}^{-1} \begin{bmatrix} \Delta M_x \\ \Delta M_y \\ \Delta M_{xy} \end{bmatrix}$$

$$\begin{bmatrix} \Delta\sigma_x/\sigma_0 \\ \Delta\sigma_y/\sigma_0 \\ \Delta\sigma_z/\sigma_0 \end{bmatrix} = \frac{Ez}{(1-\nu^2)\sigma_0} \begin{bmatrix} \alpha_{11} & \alpha_{12} & \alpha_{13} \\ \alpha_{21} & \alpha_{22} & \alpha_{23} \\ \alpha_{31} & \alpha_{32} & \alpha_{33} \end{bmatrix} \begin{bmatrix} \Delta\beta_x \\ \Delta\beta_y \\ \Delta\beta_{xy} \end{bmatrix}$$

6.

$$\frac{\sigma_x}{\sigma_0} = \sum^n \frac{\Delta\sigma_x}{\sigma_0}, \quad \frac{\sigma_y}{\sigma_0} = \sum^n \frac{\Delta\sigma_y}{\sigma_0}, \quad \frac{\tau_{xy}}{\sigma_0} = \sum^n \frac{\Delta\tau_{xy}}{\sigma_0}$$

The procedure is repeated until an ultimate load is obtained. The ultimate load is indicated by very large deflection or singularity of the matrix which is inverted to obtain a solution.

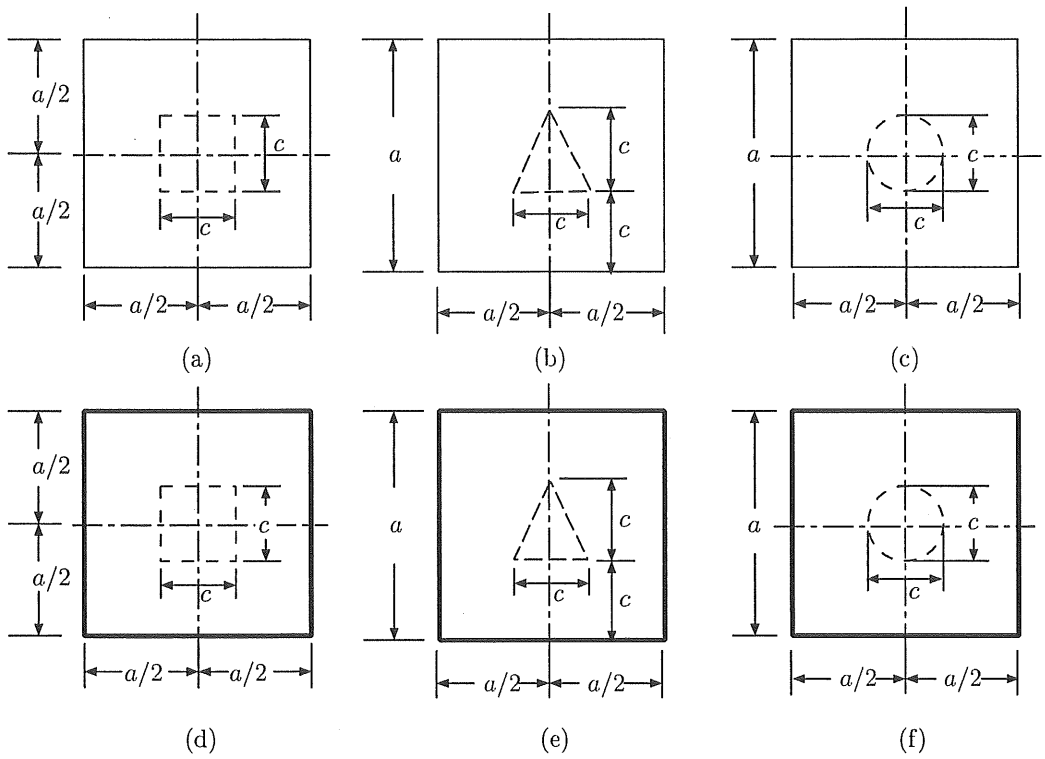

Figure 5.4: Square plates with a various-shaped hole

5.4 Numerical work

The efficiency and accuracy of numerical solutions have been investigated for the elasto-plastic bending problems of some plates with holes subjected to uniform lateral loads shown in Figure 5.4. In this chapter, both of the divisional numbers m and n are 12. The number of layers along the direction of the thickness nz is 20. The Poisson's ratio ν is 0.3.

5.4.1 Simply supported square plate with square hole

A simply supported square plate with square hole is shown in figure 5.4(a). Three cases of the length of the hole are considered. The first is c=0.0, which is the case of the plate without hole. The second is $c = a/3$. The third is $c = a/2$. The non-dimensional incremental load intensity is $\Delta q a^2/M_p$=0.2 ($M_p = \sigma_0 h^2/4$: full plastic moment). The load-deflection curves with respect to maximum deflection of the plates are shown in Figure 5.5, which shows that the ultimate load for simply supported square plate with

square hole can be established. The total ultimate loads of the plate are presented in Table 5.1 together with the results of Ref.[55] and Ref.[30]. A comparison of these results reveals a very close agreement and it may be seen that the total ultimate load will decrease when the size of the hole increases. The progression of the yield regions at different levels of loads is shown in Figure 5.6, which shows that the first yielding of the plate occurs at the four corners of the square hole, then, at the four corners of the square plate and the the yield region is expanding along the diagonal of the plate. The progression of yield region of the simply supported plate with a square hole is similar to that of the simply supported plate without holes. The redistributions of M_x, M_y, w along $\zeta = 1/6$ are illustrated in Figure 5.7 for the three levels of loads for the case of $c = a/3$.

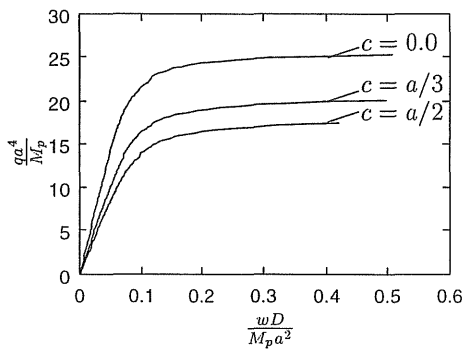

Figure 5.5: Load-deflection curves for simply supported square plate with square hole

Table 5.1: Ultimate loads $(qa^4)/M_p$ for simply supported plate with square hole

		ref.[55]		ref.[30]	
c	present	lower bound	upper bound	displacement model	hybrid model
0.0	25.2	24.9	26.5	24.8	25.2
a/3	20.1	19.5	20.8	–	–
a/2	17.4	–	–	–	–

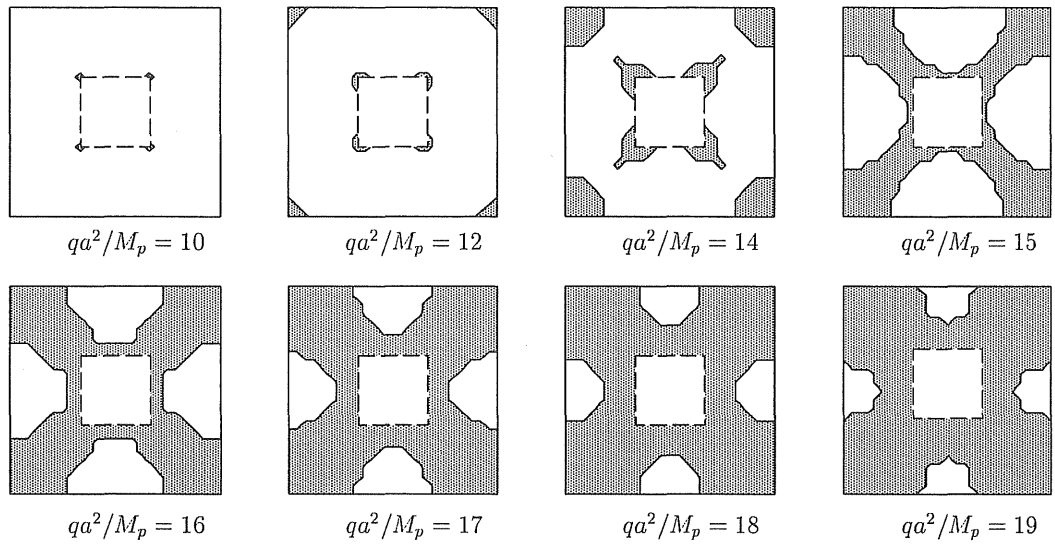

Figure 5.6: Progression of yield regions of simply supported square plate with square hole

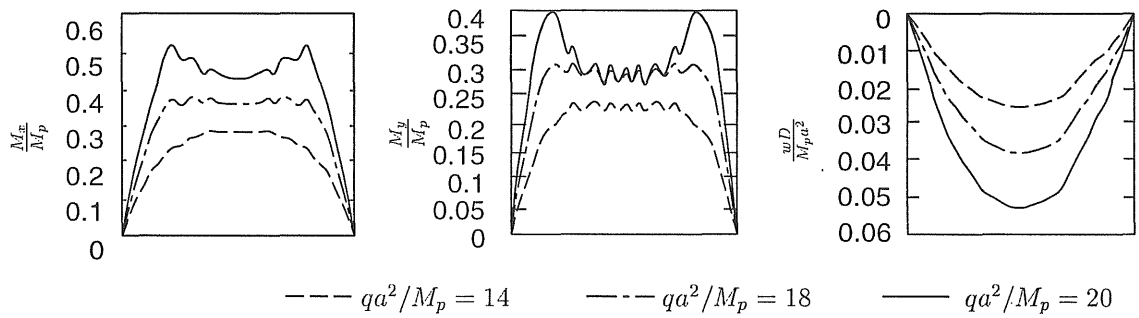

Figure 5.7: Moments and deflection for simply supported square plate with square hole

5.4.2 Simply supported square plate with triangular hole

A simply supported square plate with triangular hole is shown in figure 5.4(b). The case of $c = a/3$ is considered. The non-dimensional incremental load intensity is $\Delta qa^2/M_p$=0.2 ($M_p = \sigma_0 h^2/4$: full plastic moment). The load-deflection curve with respect to maximum deflection of the plate is shown in Figure 5.8, which shows the ultimate load has been obtained. The total ultimate load is 21.53 qa^4/M_p. The progression of the yield regions at different levels of loads is shown in Figure 5.9, which reveals the first yielding of the plate occurs at the edges of the hole, then at the four

corners of the plate, when $qa^2/M_p = 15$, the yield region is like the capital letter A, after that, the yield region is expanding mainly along the diagonal of the plate. The redistributions of M_x, M_y, w along $\zeta = 1/6$ are illustrated in Figure 5.10 for the three levels of loads.

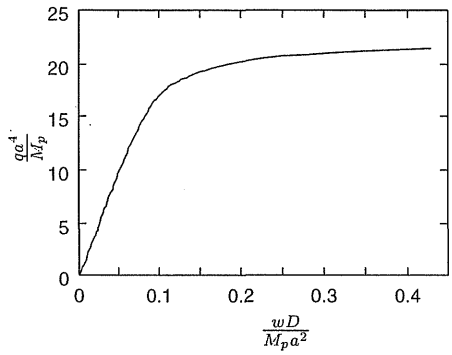

Figure 5.8: Load-deflection curve for simply supported square plate with triangular hole

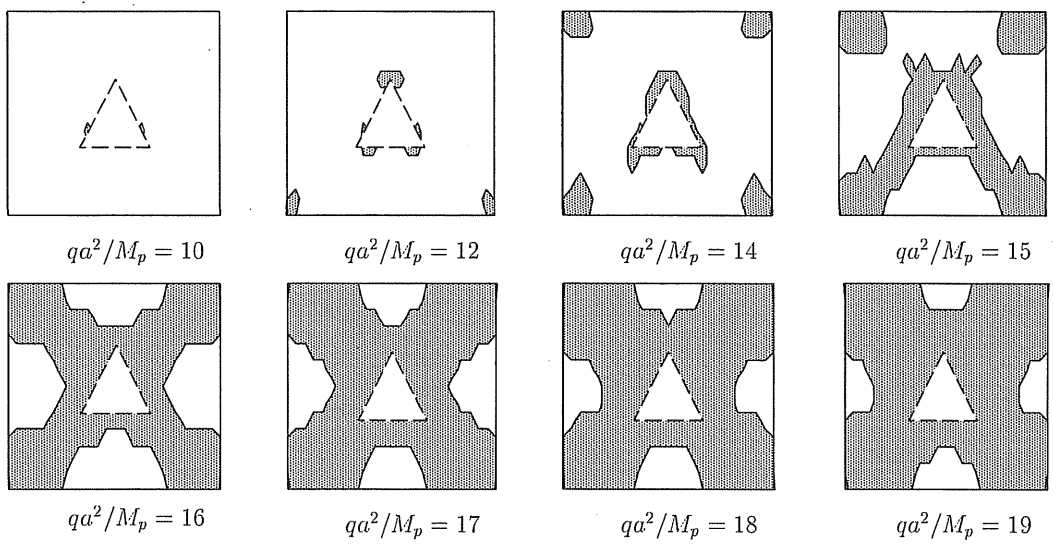

Figure 5.9: Progression of yield regions of simply supported square plate with triangular hole

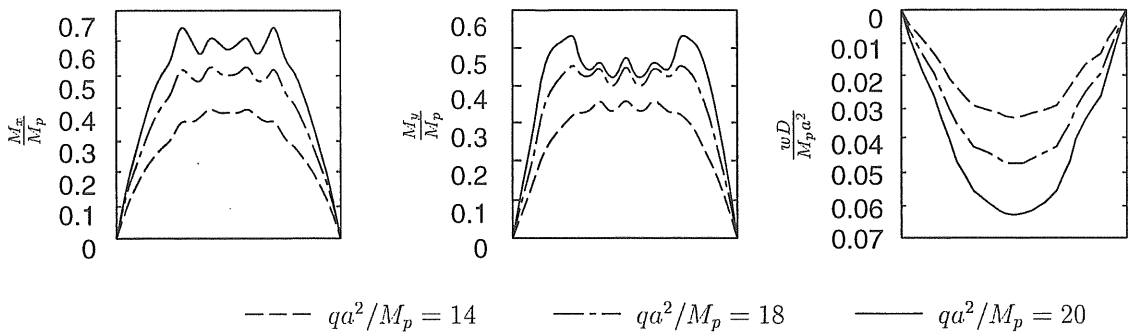

Figure 5.10: Moments and deflection for simply supported square plate with triangular hole

5.4.3 Simply supported plate with circular hole

A simply supported square plate with circular hole is shown in figure 5.4(c). The case of $c = a/3$ is considered. The non-dimensional incremental load intensity is $\Delta qa^2/M_p$=0.2. The load-deflection curve with respect to maximum deflection of the plate is shown in Figure 5.11, which shows the ultimate load is obtained. The total ultimate load is 20.7 qa^4/M_p. The progression of the plastic regions at different levels of loads is shown in Figure 5.12, which reveals that the first yielding occurs at the edges of the hole and the yield region spreads along the diagonal of the plate. The redistributions of M_x, M_y, w along $\zeta = 1/6$ are illustrated in Figure 5.13

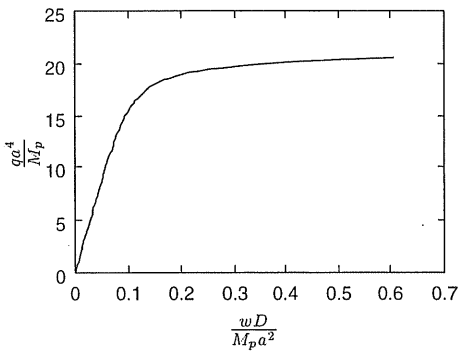

Figure 5.11: Load-deflection curve for simply supported square plate with circular hole

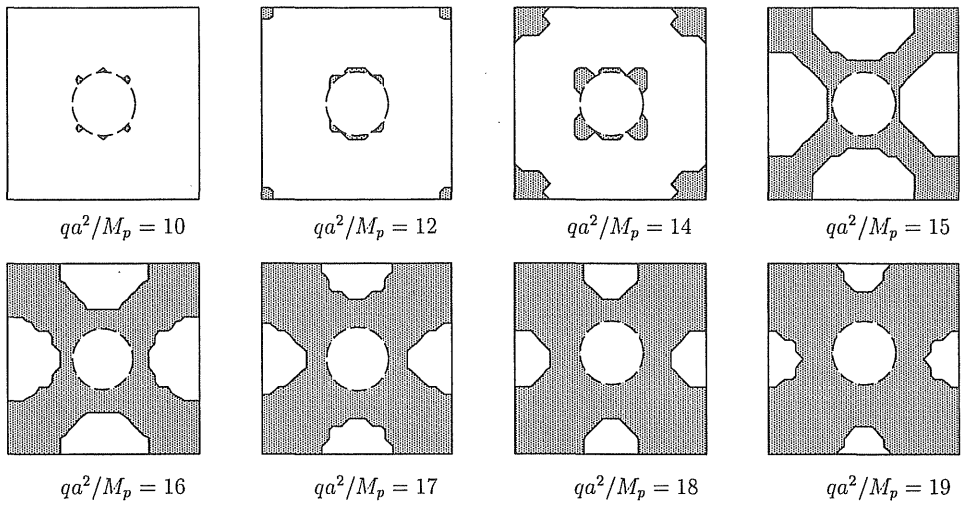

Figure 5.12: Progression of yield regions of simply supported square plate with circular hole

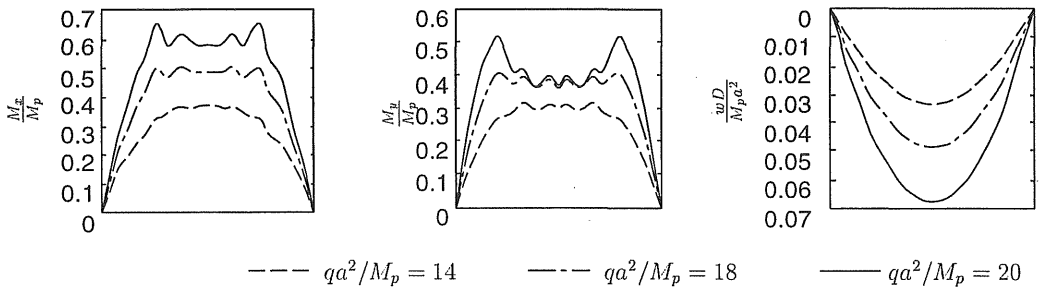

Figure 5.13: Moments and deflection for simply supported square plate with circular hole

5.4.4 Clamped square plate with square hole

The elasto-plastic analysis of the clamped square plate with square hole is shown in figure 5.4(d). Two cases of the length of the hole are considered. The first is c=0.0, which is the case of the plate without hole. The second is $c = a/3$. The non-dimensional incremental load intensity is $\Delta qa^2/M_p$=1.0. The load-deflection curves with respect to maximum deflection of the plate are shown in Figure 5.14, which reveals that the ultimate loads of these plates are obtained. The total ultimate loads of the plate are indicated in Table 5.2 together with the results of Ref.[55] and Ref.[30]. A comparison of these results reveals a very close agreement and it may be also deserved that the

Table 5.2: Ultimate loads $(qa^4)/M_p$ for clamped plate with square hole

		Ref.[55]		Ref.[30]	
c	present	lower bound	upper bound	displacement model	hybrid model
0.0	44.0	42.9	49.2	43.3	43.9
a/3	40.0	–	–	–	–

total ultimate load will decrease when the plate has a hole. The progression of the yield regions at different levels of loads is shown in Figure 5.15, which shows that the first yielding of the plate occurs at the middle of the four edges of the plate, then, at the

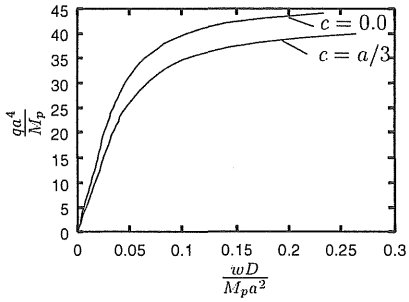

Figure 5.14: Load-deflection curves for clamped square plate with square hole

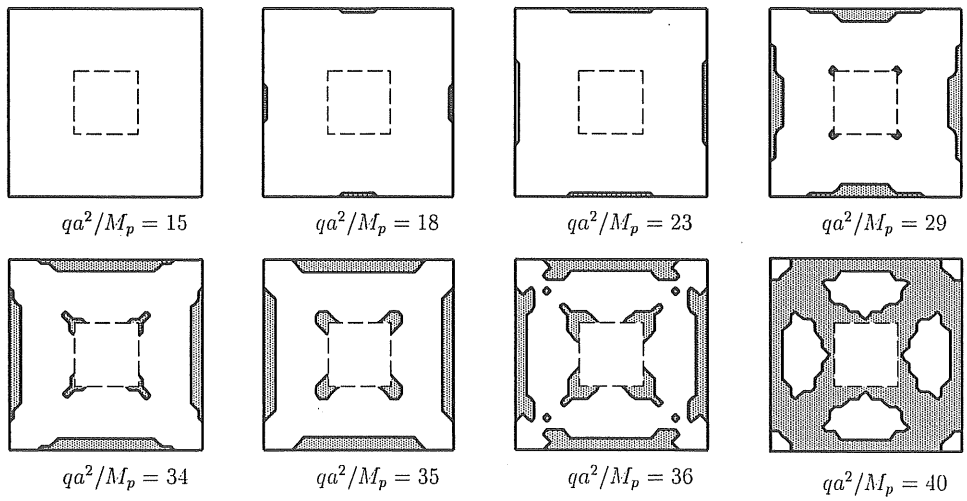

Figure 5.15: Progression of yield regions of clamped square plate with square hole

four corners of the hole, and the yield region spreads along both these edges and the diagonal of the plate. The redistributions of M_x, M_y, w along $\zeta = 1/6$ are illustrated in Figure 5.16 for the three levels loads for the case of $c = a/3$.

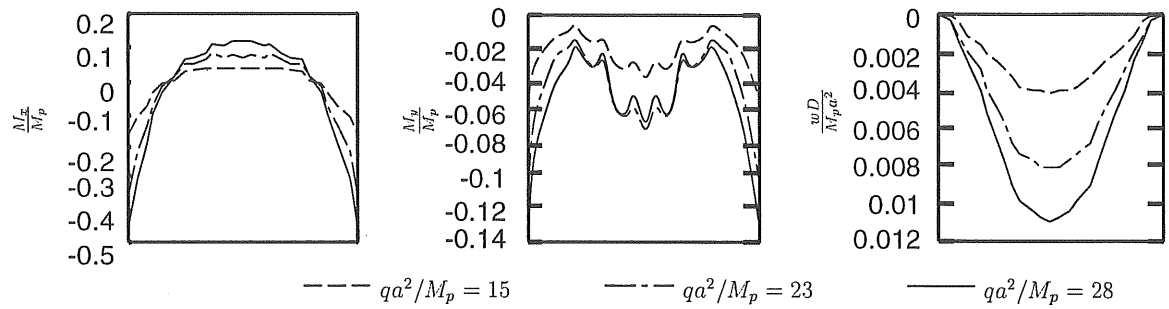

Figure 5.16: Moments and deflection for clamped square plate with square hole

5.4.5 Clamped square plate with triangular hole

The clamped square plate with triangular hole is shown in figure 5.4(e). The case of $c = a/3$ is considered. The non-dimensional incremental load intensity is $\Delta qa^2/M_p$=1.0. The load-deflection curve with respect to maximum deflection of the plate is shown in Figure 5.17, which shows the ultimate load is obtained. The total ultimate load is 42.5 qa^4/M_p. The progression of the yield regions at different levels of loads is shown in Figure 5.18, which shows that the progression of the yield regions is similar to that of clamped square plate with square hole. The redistributions of M_x, M_y, w along $\zeta = 1/6$

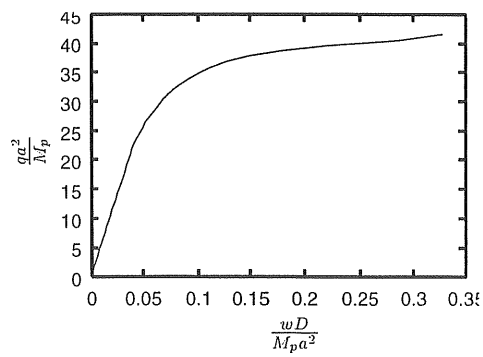

Figure 5.17: Load-deflection curve for clamped square plate with triangular hole

are illustrated in Figure 5.19 for the three levels of loads.

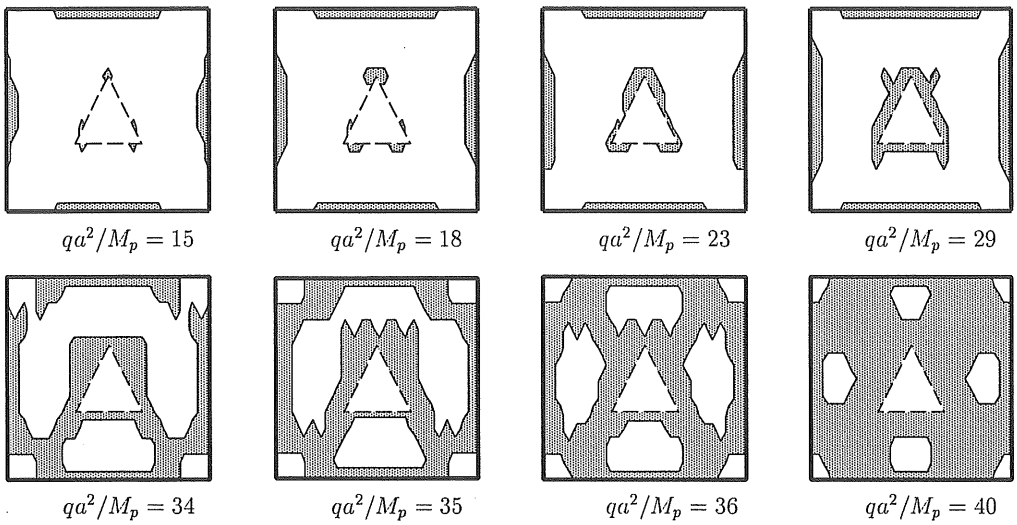

Figure 5.18: Progression of yield regions of clamped square plate with triangular hole

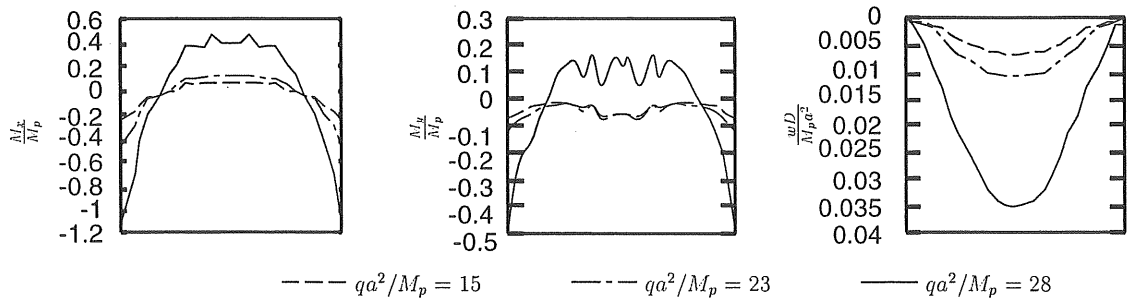

Figure 5.19: Moments and deflection for clamped square plate with triangular hole

5.4.6 Clamped plate with circular hole

A clamped square plate with circular hole is shown in figure 5.4(f). The case of $c = a/3$ is considered. The non-dimensional incremental load intensity is $\Delta qa^2/M_p$=1.0. The load-deflection curve with respect to maximum deflection of the plate is shown in Figure 5.20. The total ultimate load is 42.0 qa^4/M_p. The progression of the yield regions at different levels of loads is shown in Figure 5.21, which is similar to that of the square plate with square hole. The redistributions of M_x, M_y, w along $\zeta = 1/6$ are

illustrated in Figure 5.22 for the three levels of loads.

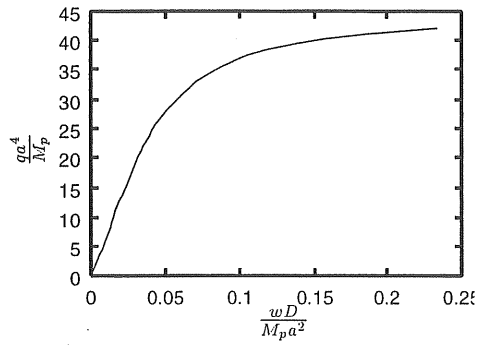

Figure 5.20: Load-deflection curve for clamped square plate with circular hole

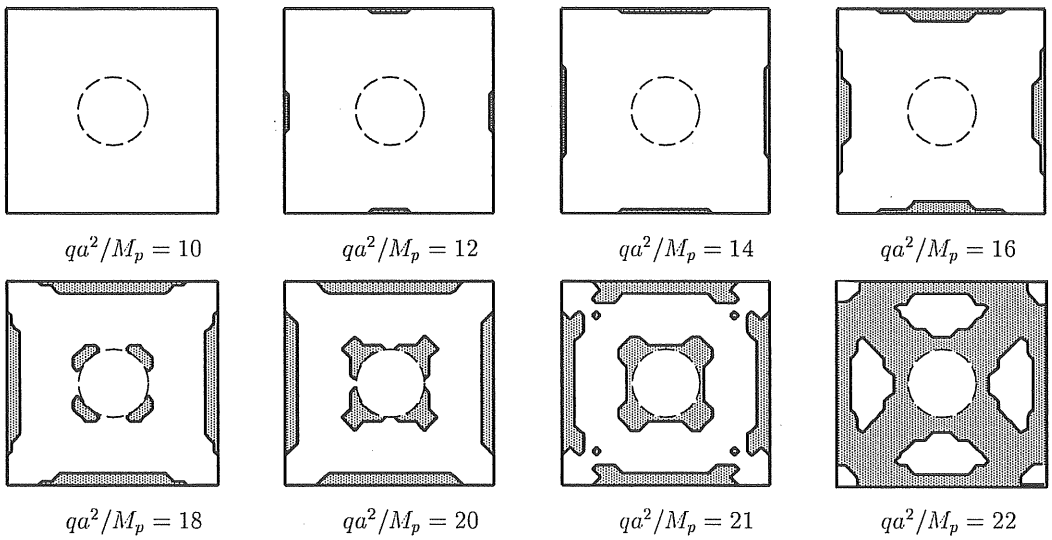

Figure 5.21: Progression of yield regions of clamped square plate with circular hole

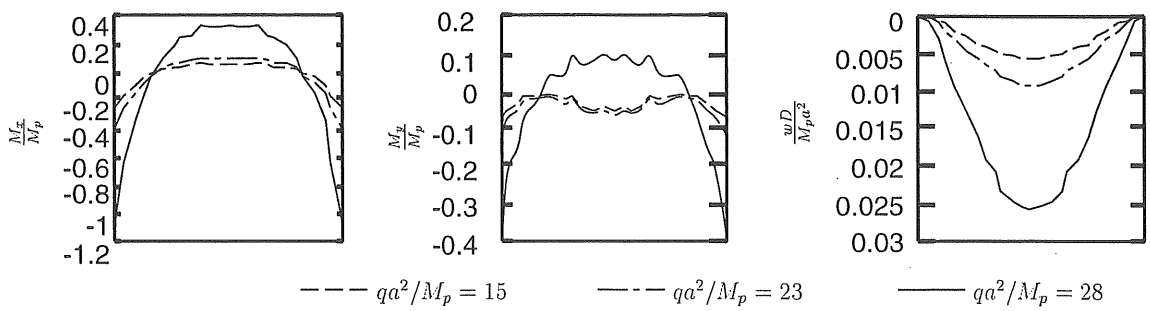

Figure 5.22: Moments and deflection for clamped square plate with circular hole

5.5 Conclusions

In this chapter, a discrete method has been used for the elasto-plastic bending problems of square plates with a various-shaped hole. The main conclusions are summarized as follows:.

1. Under the concept of an equivalent rectangular plate , that is , a plate with hole can be finally transformed into a rectangular plate with various thickness and point supports, the fundamental differential equations have been obtained.

2. By translating differential equations into integral equations and applying numerical integration, the discrete solutions are obtained.

3. Based on the discrete solutions, numerical calculation is carried out for square plates with square, triangular or circular hole. The ultimate load can be obtained for all these plates. The progression of yield region is illustrated in figures.

4. The results show that the boundary conditions of the plates have great effects on the ultimate load and the progression of yield regions. The shape and size of holes also influence the ultimate load and the progression of yield regions, and the whole ultimate load will decrease when the hole becomes larger.

5. A comparison with published results shows the results obtained by the discrete method has good convergency and adequate accuracy.

Chapter 6

Conclusions

Conclusions

In this thesis, a general discrete method has been proposed for elastic and plastic problems. In order to investigate the efficiency and accuracy of the method, elastic bending, free vibration, and elasto-plastic bending problems of irregular-shaped plates are carried out. The main work and conclusions are summarized as follows.

In chapter 1, a review of published literature and the outline of this thesis are presented. Because the fundamental differential equations of the problems of irregular-shaped plates are the simultaneous partial differential equations with variable coefficients, it is almost impossible to obtain the analytical solutions. In order to analyze the problems, many numerical method are used. Almost all the methods need the assumption of deflection at first. For some cases, they may encounter some difficulties such as the phenomenon of shear locking, the corner problems and etc. In order to solve these problems, special treatment is needed. On the other hand, the problems of irregular-shaped plates are generally more difficult than those of rectangular plates because the boundary of the irregular-shaped plate is more difficult to be described easily and accurately. All these make the calculation more complex and need more computer memory space and time. So it is necessary to find another method to solve the problems of irregular-shaped plates efficiently and simply in order that even not very large-size digital computer can be used to solve the problem of irregular-shaped plates quickly and accurately. It is the purpose of this thesis. In this thesis, a concept of an equivalent rectangular plate is developed for analyzing the bending and free vibration problems of irregular-shaped plates. A unite method is obtained for these problems.

In chapter 2, by adding some parts, an irregular-shaped plate can be finally considered as an equivalent rectangular plate with various thickness and point supports. Under the concept of the equivalent rectangular plate, the problems of irregular-shaped plates can be translated into the problems of equivalent rectangular plates. And then, all the analyses can be carried out on the equivalent rectangular plate. The fundamental differential equations are derived. By translating the differential equations into integral equations and applying numerical integration, the semi-analytical discrete so-

lutions are obtained. By increasing the number of crosswise line divided equally, the governing differential equations and the boundary conditions are satisfied to any desired degree of accuracy in theory, and the quantities at any intersection point of crosswise line are only related to the quantities of the boundary points. So the discrete method is a semi-analytical method and it can save computer memory space and time.

In chapter 3, in order to investigate the efficiency and accuracy of the discrete solution based on the equivalent rectangular plate, the numerical analyses are carried out for the bending problems of irregular-shaped plates such as plate with opening, circular, semi-circular, elliptic, triangular, skew and rhombic plates. It is shown that the concept of the equivalent rectangular plate is proper and the numerical solutions have the good convergency and adequate accuracy for various types of irregular-shaped plates even if the divisional numbers m, n are not very large. With the increment of divisional numbers, the solutions can have more adequate accuracy.

In chapter 4, the discrete method is extended for the free vibration analysis of irregular-shaped plates. Using the similar method proposed in chapter 2, in theory, the discrete solutions can be obtained from the fundamental differential equations of vibration problems. But it is found the method is difficult to find the frequency parameters in the numerical calculation. In order to improve the defect of this method, the discrete method with Green function is proposed to analyze the vibration problems. Three sections consist of this chapter.

In the first section, the free vibration problems of rectangular plates with different boundary conditions and variable thickness are analyzed. The Green function of the bending problem of these plates is given by the static displacement function of the plates with a unit concentrated load. By applying the Green function, the displacement amplitude at any point of the rectangular plate during the free vibration can be given. Using the non-dimensional expressions and the numerical integration method mentioned in chapter 2, the characteristic equation of the free vibration of a rectangular plate with variable thickness can be obtained. The frequency parameters and their modes of free vibration are obtained and illustrated in tables and figures. These tables and figures show that the boundary conditions and the thickness of the plates affect the natural frequency parameters and nodal lines of modes of free vibration. It is observed

that the frequency parameters increase with an increase in the constraints on the plate and there are some changes of mode order for some plates with different thickness. The numerical results compared with other published ones show that the numerical solutions by the discrete method have good convergency and adequate accuracy.

In the second section, under the concept of the equivalent rectangular plate, the discrete method with Green function proposed in the previous section is extended for the free vibration analysis of rectangular plates with various-shaped holes. In this section, the shapes of holes are circular, semi-circular, elliptic, square, rectangular, triangular and rhombic. The positions of holes are not limited at the central part of plates. They can be at any part of the plates. All these will make up the deficiency of the previously published literature. Some new data are obtained. Numerical results show that the numerical solutions by the proposed method have the good convergency and adequate accuracy. The effects of Poisson's ratio, the size, shape and position of the hole on the vibration characteristics are investigated and illustrated in tables and figures. It is observed that Poisson's ratio and the size of a hole have some effects on the frequency parameters but have only a few effects on the nodal lines of modes of free vibration. On the contrary, the position of the hole has some effects on the nodal lines of modes of free vibration, but have only a few effects on the frequency parameters. The shape of the hole and the boundary conditions of the plates influence both the frequency parameters and the nodal lines of modes.

In the third section, under the concept of an equivalent rectangular plate, the discrete method with Green function is also used for the free vibration analysis of right triangular plates with various thickness, different boundary conditions, aspect ratios and thickness ratios. The Green function of the bending problem of these plates is given by the static displacement function of the plates with a unit concentrated load and point supports. The characteristic equation of the free vibration of a rectangular plate with variable thickness and point supports can be finally obtained. The frequency parameters and their modes of free vibration are obtained and illustrated in tables and figures.

In chapter 5, under the concept of the equivalent rectangular plate, the discrete method is proposed for the elasto-plastic bending analysis of square plates with various-

shaped holes. In order to analyze these problems, the Prandtle-Reuss's law and von Mises yield criteria are used. Under the assumptions that the increments are infinitesimal and all the governing equations may be linearized, the fundamental differential equations of elasto-plastic bending analysis of rectangular plates with various thickness and point supports are derived. Then, the discrete solutions are obtained by translating the differential equations into integral equations and applying numerical integration. In order to consider the expansion of the yield regions in the direction of the thickness of the plate, the thickness of the plate is divided into many layers. Numerical results have been carried out for square plates with square, triangular or circular hole and compared with previously published results. The ultimate load can be obtained for all these plates. The progression of yield region is illustrated in figures. The results show that the boundary conditions of the plates have great effects on the ultimate load and the progression of yield regions. The ultimate loads of clamped plates with holes are about two times of those of simply supported plates with hole. The progression of yield regions of clamped and simply supported plates with holes is quite different. For clamped plate with hole, the first yielding occurs at the middle of the four edges of the plate, then, at the edges of the hole, and then the yield region spreads along both the four edges and the diagonal of the plate. For the simply supported plate, first yielding occurs at the edges of the hole, then, at the four corners of the plate and then the yield region spreads mainly along the diagonal of the plate. A comparison with the published results shows the results obtained by the discrete method have good convergency and adequate accuracy. The method used here can be used not only for the elasto-plastic bending problems of square plates with holes, but also for the same problems of the irregular-shaped plates such as triangular, circular, rhombic plates and the free vibration problems of elasto-plastic irregular-shaped plates. These will be studied in the future.

In chapter 6, the main work and conclusions are summarized.

In brief, the discrete method has been proposed for the elastic bending, free vibration, elasto-plastic bending analyses of irregular-shaped plates. Numerical calculation has been carried out and it is shown that the results obtained by the proposed method have good convergency and adequate accuracy.

Bibliography

[1] H.D.CONWAY and M.K.HUANG 1952 *Journal of Mechanics* Mach, 5-8. The bending of uniformly loaded sectorial plates with clamped edges.

[2] S.VAIDYANATHAN, H.R.BUSBY and D.R.Houser 1994 *Computers and Structures* **51**, 255-266. A numerical approach to the static analysis of an annular sector Mindlin plate with applications to bevel gear design.

[3] H.J.FLETCHER 1959 *Journal of Applied Mechanics* December, 625-628. Bending of isosceles right triangular plates.

[4] H.D.CONWAY 1962 *Journal of Applied Mechanics* December, 755-756. Triangular plates analyzed by point matching.

[5] T.MIZUSAWA 1994 *Computers and Structures* **53**, 439-448. Application of the spline element method to analyze the bending of skew plates.

[6] W.K.LO and L.T.LEE 1996 *Computers and Structures* **58**, 957-971. Equivalent systems for variable thickness circular plates.

[7] S.F.Ng and X.Chen 1995 *Computers and Structures* **54**, 111-118. Analysis of arbitrary mindlin plates or bridge decks by spline finite strip method.

[8] N.C.HAMOUCHE, Z.U.A.WARSI and J.C.MCWHORTER III 1997 *Computers and Structures* **63** , 159-171. A spectral solution for the bending of arbitrarily shaped plates.

[9] K.M.LIEW, K.C.HUNG and M.K.LIM 1995 *Journal of Sound and Vibration* **182**, 77-90. Vibration of Mindlin plates using boundary characteristic orthogonal polynomials.

[10] G.AKSU and S.A.AL-KAABI 1987 *Journal of Sound and Vibration* **119**, 189-205. Free vibration analysis of Mindlin plates with linearly varying thickness.

[11] N.LI and D.J.GORMAN 1993 *Journal of Sound and Vibration* **165**, 361-368. Free vibration analysis of simply supported rectangular plates with internal line support along diagonals.

[12] F.JU, H.P.LEE and K.H.LEE 1995 *Journal of Sound and Vibration* **183**, 533-545. Free vibration of plates with stepped variations in thickness on non-homogeneous elastic foundations.

[13] C.S.KIM and S.M.DICKINSON 1990 *Journal of Sound and Vibration* **141**, 291-311. The free flexural vibration of right triangular isotropic and orthotropic plates.

[14] B.SINGH and V.SAXENA 1996 *Journal of Sound and Vibration* **194**, 471-496. Transverse vibration of triangular plates with variable thickness.

[15] D.J.GORMAN 1983 *Journal of Sound and Vibration* **89**, 107-118. A highly accurate analytical solution for free vibration analysis of simply supported right triangular plates.

[16] SHAUKAT MIRZA and MOHAN BIJLANI 1985 *Computers and Structures* **21**, 1129-1135. Vibration of triangular plates of variable thickness.

[17] J.YUAN and S.M.DICKINSON 1996 *Computers and Structures* **58**, 1261-1264. On the vibration of annular, circular and sectorial plates with cut-outs or on parial supports.

[18] K.Y.LAM, K.M.LIEW and S.T.Chow 1992 *Journal of Sound and Vibration* **154**, 261-269. Use of two-dimensional orthogonal polynomials for vibration analysis of circular and elliptical plates.

[19] O.G.MCGEE, W.D.GRAVES, T.S.BUTALIA and M.I.OWINGS 1994 *Computers and Structures* **53**, 679-694. Nature vibrations of shear deformable rhombic plates with clamped and free edge conditions.

[20] R.S.SRINIVASAN and K.MUNASWAMY 1975 *Journal of Sound and Vibration* **39**, 207-216. Frequency analysis of skew orthotropic point supported plates.

[21] R.ALI and S.J.ATWAL 1980 *Computers and Structures* **12**, 819-823. Prediction of natural frequencies of vibration of rectangular plates with rectangular cutouts.

[22] P.G.YOUNG and S.M.DICKINSON 1994 *Journal of Sound and Vibration* **177**, 93-109. Further studied on the vibration of plates with curved edges, including complicating effects.

[23] H.T.SALIBA 1986 *Journal of Sound and Vibration* **110**, 87-97. Free vibration analysis of simply supported symmetrical trapezoidal plates.

[24] H.T.SALIBA 1988 *Journal of Sound and Vibration* **126**, 237-247. Transverse free vibration of fully clamped symmetrical trapezoidal plates.

[25] T.KUSUDA 1960 *Journal of the Society of Naval Architects of Japan* **107**, 195-202. Plastic analysis of plate structures subjected to transverse load.

[26] K.B.ANJAN and T.H.JOHN 1967 *Journal of the Structural Division. Proceedings of the American Society of Civil Engineers* **ST 5**, 279-295. Elasto-plastic plate analysis by finite differences.

[27] R.KARAKUZU, A.ÖZEL and O.SAYMAN 1997 *Computers and Structures* **63**, 551-558. Elastic-plastic finite element analysis of metal matrix plates with edge notches.

[28] H.S.ALFREDO and A.L.LEONARD 1968 *Journal of the Engineering Mechanics Division. Proceedings of the American Society of Civil Engineers* **EM 1**, 271-293. Discrete model analysis of elastic-plastic plates.

[29] M.RISTINMAA 1994 *Computers and Structures* **53**, 93-103. Consistent stiffness matrix in FE calculations of elasto-plastic bodies.

[30] NAOYUKI WATANABE and KYOHEI KONDO *Computers and Structures* **28**, 495-503. A new simplified finite element method for elastic-plastic analysis of plate bending problems.

[31] T.SAKIYAMA and M.HUANG 1999 *Structural Engineering and Mechanics* **7**, 289-302. Elastic bending analysis of irregular-shaped plates.

[32] T.SAKIYAMA and M.HUANG 1998 *Journal of Sound and Vibration* **216**, 379-397. Free vibration analysis of rectangular plates with variable thickness.

[33] T.SAKIYAMA and M.HUANG 1998 *Reports of the Faculty of Engineering Nagasaki University* **28**, 163-171. Free vibration analysis of rectangular plates with variable thickness.

[34] T.SAKIYAMA and M.HUANG 1999 *Reports of the Faculty of Engineering Nagasaki University* **29**, 227-236. Free vibration analysis of irregular-shaped plates with variable thickness.

[35] M.HUANG and T.SAKIYAMA 1999 *Journal of Sound and Vibration* **226**, 769-786. Free vibration analysis of rectangular plates with variously-shaped holes.

[36] T.SAKIYAMA and M.HUANG *Journal of Sound and Vibration.* Free vibration analysis of right triangular plates with variable thickness.(accepted)

[37] S. TIMOSHENKO and S.W.KRIEGER 1959 *McGRAW-HILL* **Second Edition** Theory of plates and shells

[38] A. SAITO, T.SHIMAZAKI and S.KIMURA 1958 *Trans. Japan Society of Mechanical Engineers* **147**, 853-861. Bending of elliptic plates under a concentrated load.

[39] S.IWAHARA 1980 *Trans. Architecture Institute of Japan* **288**, 85-96. Analytical study about the bending of elastic plates with opening hole under uniform load, part 2: square plate with a square hole.

[40] T.OTA, M.HAMADA, T.SAGIJIMA, Y.NISHIMURA and H.MASUI 1962 *Trans. Japan Society of Mechanical Engineers* **188**, 421-427. Statical deflection of a rhomboidal plate with clamped edges subjected to uniformly distributed pressure.

[41] T. SAKIYAMA AND H.MATSUDA 1983 *Proc. Japan Society of Civil Engineers* **338**, 21-28. Bending analysis of rectangular plates with variable thickness.

[42] A.W.Leissa 1969 *NASA SP*-160, 43-45. Vibration of plates.

[43] R.W.Claassen and C.J.Thorne 1960 *NOTS Tech. Pub.* 2379, *NAVWEPS Rept.* 7016. U.S.Naval Ordnance Test Station. Transverse vibrations of thin rectangular isotropic plates.

[44] V.V.Bolotin 1961 *Inshen. Sbornik.* **31**, 3-14. Dynamic edge effect in the elastic vibrations of plates.

[45] R.W.Claassed and C.J.Thorne 1962 *Journal of Aerospace Science* **29**, 1300-1305. Vibration of a rectangular cantilever plate.

[46] D.Young 1950 *Journal of Applied Mechanics* **17**, 448-453. Vibration of rectangular plates by the Ritz method.

[47] K.M.Liew, K.C.Hung and M.K.Lim 1995 *Journal of Sound and Vibration* **182**, 77-90. Vibration of Mindlin plates using boundary characteristic orthogonal polynomials.

[48] F.C.Appl and N.R.Byers 1965 *Journal of Applied Mechanics* **32**, 163-167. Fundamental frequency of simply supported rectangular plates with linearly varying thickness.

[49] C.V.Joga Rao and G.Pickett 1961 *Journal of the Aeronautical Society of India* **13**, 83-88. Vibrations of plates of irregular shapes and plates with holes.

[50] J.N.Reddy 1982 *Journal of Sound Vibration* **83**, 1-10. Large amplitude flexural vibration of layered composite plates with cutouts.

[51] T.Kumai 1952 *Proceeding of second Japanese national congress of applied mechanics* 339-342. The flexural vibration of a square plate with a central hole.

[52] R.F.Hegarty and T.Ariman 1975 *International Journal of Solids and Structures* **11**, 895-906. Elasto-dynamic analysis of rectangular plates with circular holes.

[53] K.M.Liew, C.W.Lim and M.K.Lim 1994 *Journal of Sound and Vibration* **177**, 479-501. Transverse vibration of trapezoidal plates of variable thickness: unsymmetric trapezoids.

[54] K.S.YAMASHITA Matrix method for strength of materials. *Japan Society of Steel Structure*

[55] The structural mechanics handbook 1986. *Japan Society of Civil Engineers*

[56] P.GAGNON, C.GOSSELIN and L.CLOUTIER 1997 *Computers and Structures* **63**, 349-362. A finite strip element for the analysis of variable thickness rectangular thick plates.

[57] H.TAKABATAKE, H.MORIMOTO, T.FUJIWARA and T.HONMA 1996 *Computers and Structures* **58**, 263-275. Simplified analysis of circular plates including voids.

[58] A.EL-ZAFRANY, S.FADHIL and M.Debbih 1995 *Computers and Structures* **56**, 565-576. An efficient approach for boundary element bending analysis of thin and thick plates.

[59] G.K.FU and S.J.BOULOS 1996 *Computers and Structures* **58**, 221-232. Finite element analyses of irregular thick plates for signal pole design.

[60] C.G.BOAY 1993 *Computers and Structures* **48**, 529-533. Free vibration of rectangular isotropic plates with and without a concentrated mass.

[61] S.S.A.GHAZI, F.A.BARKI and H.M.SAFWAT 1997 *Computers and Structures* **62**, 395-407. Free vibration analysis of penta, hepta-gonal shaped plates.

[62] C.M.WANG and V.THEVENDRAN 1993 *Journal of Sound and Vibration* **163**, 137-149. Vibration analysis of annular plates with concentric supports using a variant of Rayleigh-Ritz method.

[63] O.G.MCGEE, A.W.LEISSA and C.S.HUANG 1993 *Journal of Sound and Vibration* **164**, 565-569. Vibrations of completely free sectorial plates.

[64] H.T.SALIBA 1993 *Journal of Sound and Vibration* **164**, 383-397. Theoretical free vibration analysis of rectangular cantilever plates with rigid point supports.

[65] K.H.LOW 1993 *Journal of Sound and Vibration* **160**, 111-121. Analytical and experimental investigation on a vibrating rectangular plate with mounted weights.

[66] H.T.SALIBA 1995 *Journal of Sound and Vibration* **183**, 765-778. Transverse free vibrations of right triangular thin plates with combinations of clamped and simply supported boundary conditions: a highly accurate simplified solution.

[67] A.ACHONG 1995 *Journal of Sound and Vibration* **183**, 157-168. Vibrational analysis of circular and elliptical plates carrying point and ring masses and with edges elastically restrained.

[68] K.M.LIEW 1993 *Journal of Sound and Vibration* **165**, 329-340. On the use of *pb*-2 Rayleigh-Ritz method for free flexural vibration of triangular plates with curved internal supports.

[69] K.M.LIEW,K.C.HUNG and M.K.LIM 1995 *Journal of Sound and Vibration* **182**, 709-727. Three-dimensional vibration of rectangular plates: effects of thickness and edge constraints.

[70] I.V.ANDRIANOV and G.A.KRIZHEVSKY 1993 *Journal of Sound and Vibration* **162**, 231-241. Free vibration analysis of rectangular plates with structural inhomogeneity.

[71] G.S.PALANI, NAGESH R.IYER and T.V.S.R.APPA RAO 1993 *Journal of Sound and Vibration* **166**, 409-427. An efficient finite element model for static and vibration analysis of plates with arbitrarily located eccentric stiffeners.

[72] B.SINGH and S.CHAKRAVERTY 1993 *Journal of Sound and Vibration* **162**, 537-546. Transverse vibration of annular circular and elliptic plates using the characteristic orthogonal polynomials in two dimensions.

[73] A.W.LEISSA, O.G.MCGEE and C.S.HUANG 1993 *Journal of Sound and Vibration* **161**, 227-239. Vibrations of circular plates having V-notches or sharp radial cracks.

[74] S.C.FAN and M.H.LUAH 1993 *Journal of Sound and Vibration* **165**, 85-100. A nine-node spline element for free vibration analysis of general plates.

[75] S.KUKLA and B.SKALMIERSKI *Journal of Sound and Vibration* **187**, 339-343. Free vibration of a rectangular plate loaded by a non-uniform in-plane force.

[76] R.B.BHAT and G.MUNDKUR 1993 *Journal of Sound and Vibration* **161**, 157-171. Vibration of plates using plate characteristic functions obtained by reduction of partial differential equation.

[77] C.RAJALINGHAM and R.B.BHAT 1993 *Journal of Sound and Vibration* **161**, 109-118. Axisymmetric vibration of circular plates and its analog in elliptical plates using characteristic orthogonal polynomials.

[78] M.MUKHOPADHYAY 1979 *Journal of Sound and Vibration* **63**, 87-95. A semi-analytic solution for free vibration of annular sector plates.

[79] L.T.LEE and D.C.LEE 1997 *Computers and Structures* **65**, 149-156. Free vibration of rectangular plates on elastic point supports with the application of a new type of admissible function.

[80] J.YUAN and S.M.DICKINSON 1996 *Computers and Structures* **58**, 1261-1264. On the vibration of annular, circular and sectorial plates with cut-outs or on partial supports.

[81] E.ROMANELLI and P.A.A.LAURA 1997 *Computers and Structures* **62**, 795-797. An approximate method for analyzing transverse vibrations of circular, annular plates of non-uniform thickness and a free inner boundary.

[82] H.L.TUNG and Y.H.ERNEST 1958 *Journal of the Engineering Mechanics Division. Proceedings of the American Society of Civil Engineers* **EM 1**, 199-210. Elasto-plastic bending of rectangular plates.

[83] W.M.GERALD and H.G.KURT 1971 *Journal of the Structural Division. Proceeding of the American Society of Civil Engineers* **ST 7**, 1863-1878. Elastic-plastic bending of rectangular plates.

[84] W.PRAGER 1952 *Proceedings, 8th International Congress on Theory and Applied Mechanics, Istanble* **2**, 65-72. The General theory of limit design.

Appendix

From equations (2.2d), (2.2e), the following equations can be obtained.

$$\frac{\partial X_7}{\partial \eta} = \overline{D}(X_5 - \nu X_4) \tag{6.1a}$$

$$\frac{\partial X_6}{\partial \zeta} = \mu \overline{D}(X_4 - \nu X_5) \tag{6.1b}$$

$$\overline{D} = \frac{I}{(1-\nu^2)\mu} = \frac{D_0}{D}$$

Integrating the equation (6.1a) over the area $[0, \eta_i]$

$$\int_0^{\eta_i} \frac{\partial X_7}{\partial \eta} d\eta = \int_0^{\eta_i} \overline{D}(X_5 - \nu X_4) d\eta \tag{6.2}$$

By applying the trapezoidal rule of the numerical integration to the above equation

$$X_{7i0} - X_{700} = \sum_{k=0}^{i} \beta_{ik} \overline{D}_{k0}(X_{5k0} - \nu X_{4k0}) \tag{6.3}$$

thus,

$$\sum_{k=1}^{i} \beta_{ik} \overline{D}_{k0} X_{5k0} = -\beta_{i0} \overline{D}_{00} X_{500} + \nu \sum_{k=0}^{i} \beta_{ik} \overline{D}_{k0} X_{4k0} + X_{7i0} - X_{700} \tag{6.4}$$

Rewriting the above equation according to the order as $i = 1, 2, \cdots, i$

$i = 1$ $\quad \beta_{11} \overline{D}_{10} X_{510} =$

$$-\beta_{10} \overline{D}_{00} X_{500} + \nu \sum_{k=0}^{1} \beta_{1k} \overline{D}_{k0} X_{4k0} + X_{710} - X_{700} \tag{6.5a}$$

$i = 2$ $\quad \beta_{21} \overline{D}_{10} X_{510} + \beta_{22} \overline{D}_{20} X_{520} =$

$$-\beta_{20} \overline{D}_{00} X_{500} + \nu \sum_{k=0}^{2} \beta_{2k} \overline{D}_{k0} X_{4k0} + X_{720} - X_{700} \tag{6.5b}$$

$i = 3$ $\quad \beta_{31} \overline{D}_{10} X_{510} + \beta_{32} \overline{D}_{20} X_{520} + \beta_{33} \overline{D}_{30} X_{530} =$

$$-\beta_{30} \overline{D}_{00} X_{500} + \nu \sum_{k=0}^{3} \beta_{3k} \overline{D}_{k0} X_{4k0} + X_{730} - X_{700} \tag{6.5c}$$

$\vdots \qquad \vdots$

$i = i$ $\quad \beta_{i1} \overline{D}_{10} X_{510} + \beta_{i2} \overline{D}_{20} X_{520} + \beta_{i3} \overline{D}_{30} X_{530} + \cdots + \beta_{ii} \overline{D}_{i0} X_{5i0} =$

$$-\beta_{i0} \overline{D}_{00} X_{500} + \nu \sum_{k=0}^{i} \beta_{ik} \overline{D}_{k0} X_{4k0} + X_{7i0} - X_{700} \tag{0.5i}$$

Putting the terms on the right side of the above equations into $A_i (i = 1, 2, \cdots, i)$ and writing the above equations in matrix form

$$\begin{bmatrix} \beta_{11} & & & & 0 \\ \beta_{21} & \beta_{22} & & & \\ \beta_{31} & \beta_{32} & \beta_{33} & & \\ \vdots & \vdots & \vdots & & \\ \beta_{i1} & \beta_{i2} & \beta_{i3} & \cdots & \beta_{ii} \end{bmatrix} \begin{bmatrix} \overline{D}_{10}X_{510} \\ \overline{D}_{20}X_{520} \\ \overline{D}_{30}X_{530} \\ \vdots \\ \overline{D}_{i0}X_{5i0} \end{bmatrix} = \begin{bmatrix} A_1 \\ A_2 \\ A_3 \\ \vdots \\ A_i \end{bmatrix} \tag{6.6}$$

From the equation (6.6), the unknowns $\{D_{i0}M_{xi0}\}$ $(i = 1, 2, 3 \cdots i)$ are obtained as

$$\begin{bmatrix} \overline{D}_{10}X_{510} \\ \overline{D}_{20}X_{520} \\ \overline{D}_{30}X_{530} \\ \vdots \\ \overline{D}_{i0}X_{5i0} \end{bmatrix} = \begin{bmatrix} b_{11} & b_{12} & b_{13} & \cdots & b_{1i} \\ b_{21} & b_{22} & b_{23} & \cdots & b_{2i} \\ b_{31} & b_{32} & b_{33} & \cdots & b_{3i} \\ \vdots & \vdots\vdots & \ddots & \vdots & \\ b_{i1} & b_{i2} & b_{i3} & \cdots & b_{ii} \end{bmatrix} \begin{bmatrix} A_1 \\ A_2 \\ A_3 \\ \vdots \\ A_i \end{bmatrix} \tag{6.7}$$

where $[b_{ij}] = [\beta_{ij}]^{-1}$

From equation (6.7), the following equation can be obtained

$$\overline{D}_{i0}X_{5i0} = \sum_{k=1}^{i} b_{ik}A_k$$

$$= b_{i1}[-\beta_{10}\overline{D}_{00}X_{500} + \nu\sum_{k=0}^{1}\beta_{1k}\overline{D}_{k0}X_{4k0} + X_{710} - X_{700}]$$

$$+b_{i2}[-\beta_{20}\overline{D}_{00}X_{500} + \nu\sum_{k=0}^{2}\beta_{2k}\overline{D}_{k0}X_{4k0} + X_{720} - X_{700}]$$

$$+b_{i3}[-\beta_{30}\overline{D}_{00}X_{500} + \nu\sum_{k=0}^{3}\beta_{3k}\overline{D}_{k0}X_{4k0} + X_{730} - X_{700}]$$

$$\vdots$$

$$+b_{ii}[-\beta_{i0}\overline{D}_{00}X_{500} + \nu\sum_{k=0}^{i}\beta_{ik}\overline{D}_{k0}X_{4k0} + X_{7i0} - X_{700}]$$

$$= b_{i1}[-\beta_{10}\overline{D}_{00}X_{500} + \nu\beta_{10}\overline{D}_{00}X_{400} + \nu\beta_{11}\overline{D}_{10}X_{410} + X_{710} - X_{700}]$$

$$+b_{i2}[-\beta_{20}\overline{D}_{00}X_{500} + \nu\beta_{20}\overline{D}_{00}X_{400} + \nu\beta_{21}\overline{D}_{10}X_{410} + \nu\beta_{22}\overline{D}_{20}X_{420} + X_{720} - X_{700}]$$

$$+b_{i3}[-\beta_{30}\overline{D}_{00}X_{500} + \nu\beta_{30}\overline{D}_{00}X_{400} + \nu\beta_{31}\overline{D}_{10}X_{410} + \nu\beta_{32}\overline{D}_{20}X_{420}$$

$$+\nu\beta_{33}\overline{D}_{30}X_{430} + X_{730} - X_{700}]$$

$$\vdots$$

$$+b_{ii}[-\beta_{i0}\overline{D}_{00}X_{500} + \nu\beta_{i0}\overline{D}_{00}X_{400} + \nu\beta_{i1}\overline{D}_{10}X_{410} + \nu\beta_{i2}\overline{D}_{20}X_{420}$$

$$+\nu\beta_{i3}\overline{D}_{30}X_{430} + \cdots + \nu\beta_{ii}\overline{D}_{i0}X_{4i0} + X_{7i0} - X_{700}]$$

$$= X_{500}(-\overline{D}_{00}\sum_{k=1}^{i} b_{ik}\beta_{k0}) + X_{400}(\nu\overline{D}_{00}\sum_{k=1}^{i} b_{ik}\beta_{k0}) + X_{700}(-\sum_{k=1}^{i} b_{ik})$$
$$+ X_{410}(\nu\overline{D}_{10}\sum_{k=1}^{i} b_{ik}\beta_{k1}) + X_{710}b_{i1}$$
$$+ X_{420}(\nu\overline{D}_{20}\sum_{k=2}^{i} b_{ik}\beta_{k2}) + X_{720}b_{i2}$$
$$\vdots$$
$$+ X_{4i0}(\nu\overline{D}_{i0}\sum_{k=i}^{i} b_{ik}\beta_{ki}) + X_{7i0}b_{ii}$$

Therefore,

$$X_{5i0} = X_{500}(-\frac{\overline{D}_{00}}{\overline{D}_{i0}}\sum_{k=1}^{i} b_{ik}\beta_{k0}) + X_{400}(\nu\frac{\overline{D}_{00}}{\overline{D}_{i0}}\sum_{k=1}^{i} b_{ik}\beta_{k0}) + X_{700}(-\frac{1}{\overline{D}_{i0}}\sum_{k=1}^{i} b_{ik})$$
$$+X_{410}(\nu\frac{\overline{D}_{10}}{\overline{D}_{i0}}\sum_{k=1}^{i} b_{ik}\beta_{k1}) + X_{710}(\frac{1}{\overline{D}_{i0}}b_{i1})$$
$$+X_{420}(\nu\frac{\overline{D}_{20}}{\overline{D}_{i0}}\sum_{k=2}^{i} b_{ik}\beta_{k2}) + X_{720}(\frac{1}{\overline{D}_{i0}}b_{i2})$$
$$\vdots$$
$$+X_{4i0}(\nu\frac{\overline{D}_{i0}}{\overline{D}_{i0}}\sum_{k=1}^{i} b_{ik}\beta_{ki}) + X_{7i0}(\frac{1}{\overline{D}_{i0}}b_{ii}) \tag{6.8}$$

Rewriting the above equation in simple form

$$X_{5i0} = a_{25i003}X_{500} + \sum_{k=0}^{i}(a_{15i0k3}X_{4k0} + a_{15i0k5}X_{7k0}) \tag{6.9}$$

$$a_{25i003} = -\frac{\overline{D}_{00}}{\overline{D}_{i0}}\sum_{k=1}^{i} b_{ik}\beta_{k0}$$

$$a_{15i003} = \nu\frac{\overline{D}_{00}}{\overline{D}_{i0}}\sum_{k=1}^{i} b_{ik}\beta_{k0} \quad a_{15i005} = -\frac{1}{\overline{D}_{i0}}\sum_{k=1}^{i} b_{ik}$$

$$a_{15i013} = \nu\frac{\overline{D}_{10}}{\overline{D}_{i0}}\sum_{k=1}^{i} b_{ik}\beta_{k1} \quad a_{15i015} = \frac{1}{\overline{D}_{i0}}b_{i1}$$

$$a_{15i023} = \nu\frac{\overline{D}_{20}}{\overline{D}_{i0}}\sum_{k=2}^{i} b_{ik}\beta_{k2} \quad a_{15i025} = \frac{1}{\overline{D}_{i0}}b_{i2}$$

$$\vdots \qquad\qquad \vdots$$

$$a_{15i0i3} = \nu\frac{\overline{D}_{i0}}{\overline{D}_{i0}}\sum_{k=i}^{i} b_{ik}\beta_{ki} \quad a_{15i0i5} = \frac{1}{\overline{D}_{i0}}b_{ii}$$

The discrete solutions expressed in equation (2.11) are

$$X_{pij} = \sum_{k=0}^{i} \Big\{ a_{1pijk1}(Q_y)_{k0} + a_{1pijk2}(M_{xy})_{k0} + a_{1pijk3}(M_y)_{k0} + a_{1pijk4}(\theta_y)_{k0} + a_{1pijk5}(\theta_x)_{k0} + a_{1pijk6}(w)_{k0} \Big\} + \sum_{l=0}^{j} \Big\{ a_{2pijl1}(Q_x)_{0l} + a_{2pijl2}(M_{xy})_{0l} + a_{2pijl3}(M_x)_{0l} + a_{2pijl4}(\theta_y)_{0l} + a_{2pijl5}(\theta_x)_{0l} + a_{2pijl6}(w)_{0l} \Big\} + \overline{q}_{pij} + \sum_{f=1}^{3} \sum_{c=0}^{m} \sum_{d=0}^{n} \overline{q}_{fpijcd} P_{fcd}$$

$(Q_y) = X_1$, $(Q_x) = X_2$, $(M_{xy}) = X_3$, $(M_y) = X_4$, $(M_x) = X_5$, $(\theta_y) = X_6$, $(\theta_x) = X_7$ and $(w) = X_8$ are integral constants.

These constants along the edges $\eta = 0$ and $\zeta = 0$ are illustrated in Figure 6.1. There are only six integral constants at each discrete point. X_1 and X_4 don't exist along the edge $\eta = 0$. X_2 and X_5 don't exist along the edge $\zeta = 0$. So it is necessary to find the relations between the existent and unexistent constants. The coefficient a_{15i0i3} is used as an example to explain the meaning of the foot of the coefficient

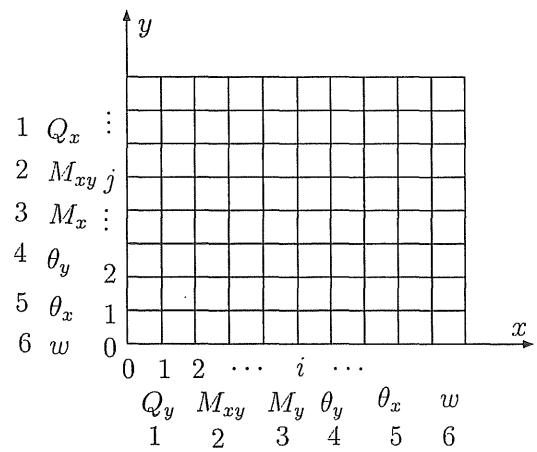

Figure 6.1:

$a_{\underline{1}5i0i3}$: the coefficient of the integral constants along the edge $\zeta = 0$.

$a_{1\underline{5}i0i3}$: the coefficient of the constant X_5.

$a_{15\underline{i}0i3}$: the coefficient at the point $(\eta, 0)$.

$a_{15i0\underline{i}3}$: the coefficient of the integral constant at poit $(\eta_i, 0)$.

$a_{5i0i\underline{3}}$: the coefficient of the constant X_4 at point $(\eta_i, 0)$..

a_{1*****} and a_{2*****} are noted as the coefficients of the integral constants along the edge $\zeta = 0$ and $\eta = 0$, respectively.

From the equation (6.1b), using the same manner, the following equation and coefficients can be obtained

$$X_{40j} = a_{140j03}X_{400} + \sum_{l=0}^{j}(a_{240jl3}X_{50j} + a_{240jl4}X_{60l}) \tag{6.10}$$

$$a_{140j03} = -\frac{\overline{D}_{00}}{\overline{D}_{0j}}\sum_{l=1}^{j} b_{jl}\beta_{l0}$$

$$a_{240j03} = \nu\frac{\overline{D}_{00}}{\overline{D}_{0j}}\sum_{l=1}^{j} b_{jl}\beta_{l0} \quad a_{240j04} = -\frac{1}{\mu\overline{D}_{0j}}\sum_{l=1}^{j} b_{jl}$$

$$a_{240j13} = \nu\frac{\overline{D}_{01}}{\nu\overline{D}_{0j}}\sum_{l=1}^{j} b_{jl}\beta_{l1} \quad a_{240j14} = \frac{1}{\mu\overline{D}_{0j}}b_{j1}$$

$$a_{240j23} = \nu\frac{\overline{D}_{02}}{\overline{D}_{0j}}\sum_{l=2}^{j} b_{jl}\beta_{l2} \quad a_{240j24} = \frac{1}{\mu\overline{D}_{0j}}b_{j2}$$

$$\vdots \qquad\qquad \vdots$$

$$a_{240jj3} = \nu\frac{\overline{D}_{0j}}{\overline{D}_{0j}}\sum_{l=j}^{j} b_{jl}\beta_{lj} \quad a_{240jj4} = \frac{1}{\mu\overline{D}_{0j}}b_{jj}$$

From the equation (2.2h), the following equation can be obtained

$$\frac{\partial X_8}{\partial \zeta} = \mu K X_1 - \mu X_6 \tag{6.11}$$

Integrating the above equation over $[0, \zeta_j]$,

$$\int_0^{\zeta_j}\frac{\partial X_8}{\partial \zeta}d\zeta = \int_0^{\zeta_j}(\mu K X_1 - \mu X_6)d\zeta \tag{6.12}$$

By applying the trapezoidal rule of the numerical integration to the above equation

$$X_{80j} - X_{800} = \mu\sum_{l=0}^{j} K_{0l}\beta_{jl}X_{10l} - \mu\sum_{l=0}^{j}\beta_{jl}X_{60l} \tag{6.13}$$

$$\mu\sum_{l=1}^{j} K_{0l}\beta_{jl}X_{10l} = -\mu K_{00}\beta_{j0}X_{100} + \mu\sum_{l=0}^{j}\beta_{jl}X_{60l} + X_{80j} - X_{800} \tag{6.14}$$

Putting the terms on the right of the above equations into $B_j (j = 1, 2, \cdots, j)$ and writing the above equations in matrix form

$$\begin{bmatrix} \beta_{11} & & & & 0 \\ \beta_{21} & \beta_{22} & & & \\ \beta_{31} & \beta_{32} & \beta_{33} & & \\ \vdots & \vdots & \vdots & & \\ \beta_{j1} & \beta_{j2} & \beta_{j3} & \cdots & \beta_{jj} \end{bmatrix} \begin{bmatrix} \mu K_{01}X_{101} \\ \mu K_{02}X_{102} \\ \mu K_{03}X_{103} \\ \vdots \\ \mu K_{0j}X_{10j} \end{bmatrix} = \begin{bmatrix} B_1 \\ B_2 \\ B_3 \\ \vdots \\ B_j \end{bmatrix} \tag{6.15}$$

From the equation (6.15), the unknowns $\{\mu K_{0j} X_{1i0}\}$ $(j = 1, 2, 3 \cdots j)$ are obtained as

$$\begin{bmatrix} \mu K_{01} X_{101} \\ \mu K_{02} X_{102} \\ \mu K_{03} X_{103} \\ \vdots \\ \mu K_{0j} X_{10j} \end{bmatrix} = \begin{bmatrix} b_{11} & b_{12} & b_{13} & \cdots & b_{1j} \\ b_{21} & b_{22} & b_{23} & \cdots & b_{2j} \\ b_{31} & b_{32} & b_{33} & \cdots & b_{3j} \\ \vdots & \vdots & \vdots & \ddots & \vdots \\ b_{j1} & b_{j2} & b_{j3} & \cdots & b_{jj} \end{bmatrix} \begin{bmatrix} B_1 \\ B_2 \\ B_3 \\ \vdots \\ B_j \end{bmatrix} \tag{6.16}$$

Rewriting the above equation as

$$\mu K_{0j} X_{10j} = \sum_{l=1}^{j} b_{jl} B_l \tag{6.17}$$

Using the equation (6.17) and replacing $\{B_l\}$ by the terms at right side of the equation (6.14)

$$\begin{aligned} X_{10j} = X_{100}(\frac{K_{00}}{K_{0j}} \sum_{l=1}^{j} b_{jl}\beta_{l0}) &+ X_{600}(\frac{1}{K_{0j}} \sum_{l=1}^{j} b_{jl}\beta_{l0} + X_{800}(\frac{1}{\mu K_{0j}} \sum_{l=1}^{j} b_{jl}) \\ &+ X_{601}(\frac{1}{K_{0j}} \sum_{l=1}^{j} b_{jl}\beta_{l1} + X_{801}(\frac{1}{\mu K_{0j}} b_{j1}) \\ &+ X_{602}(\frac{1}{K_{0j}} \sum_{l=2}^{j} b_{jl}\beta_{l2} + X_{802}(\frac{1}{\mu K_{0j}} b_{j2}) \\ &\vdots \\ &+ X_{60j}(\frac{1}{K_{0j}} \sum_{l=j}^{j} b_{jl}\beta_{lj} + X_{801}(\frac{1}{\mu K_{0j}} b_{jj}) \end{aligned} \tag{6.18}$$

Writing the above equation in simple form

$$X_{40j} = a_{110j01} X_{100} + \sum_{l=0}^{j} (a_{210jl4} X_{60l} + a_{210jl6} X_{80l}) \tag{6.19}$$

$$a_{110j01} = -\frac{K_{00}}{K_{0j}} \sum_{l=1}^{j} b_{jl}\beta_{l0}$$

$$a_{210j04} = \frac{1}{K_{0j}} \sum_{l=1}^{j} b_{jl}\beta_{l0} \quad a_{210j06} = -\frac{1}{\mu K_{0j}} \sum_{l=1}^{j} b_{jl}$$

$$a_{210j14} = \frac{1}{K_{0j}} \sum_{l=1}^{j} b_{jl}\beta_{l1} \quad a_{210j16} = \frac{1}{\mu K_{0j}} b_{j1}$$

$$a_{210j24} = \frac{1}{K_{0j}} \sum_{l=2}^{j} b_{jl}\beta_{l2} \quad a_{210j26} = \frac{1}{\mu K_{0j}} b_{j2}$$

$$\vdots$$

$$a_{210jj4} = \frac{1}{K_{0j}} \sum_{l=j}^{j} b_{jl}\beta_{lj} \quad a_{210jj6} = \frac{1}{\mu K_{0j}} b_{jj}$$

From the equation (2.2g), in the same manner, the following equations and coefficients are obtained.

$$X_{2i0} = a_{22i001}X_{200} + \sum_{k=0}^{j}(a_{12i0k5}X_{7k0} + a_{12i0k6}X_{8k0}) \tag{6.20}$$

$$a_{22i001} = -\frac{K_{00}}{K_{i0}} \sum_{k=1}^{i} b_{ik}\beta_{k0}$$

$$a_{12i005} = \frac{1}{K_{i0}} \sum_{k=1}^{i} b_{ik}\beta_{k0} \quad a_{12i006} = -\frac{1}{K_{i0}} \sum_{k=1}^{i} b_{ik}$$

$$a_{12i015} = \frac{1}{K_{i0}} \sum_{k=1}^{i} b_{ik}\beta_{k1} \quad a_{12i016} = \frac{1}{K_{i0}} b_{i1}$$

$$a_{12i025} = \frac{1}{K_{i0}} \sum_{k=2}^{i} b_{ik}\beta_{k2} \quad a_{12i026} = \frac{1}{K_{i0}} b_{i2}$$

$$\vdots$$

$$a_{12i0i5} = \frac{1}{K_{i0}} \sum_{k=1}^{i} b_{ik}\beta_{ki} \quad a_{12i0i6} = \frac{1}{K_{i0}} b_{ii}$$

From the equations (6.9), (6.10), (6.19) and (6.20), the coefficients can be simply expressed in following forms

$$a_{25i003} = \frac{\overline{D}_{00}}{\overline{D}_{i0}}\overline{\alpha}_i, \quad a_{140j03} = \frac{\overline{D}_{00}}{\overline{D}_{0j}}\overline{\alpha}_i, \quad a_{15i0k3} = \nu\frac{\overline{D}_{k0}}{\overline{D}_{i0}}\overline{\beta}_{ik}$$

$$a_{240jl3} = \nu\frac{\overline{D}_{0l}}{\overline{D}_{0j}}\overline{\beta}_{jl}, \quad a_{15i0k5} = \frac{1}{\overline{D}_{i0}}\overline{\gamma}_{ik}, \quad a_{240jl4} = \frac{1}{\mu\overline{D}_{0j}}\overline{\gamma}_{jl}$$

$$a_{110j01} = \frac{K_{00}}{\overline{K}_{0j}}\overline{\alpha}_j, \quad a_{210jl4} = \frac{1}{K_{0j}}\overline{\beta}_{jl}, \quad a_{210jl6} = \frac{1}{\mu K_{0j}}\overline{\gamma}_{jl}$$

$$a_{22i001} = \frac{K_{00}}{K_{i0}}\overline{\alpha}_i, \quad a_{12i0k5} = \frac{1}{K_{i0}}\overline{\beta}_{ik}, \quad a_{12i0k6} = \frac{1}{K_{i0}}\overline{\gamma}_{ik},$$

$$\overline{\alpha}_i = (-1)^i, \quad \overline{\alpha}_j = (-1)^j, \quad \overline{D}_{i0} = D_0/D_{i0}, \quad \overline{D}_{0j} = \mu D_0/D_{0j},$$

$$\overline{\beta}_{ik} = \delta_{ik} + (-1)^{(i+1)}\delta_{0k}, \quad \overline{\beta}_{jl} = \delta_{jl} + (-1)^{(j+1)}\delta_{0l}, \quad \overline{\gamma}_{ik} = \frac{4m(-1)^{i+k}}{1+\delta_{ik}+\delta_{0k}},$$

$$\overline{\gamma}_{jl} = \frac{4n(-1)^{j+l}}{1+\delta_{jl}+\delta_{0l}}, \quad \overline{\gamma}_{ik} = \begin{cases} 0 & (i<k) \\ \overline{\gamma}_{ik} & (i \geq k) \end{cases}, \quad \overline{\gamma}_{jl} = \begin{cases} 0 & (j<l) \\ \overline{\gamma}_{ik} & (j \geq l) \end{cases}$$

But for elsto-plastic problems, the coefficients are expressed as follows

$$a_{25i003} = \frac{1}{t_{11}(i,0)} \frac{\overline{D}_{00}}{\overline{\overline{D}}_{i0}} \overline{\alpha}_i \qquad a_{140j03} = \frac{1}{t_{22}(0,j)} \frac{\overline{D}_{00}}{\overline{\overline{D}}_{0j}} \overline{\alpha}_i$$

$$a_{15i0k3} = -\frac{t_{12}(k,0)}{t_{11}(i,0)} \frac{\overline{D}_{k0}}{\overline{\overline{D}}_{i0}} \overline{\beta}_{ik} \qquad a_{240jl3} = -\frac{t_{21}(0,l)}{t_{22}(0,j)} \frac{\overline{D}_{0l}}{\overline{\overline{D}}_{0j}} \overline{\beta}_{jl}$$

$$a_{15i0k2} = -\frac{t_{13}(k,0)}{t_{11}(i,0)} \frac{\overline{D}_{k0}}{\overline{\overline{D}}_{i0}} \overline{\beta}_{ik} \qquad a_{240jl2} = -\frac{t_{23}(0,l)}{t_{22}(0,j)} \frac{\overline{D}_{0l}}{\overline{\overline{D}}_{0j}} \overline{\beta}_{jl}$$

$$a_{15i0k5} = \frac{1}{(1-\nu^2)\overline{D}_{i1} t_{11}(i,0)} \overline{\gamma}_{ik} \qquad a_{240jl4} = \frac{1}{\mu(1-\nu^2)\overline{D}_{1j} t_{22}(0,j)} \overline{\gamma}_{jl}$$

$$a_{110j01} = \frac{K_{00}}{K_{0j}} \overline{\alpha}_j \quad a_{210jl4} = \frac{1}{K_{0j}} \overline{\beta}_{jl} \quad a_{210jl6} = \frac{1}{\mu K_{0j}} \overline{\gamma}_{jl}$$

$$a_{22i001} = \frac{K_{00}}{K_{i0}} \overline{\alpha}_i \quad a_{22i0k5} = \frac{1}{K_{i0}} \overline{\beta}_{ik} \quad a_{12i0k6} = \frac{1}{K_{i0}} \overline{\gamma}_{ik}$$

Where $[t_{ij}] = [a_{ij}]^{-1}$ and $[a_{ij}]$ is expressed in the equation (5.9).

Acknowledgement

This thesis was accomplished under the supervision of Professor Takeshi Sakiyama. I would like to express my greatest gratitude to him for his enlightening guidance and great help. I feel very lucky to be one of his students and I attribute all my achievements to him.

I would also like to express my particular and sincere thanks to Associate Professor Hiroshi Matsuda and Associate Professor Chihiro Morita for their enthusiastic support and valuable amendments to the thesis. A lot of their good suggestions have been adopted in this thesis.

I am very thankful to the members of the dissertation committee, Professor Teisuke Sueoka, Professor Minoru Shugyo and Professor Yutaka Yoshitake for their critical reviews and constructive advice.

I am also indebted to Mr. Aoi Koga, Mr. Jianping Li, Ms. Naomi Sakaue and Ms. Hatsumi Tanabe for their kindness and valuable help.

I want to thank all the students in Professor Sakiyama's laboratory and all my friends for their friendship and help.

Finally, I want to express my deepest gratitude to my parents, brother, sister, my husband and my daughter for their love, understanding and support.